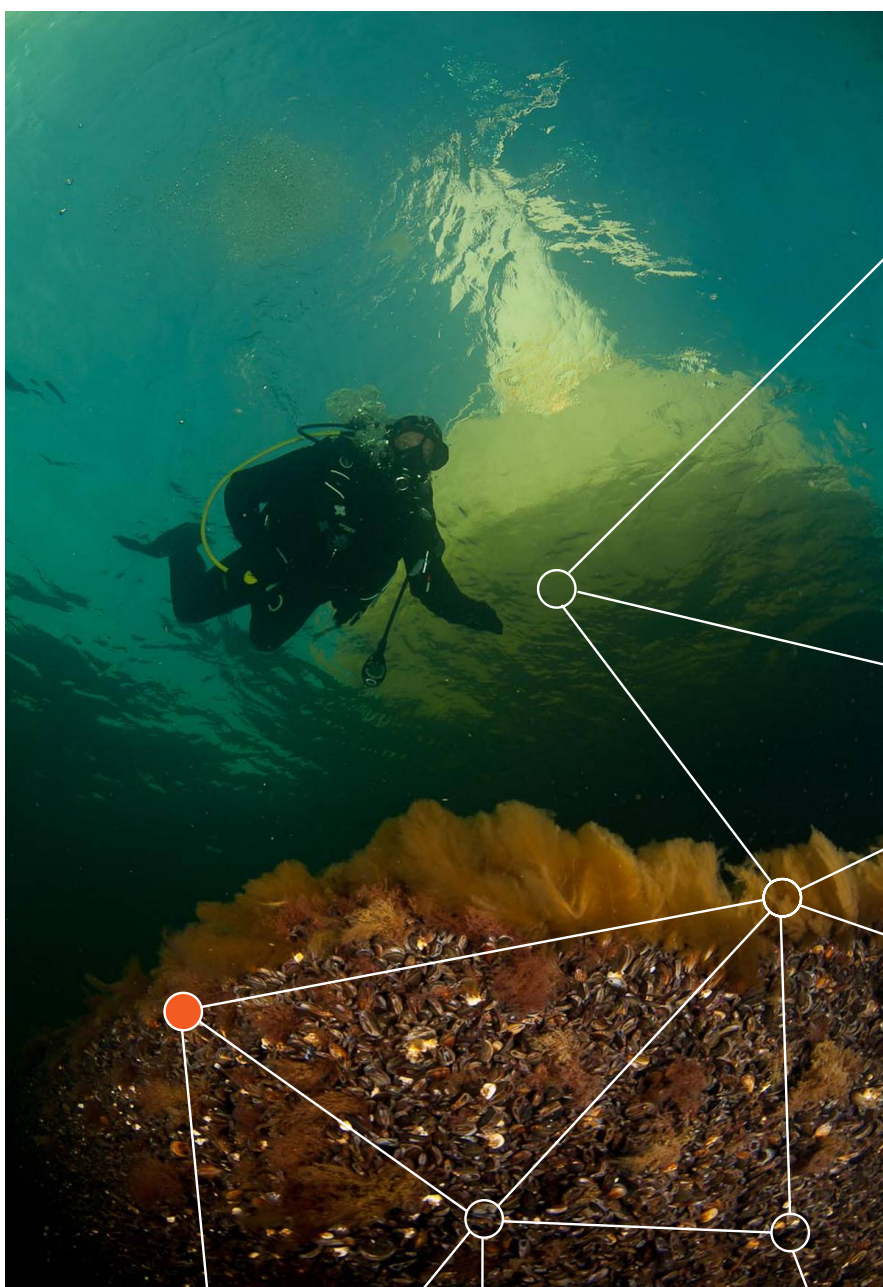


Evaluation of a wideband echosounder for fisheries and marine ecosystem science

**ICES COOPERATIVE
RESEARCH REPORT**

RAPPORT
DES RECHERCHES
COLLECTIVES



2016 USA–Norway EK80 Workshop Report:
Evaluation of a wideband echosounder for
fisheries and marine ecosystem science

Authors

David A. Demer • Lars N. Andersen • Chris Bassett • Laurent Berger
Dezhang Chu • Jeff Condiotty • George R. Cutter Jr. • Briony Hutton
Rolf Korneliussen • Naig Le Bouffant • Gavin Macaulay
William L. Michaels • David Murfin • Armin Pobitzer • Josiah S. Renfree
Thomas S. Sessions • Kevin L. Stierhoff • Charles H. Thompson



ICES

International Council for
the Exploration of the Sea

CIEM

Conseil International pour
l'Exploration de la Mer

International Council for the Exploration of the Sea Conseil International pour l'Exploration de la Mer

H. C. Andersens Boulevard 44–46
DK-1553 Copenhagen V
Denmark
Telephone (+45) 33 38 67 00
Telefax (+45) 33 93 42 15
www.ices.dk
info@ices.dk

Recommended format for purposes of citation:

Demer, D. A., Andersen, L. N., Bassett, C., Berger, L., Chu, D., Condiotty, J., Cutter, G. R., *et al.* 2017. 2016 USA–Norway EK80 Workshop Report: Evaluation of a wideband echosounder for fisheries and marine ecosystem science. ICES Cooperative Research Re-port No. 336. 69 pp. <https://doi.org/10.17895/ices.pub.2318>

Series Editor: Emory D. Anderson

The material in this report may be reused for non-commercial purposes using the recommended citation. ICES may only grant usage rights of information, data, images, graphs, etc. of which it has ownership. For other third-party material cited in this report, you must contact the original copyright holder for permission. For citation of datasets or use of data to be included in other databases, please refer to the latest ICES data policy on the ICES website. All extracts must be acknowledged. For other reproduction requests please contact the General Secretary.

This document is the product of an Expert Group under the auspices of the International Council for the Exploration of the Sea and does not necessarily represent the view of the Council.

Cover image: © OCEANA/Carlos Suárez

DOI: <http://doi.org/10.17895/ices.pub.2318>

ISBN 978-87-7482-199-1

ISSN 1017-6195

© 2017 International Council for the Exploration of the Sea

Contents

Foreword	i–iv
1 Introduction	1
1.1 Wide-bandwidth echosounders	2
1.1.1 Advantages.....	2
1.1.2 Challenges	3
1.2 Simrad EK80	3
1.2.1 Transmit pulse	4
1.2.2 Frequency bandwidth.....	4
1.2.3 Stage 1 and stage 2 filters and decimators	7
1.2.4 FM-data processing	8
1.3 Calibration	11
1.3.1 Standard sphere uncertainty.....	11
1.3.2 Frequency-dependent source level	12
1.3.3 Frequency-dependent beamwidth.....	12
2 Investigations	13
2.1 Data volume and processing speed	13
2.1.1 Lossless reduction during collection	13
2.1.2 Lossy reduction during collection.....	14
2.1.3 Increased processing speed.....	14
2.2 Transmit power.....	14
2.2.1 Voltage droop	19
2.2.2 Non-linear effects	20
2.2.3 Cross-channel interference.....	22
2.3 Trigger stability.....	27
2.4 Noise measurements	29
2.4.1 EK60 CW.....	29
2.4.2 EK80 CW.....	31
2.4.3 EK80 FM	31
2.4.4 EK60 and EK80 on board FSV “Reuben Lasker”	32
2.5 Target-spectra measurements	33
2.5.1 FFT length.....	33
2.5.2 FFT position	34
2.5.3 Target separation.....	34
2.5.4 Calibration.....	35
2.5.5 Effective pulse duration.....	35
2.5.6 Single-target detection.....	36
2.6 Nautical area backscattering coefficients	40
2.6.1 Simulated echo.....	41
2.6.2 Sphere echo	42
2.6.3 Transmit pulses	43

2.7	Targets near one another or boundaries.....	45
2.7.1	Targets near the seabed	46
3	Discussion	49
3.1	Research findings.....	49
3.2	Future EK80 research	51
4	Acknowledgements.....	52
5	References	53
Annex 1: Simrad ES38-7 transducer.....		55
A.1	Impedance.....	55
A.2	Bandwidth	57
A.3	Beam pattern.....	58
A.4	Transmit spectra.....	61
A.5	Conclusion	62
Annex 2: Terms, symbols, and units		63
Annex 3: Author contact information.....		69

Foreword

For more than a decade, the Simrad–Kongsberg (Simrad) EK60 echosounder has been a worldwide standard for providing estimates of fish biomass and distributions, conducting ecosystem surveys, and observing the behaviours of aquatic organisms and their associations with oceanographic and seabed environments. However, components of EK60 general purpose transceivers (GPTs) are no longer commercially available, the GPT-control and data acquisition software, ER60, is no longer developed, and both have been recently superseded by the more advanced Simrad EK80 echosounder system. To facilitate a rapid and successful transition to the operational use of EK80, it is necessary to ensure the continuation of accurate and precise measurements used in time-series for stock assessments and marine ecosystem research.

At recent meetings of the USA–Norway Science Bilateral on Fisheries and the International Council for the Exploration of the Sea (ICES) Fisheries Acoustic Science and Technology Working Group, scientists discussed the terms of reference for conducting an EK80 workshop. NOAA’s Southwest Fisheries Science Center in San Diego, California, USA was chosen as the location for the workshop because of its state-of-the-art Ocean Technology Development Tank and access to ship time on board NOAA’s FSV “Reuben Lasker”. The EK80 workshop was scheduled in two phases: laboratory tank experiments conducted during 6–9 and 12–16 September 2016 and field experiments conducted during 19–23 September 2016. Workshop participants were from the USA, Norway, France, and Australia.

This workshop report provides technical results and recommendations that are necessary to expedite the operational use of EK80 in standardized surveys and to improve scientific information for the conservation and management of living marine resources. As more is learned about the EK80 wideband transceiver (WBT), its firmware and software will be refined by the manufacturer (Lars Andersen, Simrad, pers. comm.). Accordingly, commercial analysis software will be revised (Briony Hutton, Echoview [<https://www.echoview.com/>], and Rolf Korneliussen, Large Scale Survey System [LSSS; <http://cmr.no/projects/10396/lsss/>], pers. comms.). Recommended settings and algorithms for data collection and analysis will be collaboratively optimized for research and operational surveys. This report documents the state of the technology as of September 2016. There will likely be future EK80 workshops with updated reports.

Workshop results

Conventional narrow-bandwidth echosounders, such as EK60, transmit pulses containing a single-frequency, sinusoidal, continuous wave (CW) signal. Wide-bandwidth echosounders, such as EK80, are capable of transmitting either CW pulses at selected discrete frequencies or pulses containing a range of frequencies, commonly linear low-to-high frequency modulated (FM) signals.

EK80 may be configured to closely emulate EK60 by transmitting CW pulses simultaneously at multiple frequencies, e.g. 18, 38, 70, 120, 200, and 333 kHz. Even when similarly configured, however, EK80 has wider bandwidth receiver filters and outputs complex waveform data from each transducer sector at higher decimated sampling rates than EK60.

During this workshop, experiments were conducted that confirmed, for the first time, that EK60 and EK80, operating in CW mode, provide equivalent measures of integrated volume backscattering coefficients for echoes from calibration spheres. This important finding supports the operational transition from EK60 to EK80, operating in

CW mode, for fisheries surveys. Comparisons should also be made for data collected with EK60 and EK80 multiplexed to the same transducers during fisheries surveys.

EK80 can also be configured to transmit wideband FM pulses sequentially or simultaneously, potentially spanning large portions of the frequency range from 10 to 500 kHz. This feature offers the potential for greatly improved range resolution, signal-to-noise ratio, and characterizations of the frequency responses of target strength and volume backscattering strength. Wideband frequency responses may be used to improve target identification, thereby reducing uncertainty in estimates of animal abundance.

The many advantages of wideband vs. narrowband echosounders come with additional complexities associated with system calibrations, data storage, processing speed, signal processing and analyses, and interpretation. This is largely due to necessarily wider receiver bandwidths, higher sampling rates, and the frequency dependence of many environmental and system parameters, e.g. acoustic absorption, transducer efficiency and beamwidths, and scatterer reflectivity and directivity. For example, compared to narrowband data, wideband data may be inherently more susceptible to noise and more voluminous.

EK80 may collect 1–2 orders of magnitude more data than EK60, depending on the bandwidth and other configurations. This is because EK60 outputs envelope-detected power and split-beam phase data, and EK80 outputs complex waveform data for each channel, with at least twice as many samples per pulse duration. This additional EK80 data may allow better detection of single targets in either CW or FM mode and analysis of backscattering spectra in FM mode.

Recommendations

- Generally, all of the information available in EK80 data should be preserved to allow for future alternative investigations and because research cruises are expensive. Strategies for reducing data volume and increasing processing efficiency may be considered in terms of (i) lossless reduction during collection; (ii) lossy reduction during collection; and (iii) increased processing speed.
- To reduce data volume, Simrad should enable bandwidth-dependent logging ranges and faster and programmable alternation between CW to FM and active to passive modes. Simrad could better optimize filter bandwidth and decimation or provide users more flexibility to do so, and implement conventional data-compression algorithms.
- To store and process less data for specific objectives, Simrad could emulate EK60 data output, i.e. power and angle values with four samples per pulse; use more aggressive filtering and decimation schemes; implement programmable data collection, e.g. mostly CW with periodic FM, and alternating active and passive modes, or both; collect passive data routinely prior to each transmit signal to continuously estimate the signal-to-noise ratio and perhaps use this metric to limit data collection; and facilitate multiple narrowband signals within the allowable bandwidth.
- Multiple narrowband datasets could be analyzed as for EK60 data. Preprocessing may be used to generate matched filter data, with or without decimation. Preprocessed datasets could be limited by time, location, intensity, range, signal-to-noise ratio, bandwidths, and data types or objects of interest (e.g. single targets).

- The EK80 transmitter may not have sufficiently low output impedance to consistently produce a rectangular-pulse envelope. Transmit pulses tend to droop more with increasing pulse duration and frequency. This may have ramifications for accurate measurements of volume backscattering strength spectra. Further investigation is warranted.
- Transmit pulses from multiple EK80 WBTs may be simultaneous or sequential. When transmitting simultaneously, harmonic energy generated by lower-frequency transmissions may cause cross-channel interference, which may bias the higher-frequency data. In this case, the transmit power should be set to minimize non-linear effects, and perhaps orthogonal, non-interfering pulse signals could be used for the various frequency bands. Further investigation is warranted. Sequential transmissions eliminate cross-talk between EK80 channels, but reduces the transmit repetition rate.
- EK80 may input or output trigger signals via either an auxiliary connector on the transceiver or serial input on the computer running EK80 software. To obtain stable triggering with low latency, the auxiliary port must be used. Triggering on the serial port causes large and variable latency.
- Due to wider receiver bandwidths, noise is higher and more variable in EK80 data than in EK60. For both active and passive modes, noise decreases with increasing pulse duration, and configurations with fast-ramp (abrupt rise and fall) pulses have less noise than those with slow-ramp (gradual rise and fall) pulses. For all EK80 applications, spikes in the noise spectra should be investigated and mitigated, whenever possible, before data collections. Further investigation is warranted.
- Acoustic surveys may require targets to be resolved close to one another or near a boundary, e.g. the seabed. EK80 operating in FM mode has high range resolution, but matched-filter processing introduces side lobes related to the length of the transmitted pulse and the frequency content of the signal which may limit target detection and characterization. If the echo from one target is much weaker than another, e.g. a fish near the seabed, the side lobes from the stronger target may eclipse the weaker echo. Even if echoes from nearby targets are resolved, their backscattering spectra may not be separable. Slow ramping of the transmit signal suppresses the side lobes and improves range resolution, but echoes from resolved targets have reduced bandwidth for spectral characterization. Further investigation is warranted.

Next steps

To transition from EK60 to EK80, each EK60 GPT must be replaced with an EK80 WBT, and ER60 replaced with EK80 software. WBTs may be used with existing transducers, but some newer model transducers are better suited for wideband performance (e.g. see Annex 1: Simrad ES38-7 Transducer). Each WBT is licensed to operate within a portion of the total frequency range of 10–500 kHz, e.g. 10–30, 25–50, 45–90, 85–170, 150–300, or 250–500 kHz.

The current (2017) cost to transition each ship to EK80 is ca. US\$260–300k, including five or six WBT (~\$40k each), one ES38-7 transducer (~\$25k), data collection and processing computers (~\$10k), and a 50 TB data server (~\$25k). An unlicensed EK80 transceiver can be purchased for a spare (an additional \$40k) and later licensed for any frequency bandwidth, as required.

Due to the vast potential and significant complexity of wideband echosounders, a transition from EK60 to EK80 must be accompanied by a commitment to conduct further research and development on standard operating procedures for calibration, target-strength estimation, echo classification, marine resource surveys, and ecosystem investigations. This work will be efficiently conducted through additional collaborative workshops and research and development efforts (see Figure 1) and training courses for current and future practitioners, including both theory and practice.



Figure 1. Experimental design, and data collection and analysis activities in Southwest Fisheries Science Center conference rooms (top row) and the Ocean Technology Development Tank during the USA–Norway EK80 Workshop, September 2016. Performances of EK60 and EK80 (middle left) were evaluated and compared systematically using horizontally (middle right) and vertically (bottom) projecting transducer arrays.

1 Introduction

Underwater acoustic technologies have improved the accuracy, precision, efficiency, and timeliness of scientific information used for the conservation and management of living marine resources. For more than a decade, the Simrad–Kongsberg (Simrad) EK60 echosounder has been a worldwide standard for providing estimates of fish biomass and distributions, conducting ecosystem surveys, and observing the behaviours of aquatic organisms and their associations with oceanographic and seabed environments. However, EK60 has been recently superseded by the more advanced Simrad EK80 echosounder. Components of EK60 general purpose transceivers (GPTs) are no longer commercially available, and ER60 software has been replaced by EK80 software. For transitional purposes, EK80 software can be used with EK60 GPTs and EK80 wideband transceivers (WBTs), or combinations of the two.

To facilitate a rapid and successful transition to the operational use of EK80, it is necessary to ensure the continuation of accurate and precise measures for time-series used in stock assessments and marine ecosystem research. Therefore, scientists at the 2015 ICES Symposium on Marine Ecosystem Acoustics agreed to collaboratively conduct a series of laboratory and field experiments to characterize and compare the features and functions of EK60 and EK80.

Scientists from the USA and Norway have a long history of collaborating on fisheries acoustic science and technology development. At recent meetings of the USA–Norway Science Bilateral on Fisheries and the ICES Fisheries Acoustic Science and Technology Working Group, scientists discussed the terms of reference for conducting an EK80 workshop. The National Oceanic and Atmospheric Administration’s (NOAA’s) Southwest Fisheries Science Center (SWFSC) in San Diego, California, USA was chosen as the location for the workshop because of its state-of-the-art Ocean Technology Development Tank (aka the Technology Tank) and access to ship time on board NOAA’s FSV “Reuben Lasker” (Figure 1.1). The EK80 workshop was scheduled in two phases: laboratory tank experiments conducted during 6–9 and 12–16 September 2016 and field experiments conducted during 19–23 September 2016. Acoustic experts from the USA, Norway, France, and Australia, participated in the EK80 workshop experiments and contributed to this technical report (Figure 1.2).

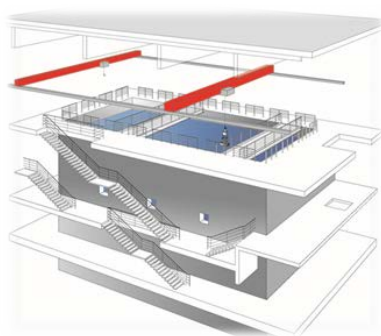


Figure 1.1. Experimentation with Simrad EK80 wide-bandwidth echosounder was conducted in the SWFSC’s 20 m by 10 m by 10 m seawater Ocean Technology Development Tank (left; Demer *et al.*, 2015), and on board NOAA’s FSV “Reuben Lasker” (right).



Figure 1.2. EK80 Workshop participants (left to right, front row) David Demer, Bill Michaels, Bryony Hutton, Reka Domokos, Jeff Condiotty, Dezhang Chu, Josiah Renfree, and Randy Cutter; (left to right, back row) David Murfin, Charles Thompson, Chris Bassett, Steve Sessions, Rolf Korneliussen, Gavin Macaulay, and Lars Andersen. Other participants not pictured include Laurent Berger, Naig Le Bouffant, and Armin Pobitzer.

This workshop report provides technical results and recommendations necessary to expedite the operational use of the Simrad EK80 wide-bandwidth scientific echosounders in standardized surveys and to improve scientific information for the conservation and management of living marine resources. This report represents the state of EK80 in September 2016. There will likely be future workshops and updated reports which document this evolving technology. As more is learned about EK80, its firmware and software will be revised by the manufacturer (Lars Andersen, pers. comm.), and analysis software will be updated accordingly. Recommended settings and algorithms for data collection and analysis will be collaboratively optimized for research and operational surveys.

1.1 Wide-bandwidth echosounders

Acoustic backscatter is used to detect, identify, enumerate, and map underwater targets. Conventional narrow-bandwidth (narrowband) echosounders, such as EK60, transmit pulses containing a single-frequency sinusoidal, continuous wave (CW) signal. In comparison, wide-bandwidth (wideband) echosounders transmit pulses containing a range of frequencies, often a linear low-to-high frequency modulated (FM) signal. The resulting wideband backscatter theoretically offers improved signal-to-noise ratio (SNR ; non-dimensional), range resolution (Δr ; m), and characterization of the wavelength-dependent echo, known as the frequency response. The latter may be used to improve target identification, thereby reducing uncertainty in estimates of target abundance.

1.1.1 Advantages

The Δr of a narrowband echosounder is half the length of the transmitted pulse $c_w \tau$ (m), where c_w (m s^{-1}) is the speed of sound in water and τ (s) is the pulse duration. To improve the Δr , data from wideband systems may be analysed using matched-filter (MF) processing, also known as pulse-compression processing (Turin, 1960; Chu and Stanton, 1998; Ehrenberg and Torkelson, 2000; Stanton and Chu, 2008a). By correlating the recorded echo with a replica of the transmitted signal, equivalent to multiplying the echo spectrum with the conjugate of the signal spectrum, Δr is not related to τ but rather is proportional to the inverse of the signal bandwidth

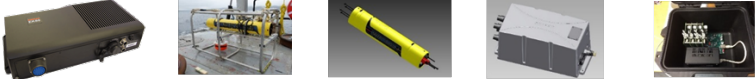
b_f (kHz), and the increase in SNR , relative to no MF processing, is theoretically equal to the time-bandwidth product τb_f (dimensionless) (Ehrenberg and Torkelson, 2000; Stanton and Chu, 2008a). The improved Δr allows for detection of targets near to each other, e.g. inside an aggregation or near a boundary such as the seabed, provided they have similar scattering strengths. In other words, MF processing of wideband data may allow targets to be detected closer to a boundary, such as the seabed (Ona and Mitson, 1996; Demer *et al.*, 2009), provided that the filter side lobes (see 2.7 Targets near one another or boundaries) do not mask the target (Lavery *et al.*, 2017).

1.1.2 Challenges

The many advantages of wideband vs. narrowband echosounders come with additional complexities associated with system calibrations, data storage, processing speed, signal processing and analyses, and interpretation. This is largely due to necessarily wider receiver bandwidths, higher sampling rates, and the frequency dependence of many environmental and system parameters, e.g. acoustic absorption, transducer efficiency and beamwidths, and scatterer reflectivity and directivity. For example, compared to narrowband data, wideband data may be inherently more susceptible to noise and more voluminous.

1.2 Simrad EK80

Simrad has recently released multiple-wideband, scientific echosounder products based on EK80 technology, presently including (i) the WBT, a self-contained echosounder for deep and/or long-term deployments; (ii) wideband autonomous transceiver (WBAT); (iii) wideband transceiver in a tube (WBT-Tube) designed for deep deployments with external power and Ethernet, e.g. on moorings or remotely operated vehicles; (iv) a small, low-power, multichannel wideband transceiver (WBT-Mini) for use in autonomous underwater and surface vehicles; and (v) a portable splash-proof WBT (WBT Portable) (Table 1.1). Hereafter in this document, these products will be referred to generically as EK80. Although EK80 investigations described below are focused on the WBT, the results may be applicable to some or all of the other EK80 products.



	WBT	WBAT	WBT-Tube	WBT-Mini	WBT Portable
Power	External	Internal Battery	External	External	External
Transmit Power	4 x 500W	4 x 200W	8 x 200W	4 x 200W	4 x 200W
Control	EK80	Mission Planner	EK80	EK80 / Mission Planner	EK80 wireless
Multiplexing	-	Built-in	Built-in	Built-in	Built-in
Channels	4	4 + MUX	8 + MUX	4 + MUX	4 + MUX
Interface	-	RS-422	-	RS-422	-
Pulse Duration	64 μ s to 8ms	64 μ s to 2ms	64 μ s to 2ms	64 μ s to 2ms	64 μ s to 2ms
Pulse types	CW, FM	CW, FM	CW, FM	CW, FM	CW, FM
Transducer Types	Single- and/or split-beam	Single- and/or split-beam	Single- and/or split-beam	Single- and/or split-beam	Single- and/or split-beam
Depth Rating	-	1000 m	4000 m	1 m	Splash proof
Frequency Range	10 to 500 kHz	30 to 500 kHz	30 to 500 kHz	30 to 500 kHz	30 to 500 kHz
Licensing	Yes	No	Yes	Yes / No	Yes

Table 1.1. Simrad EK80 product line and its respective features and specifications (table courtesy of Simrad).

1.2.1 Transmit pulse

EK80 is configured and controlled by a computer running EK80 software. EK80 may be configured to closely emulate EK60 by transmitting CW pulses simultaneously at multiple discrete frequencies, e.g. $f = 18, 38, 70, 120, 200,$ and 333 kHz. Even when similarly configured, however, there are some inherent differences between the two systems. For example, EK80 has wider bandwidth receiver filters and outputs complex waveform data from each transducer quadrant or section at higher decimated sampling rates than EK60.

EK80 can also be configured to transmit CW pulses at non-traditional frequencies, wideband FM pulses, or a combination of CW and FM pulses, sequentially or simultaneously from the same array of transducers, potentially spanning large portions of the frequency range from 10 to 500 kHz. FM signals offer the potential for greatly improved Δr , SNR , and characterizations of the frequency responses of target strength (TS ; dB *re* 1 m²) and volume backscattering strength (S_v ; dB *re* 1 m⁻¹), e.g. $TS(f)$ and $S_v(f)$.

1.2.2 Frequency bandwidth

Each WBT is licensed to operate within a portion of the total EK80 frequency range, $f = 10\text{--}500$ kHz, e.g.: $f = 10\text{--}30, 25\text{--}50, 45\text{--}90, 85\text{--}170, 150\text{--}300,$ or $250\text{--}500$ kHz. The bandwidth allowed by the license file may be further constrained to match the operational bandwidth of the transducer (e.g. see Table 1.2), the bandwidth associated with the duration of a CW pulse or the lower and upper frequencies selected for an FM pulse. EK80 may be used with the transducers used for EK60, although some newer models may be better suited for wideband performance. EK80 may also be used with transducers from other manufacturers, but perhaps not with optimal performance and not with Simrad support.

The quality factor q (unitless) for a transducer is measured as the centre frequency divided by the bandwidth. Simrad transducers with large quality factors, e.g. ES18-11C and ES38B, have bandwidths that are ca. 10% of their nominal frequencies (e.g. 2 and

4 kHz, respectively). Simrad transducers made with composite materials, e.g. ES70-7C, ES120-7C, ES200-7C, and ES333-7C, have low q and b_f that are ca. half of the nominal f , e.g. 35, 60, 100, and 166.5 kHz, respectively. These bandwidths correspond approximately to the range of frequencies where the transducer impedances have magnitudes $\geq 50 \Omega$ and phases (lags between voltage and current) $\geq -45^\circ$ and $\leq 45^\circ$. EK80 software limits the bandwidths for FM pulses transmitted by commonly used Simrad transducers, as indicated in Table 1.2.

Table 1.2. Nominal frequency, f_{nom} , and frequency range for commonly used Simrad transducers; and decimation factors and resulting sampling rates for stage 1 and stage 2 filters, EK80 V. 1.10.2.

Transducer model	Frequency range		Stage 1		Stage 2	
	f_{nom} (kHz)	Min-Max (kHz)	Decimation	Sampling rate (kHz)	Decimation	Sampling rate (kHz)
ES18*	18	18	6	23.4	7	36
ES38B*	38	38	6	187.5	10	25
ES38-7	38	34–45	64	187.5	1	23
ES70-7C	70	45–90	6	250	3	83
ES120-7C	120	90–170	12	125	1	125
ES200-7C	200	160–260	8	187.5	1	188
ES333-7C	333	280–450	6	250	1	250

* Presently, EK80 software does not allow use of FM signals with these transducers.

1.2.2.1 Pulse duration

The transmit-pulse duration (τ ; s) is the period from the start to the end of the digital signal applied to the transceiver. In EK80, τ may be set to values ranging from 64 to 8192 μ s, depending on the nominal transducer frequency. For CW pulses, the effective pulse duration (τ_{eff} ; s) is the total energy in the transmit pulse divided by its maximum power. For an FM pulse, τ_{eff} is the total energy in the autocorrelated transmit signal divided by the maximum power of the autocorrelated transmit signal (see Section 1.2.4.3, Volume backscattering strength).

1.2.2.2 Transmit power

For each nominal frequency, transmit power (p_{et} ; W) may be selected from ten options that are currently defined, based on the manufacturer's experience with EK60 and CW signals. The lowest default¹ p_{et} is 1/10th of the maximum pulsed-power specification for the transducer, provided that it is not below the minimum p_{et} for the EK80 transmitter. The largest default p_{et} has been chosen to not damage the transducer. If investigations suggest other power settings may be better suited for EK80, particularly in FM mode, Simrad is committed to adjusting the default parameters accordingly (L. Andersen, pers. comm.).

¹ With expert knowledge, so as not to damage the echosounder or transducer, the default options for EK80 settings may be changed in EK80 software by carefully editing the TrList.xml and TrList_product.xml files.

1.2.2.3 Transmit interval (ping rate)

The minimum transmit interval (T_p ; s) is limited to the maximum average continuous power = 5 W, i.e. $T_p = \tau p_{et}/5$.

1.2.2.4 Ramping

The rise and fall of each transmit pulse is “ramped” using different length Hann windows (Oppenheim *et al.*, 1999). EK80 software has default options for “slow” or “fast” ramping in both CW and FM modes (Figure 1.3), but MF processing is only implemented in FM mode.

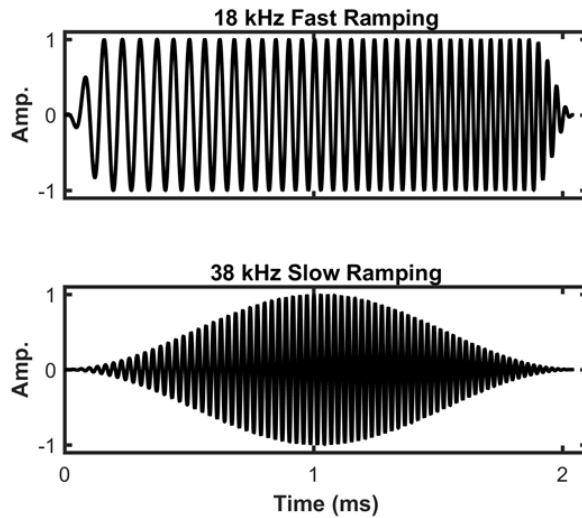


Figure 1.3. Fast (top) and slow (bottom) ramping of EK80 pulses.

A slow ramp requires half of the pulse duration to rise to the maximum value and the other half to fall, affecting the entire pulse. Compared to slow-CW pulses, fast-CW pulses have larger τ_{eff} , SNR , and Δr .

A fast ramp slightly tapers the beginning and ending of the pulse. In this case, the percentage of the half pulse that is ramped, R_f , is described by

$$R_f = \frac{2}{\tau f_{start}}, \quad (1)$$

where R_f depends on both τ and the starting frequency of the FM pulse (f_{start} ; Hz). For CW pulses, f_{start} is replaced with the centre frequency, f_c . For $\tau = 2048 \mu\text{s}$ and $f_{start} = (15, 45, 95 \text{ kHz})$ or $f_c = (18, 70, 120 \text{ kHz})$, fast ramp tapers the signal pulses by $2R_f \sim 13, 4, \text{ and } 2\%$, respectively. (Note: because two periods may be too fast for some transducers, future EK80 software may adjust the number of periods used in fast ramping, depending on the b_f .) Compared to slow-FM pulses, fast-FM pulses with MF processing have larger τ_{eff} , b_f , SNR , and sidelobe duration, but smaller Δr (see sections 1.3.2.4, Ramping and 2.7, Targets near one another or boundaries).

Depending on the application, choices of signal type (CW or FM), ramping (slow or fast), and pulse duration ($\tau = 64\text{--}8192 \mu\text{s}$) involves consideration of b_f , Δr , SNR , and MF artefacts. For example, to sample densely aggregated pelagic organisms, long fast-ramp-FM (fast-FM) pulses may be used to obtain small Δr and large b_f and SNR . However, to resolve targets near one another or a boundary, e.g. fish near the seabed, short

fast-ramp-CW (short-CW) or slow-ramp-FM (short-FM) pulses should be used to reduce MF-processing artefacts and thereby obtain small Δr , but with lower b_f , SNR , or both (see Section 2.7, Targets near one another and/or boundaries). The manufacturer could allow more ramping options to further optimize parameters for various measurement objectives.

1.2.3 Stage 1 and stage 2 filters and decimators

Received voltage $u_r(t)$ from each transducer sector is sampled at 1.5 MHz. These data are filtered and decimated in two stages to obtain the complex samples, which retain the bandwidth of the transmit signal. The data are then stored as 32-bit floating point numbers in EK80 .raw files.

The stage 1 filter has a wide bandwidth designed to avoid aliasing. Stage 2 filters have bandwidths closer to that of the transmit signal and are designed to suppress noise. The sampling rate following decimations is $> 1.25b_f$, exceeding the Nyquist sampling theorem requirement by 25%. SNR decreases by the square root of the decimation factor. To account for the decimations, the frequency spectrum, calculated using Fourier analysis, is band-shifted to the predecimated frequencies.

1.2.3.1 Stage 1 filtering and decimation

For MF processing of the filtered and decimated signal, the replica transmit signal $u_t(t)$ must be equally filtered and decimated. The stage 1 filtered transmit signal $u_{t1}(y)$ is derived by convolving (*) $u_t(t)$ with a vector of stage 1 filter coefficients b_1 stored in a field programmable gate array (FPGA),

$$u_{t1}(t) = u_t(t) * b_1 . \quad (2)$$

Then, $u_{t1}(t)$ is decimated by a factor specific to the transmit pulse parameters. The minimum decimation factor is 6.

1.2.3.2 Stage 2 filtering and decimation

Stage 2 filtering is accomplished by the same operations as the stage 1 filter, except that $u_t(t)$ is replaced by $u_{t1}(t)$ and b_1 is replaced by a vector of stage 2 filter coefficients b_2 generated by software,

$$u_{t2}(t) = u_{t1}(t) * b_2 . \quad (3)$$

Then, $u_{t2}(t)$ is decimated by a factor specific to the transmit pulse parameters. The twice-filtered, twice-decimated, replica transmit pulse $u_{t2}(t)$ is used for MF processing. The values for $u_t(t)$, b_1 , and b_2 and the decimation values are recorded in the .raw file. (Note, the filter generator will likely change with future EK80 revisions.) For illustration, both b_1 and b_2 for fast ramp could describe a sinc function, a rectangular window in the time-domain and an impulse response in the frequency-domain (Figure. 1.4).

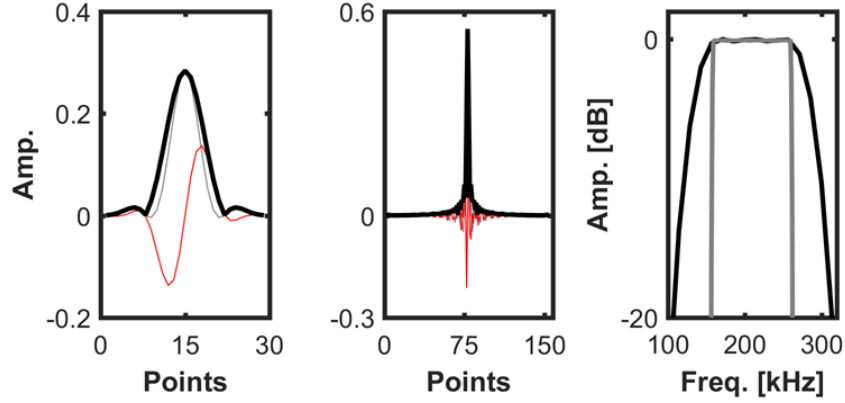


Figure 1.4. Stage 1 (left; black – envelope; grey – real; red – imaginary) and stage 2 (middle; black – envelope; grey – real; red – imaginary) filter coefficients and normalized frequency spectra (right; black – stage 1; grey – stage 2) for a 1024 μ s 160–260 kHz transmit pulse.

1.2.4 FM-data processing

EK80 data may be analysed and presented in the temporal domain as $S_p(t)$ (dB) or volume backscattering strength ($S_v(t)$; dB *re* 1 m^{-1}) or in the frequency domain as target strength ($TS(f)$; dB *re* 1 m^2) or $S_v(f)$. EK80 algorithms to calculate these values are detailed below.

1.2.4.1 Matched filter processing

Values for $S_p(t)$, $S_v(t)$, $TS(f)$, and $S_v(f)$ are derived by matched-filter (MF) processing of the filtered and decimated received-signal voltage for the i^{th} sector (beam). The transmit-signal voltages $u_t(t)$ and the received signal voltages $u_{r,i}(t)$ have been equivalently filtered and decimated as described in Section 1.2.3, Stage 1 and stage 2 filters and decimators. The MF output for the i^{th} beam, indicated by bold type, is

$$\mathbf{u}_{r,i}(t) = \frac{u_{r2,i}(t) * u_{t2}(-t)^*}{\|u_{t2}(t)\|^2}, \quad (4)$$

where $\mathbf{u}_{r,i}(t)$ is the MF-received signal for the i^{th} sector, $u_{t2}(t)$ is the filtered and decimated replica-transmit signal, and $u_{t2}(-t)^*$ is the time-reversed complex conjugate of the filtered and decimated replica signal. Note, time-reversed convolution is equivalent to cross-correlation. The average signal for all I beams ($I = 4$ for a split-beam) is

$$\mathbf{u}_r(t) = \frac{1}{I} \sum_{i=1}^I \mathbf{u}_{r,i}(t). \quad (5)$$

1.2.4.2 Point backscattering strength

The time-series of received power $p_{er}(t)$ is calculated from $\mathbf{u}_r(t)$, the receiver impedance ($z_{er} = 5.4 \text{ k}\Omega$) and the nominal transducer impedance ($z_{et} = 75 \Omega$),

$$p_{er}(t) = \left(\frac{|\mathbf{u}_r(t)|}{\sqrt{2}} \right)^2 \left(\frac{z_{er} + z_{et}}{z_{er}} \right)^2 \frac{1}{z_{et}}. \quad (6)$$

Point scattering strength, S_p , is calculated by Simrad as

$$S_p(t) = 10 \log_{10} p_{er}(t) + 40 \log_{10} r + 2\alpha r - 10 \log_{10} \left(\frac{p_{et} c_w^2}{(4\pi f_c)^2} \right) - 2G, \quad (7)$$

where p_{et} is the transmit power, r is the range, and α and G are the attenuation coefficient and system gain at the centre frequency f_c . Values for $S_p(t)$, computed at f_c , comprise a weighted average over the transmitted b_f , which does not account for the frequency-dependence of the attenuation coefficient and the system gain.

1.2.4.3 Volume backscattering strength

EK60 uses S_A correction $S_{A\text{corr}}$ (dB) to account for any difference between the ideal and real τ_{eff} . $S_{A\text{corr}}$ equals the theoretical nautical area scattering coefficient s_A (m² nautical mile⁻²) for the calibration sphere minus s_A measured for the sphere, in decibels.

EK80 uses different algorithms to correct for τ_{eff} . For CW, τ_{eff} is estimated by the ratio of the integrated received and transmitted pulses. For FM, the effective pulse duration is

$$\tau_{eff} = \frac{\sum |\mathbf{u}_t(t)|^2}{\max(|\mathbf{u}_t(t)|^2) f_s}, \quad (8)$$

where f_s is the post-decimation sampling rate. No account is made for any effects of hardware and software filters. At f_c , the transducer equivalent beam angle is

$$\psi = \psi_{nom} + 20 \log_{10} \left(\frac{f_{nom}}{f_c} \right), \quad (9)$$

where ψ_{nom} is the measured or specified equivalent beam angle at the nominal frequency f_{nom} . Simrad computes values for $S_v(t)$, computed at f_c , using

$$S_v(t) = 10 \log_{10} p_{er}(t) + 20 \log_{10} r + 2\alpha r - 10 \log_{10} \left(\frac{p_{et} c_w^3}{2(4f_c \pi)^2} \right) - 2G - 10 \log_{10} \tau_{eff} - \psi. \quad (10)$$

Note, this definition of $S_v(t)$ comprises a weighted average over the transmitted b_f , which does not account for the frequency dependence of the attenuation coefficient or the system gain.

1.2.4.4 Frequency-dependent target strength

The first step for calculating frequency-dependent target strength $TS(f)$ (dB *re* 1 m²) is to define the period ($t_1:t_2$) corresponding to samples from the target. The number of samples $f_s(t_2 - t_1)$ should be less than or equal to the number of samples in the autocorrelation of the transmit signal $\sim 2\tau$. For consistency, the vectors for $\mathbf{u}_r(t)$ and $\mathbf{u}_t(t)$ should have the same number of points N used in the fast Fourier transform (FFT) unless the signals are zero-padded to improve the frequency resolution. The reduced length transmit-signal autocorrelation is $\mathbf{u}_{t,red}(t)$.

The FFT outputs $\mathbf{U}_r(f)$ and $\mathbf{U}_{t,red}(f)$ span from 0 to f_s , with a frequency resolution f_s/N . To account for the changing amplitude of the ramped transmit pulse as a function of time, the target spectrum is normalized by the autocorrelated transmit signal spectrum,

$$\mathbf{U}_{target}(f) = \frac{\mathbf{U}_r(f)}{\mathbf{U}_{t,red}(f)}. \quad (11)$$

To account for the decimation, $\mathbf{U}_{target}(f)$ is band-shifted to estimate the actual frequency spectrum. Then, the received power from the target is

$$P_{er}(f) = \left(\frac{|\mathbf{U}_{target}(f)|}{\sqrt{2}} \right)^2 \left(\frac{z_{er} + z_{et}}{z_{er}} \right) \frac{1}{z_{et}}. \quad (12)$$

The target strength spectrum is

$$TS(f) = 10 \log_{10} P_{er}(f) + 40 \log_{10} r + 2\alpha(f)r - 10 \log_{10} \left(\frac{p_{et} c_w^2}{(4\pi f)^2} \right) - 2G(f), \quad (13)$$

where r is the range to the peak in the MF time-series and $\alpha(f)$ and $G(f)$ are the frequency-dependent attenuation coefficient and calibrated gain values.

1.2.4.5 Frequency-dependent volume backscattering strength

To calculate $S_v(f)$, the MF signal is first compensated for spherical spreading attenuation, which is equivalent to compensating the power by r^2 . Then, for the range of interest ($r_1 : r_2$) a normalized Hann ramp (raised cosine) is used to suppress discontinuities at the edges of u_r for the number of samples $N = f_s(t_2 - t_1)$,

$$b_{nHann} = \frac{b_{Hann}}{\left(\frac{\|b_{Hann}\|}{\sqrt{N}}\right)}, \quad (14)$$

where b_{Hann} is a normalized ramping function whose square integral (summation for discrete time-series) is unity. The ramped MF signal for the range of interest is obtained by scalar multiplication,

$$\mathbf{u}_{rb}(n) = \mathbf{u}_r(n) b_{nHann}(n), \quad (15)$$

which is transformed into the frequency domain $U_{rb}(f)$ and divided by the frequency response of the transmit signal $U_t(f)$ to calculate the frequency spectrum of the MF output,

$$\mathbf{U}_r(f) = \frac{U_{rb}(f)}{U_t(f)}. \quad (16)$$

Then, the received power from the volume is

$$P_{er}(f) = \left(\frac{|U_r(f)|}{\sqrt{2}}\right)^2 \left(\frac{z_{er} + z_{et}}{z_{er}}\right) \frac{1}{z_{et}}. \quad (17)$$

The volume backscattering strength spectrum is

$$S_v(f) = 10\log_{10} P_{er}(f) + 2\alpha r - 10\log_{10} \left(\frac{p_{et} c_w^3}{2(4\pi f)^2}\right) - 2G(f) - 10\log_{10}(t_2 - t_1) - \psi(f). \quad (18)$$

Values for $\psi(f)$ are estimated, as in Section 1.2.4.3, Volume backscattering strength, with f_c replaced by f .

1.2.4.6 Caveats and considerations

The wideband scattering calculations discussed above can be implemented in many different ways and are subject to a number of caveats and limiting factors that are described below.

1.2.4.6.1 Transducer and receiver impedances

Conversion of the .raw data to P_{er} , S_p , TS , and S_v involves values for the receiver and transducer impedances z_{er} and z_{et} , respectively. A prototype EK80 receiver had $z_{er} \approx 1000 \Omega$, but the commercial EK80 receiver has $z_{er} \approx 5400 \Omega$. The transducer impedance has remained $z_{et} \approx 75 \Omega$. The system calibration accounts for any differences between these nominal values and the actual impedance, but the values used during calibration must also be used in the data analysis.

Through at least version 1.8.3, EK80 software has used $z_{er} = 1000 \Omega$. Therefore, when using gain values calculated using EK80 software, the value of $z_{er} = 1000 \Omega$ must be used to achieve the correct results. If the calibration software used $z_{er} = 1000 \Omega$ and the post-processing software used $z_{er} = 5400 \Omega$, the resulting S_v would be biased by

0.51 dB. To avoid this issue, future versions of EK80 software will record the z_{er} value used to generate the calibration results in .raw files, and this value may change from $z_{er} = 1000 \Omega$ to $z_{er} = 5400 \Omega$ (L. Andersen, pers. comm.).

1.2.4.6.2 Transmit signals, filtering, and processing considerations

Depending on the application, EK80 can be configured to operate with different transmit signals, pulse durations, ramps, and filter configurations, each affecting SNR , Δr , and b_f .

1.2.4.6.3 Single-target spectrum

With MF processing, the frequency resolution is a function of τ and the FFT length. It is maximized at $1/\tau$ when the FFT length equals τ . A longer FFT length, without zero-padding, will contaminate the target spectrum with the neighbouring noise spectrum. MF processing of a signal with noise can improve Δr by the factor $1/b_f$ and increase the SNR by the factor $b_f \tau_{eff}$.

1.3 Calibration

Echosounder calibration is a critical requirement before conducting standardized survey operations to obtain quantitative measures for detecting targets and estimating biomass of organisms.

1.3.1 Standard sphere uncertainty

Calibrations using one or more standard spheres are typically done using nominal values for the sphere parameters, including density and sound speeds, resulting in uncertainty about the $TS(f)$ results. For example, calibrations are typically performed using a 38.1 mm diameter sphere made from tungsten carbide with 6% cobalt binder material, WC38.1 (Demer *et al.*, 2015). The nominal values are: longitudinal sound speed = 6864 m s⁻¹, transversal sound speed = 4161 m s⁻¹, and density = 14.9 g cm⁻³ (MacLennan and Dunn, 1984). If these values are inaccurate, the sphere $TS(f)$ will not exactly match theory, most conspicuously at the locations of nulls and where the TS from multiple spheres overlap.

To reduce uncertainty in standard sphere calibrations, EK80 measurements of $TS(f)$ are made from a sphere located sequentially on the axis of each transducer in an array. The combined $TS(f)$ are used to estimate the longitudinal and transversal sound speeds of the sphere such that the measured null locations match, in a least-squares sense, those in the theoretical $TS(f)$ (MacLennan and Dunn, 1984). (Note, longitudinal and transversal sound speeds are currently not estimated in EK80.) Coupled with measurements of the sphere diameter, weight, and derived mass density, these sound speed estimates may be used to reduce the uncertainty in standard sphere calibrations.

To mitigate backscatter from the sphere suspension, especially from knots in the monofilament lines, the downrigger lines and swivels may be separated from the sphere by lines that are doubled-back through the loop affixed in the sphere. This configuration positions all knots so they are resolvable from the sphere echo [see Demer *et al.* (2015) for more details].

To reduce calibration uncertainty at frequencies near nulls in the sphere $TS(f)$, calibrations may be performed sequentially using spheres of different sizes and perhaps material properties (Dragonette *et al.*, 1981; Foote, 2006; Stanton and Chu, 2008b; Lavery *et al.*, 2017). In this case, each calibration is made for frequencies away from the nulls,

and the resulting data are combined to obtain calibrated gain values for most or all of the operational frequency range.

1.3.2 Frequency-dependent source level

The frequency-dependent source level $SL(f)$ (dB *re* $p_{\text{ref}}^2/\rho_w c_w$ W m^{-2} at 1 m) is equal to the source intensity i_s (W m^{-2}) referred to the intensity of a plane wave with reference pressure, $p_{\text{ref}} = 1 \mu\text{Pa}$, in water with mass density ρ_w (kg m^{-3}) and sound speed c_w (m s^{-1}). Assuming negligible absorption loss to 1 m, $\rho_w = 1035 \text{ kg m}^{-3}$, and $c_w = 1500 \text{ m s}^{-1}$,

$$SL(f) = 10\log_{10}(p_{et}g_0(f)) - 10\log_{10}(4\pi) + 181.91. \quad (19)$$

Solving this equation with typical values for p_{et} and gain at the nominal frequency $g(f_{nom})$, SL values are in the order of 226, 229, 226, 221, 216, and 212 dB *re* $1 \mu\text{Pa}$ at 1 m for EK80 configured with ES18-11C, ES38B, ES70-7C, ES120-7C, ES200-7C, and ES333-7C transducers, respectively.

1.3.3 Frequency-dependent beamwidth

Transducer beamwidth $b(f)$ ($^\circ$) is a function of the aperture diameter, d (m) and the acoustic wavelength, λ (m). It may be derived from the transducer beamwidth at f_{nom} (Bodholt, 2002):

$$b(f) = \frac{\lambda}{d} \frac{180^\circ}{\pi} = b(f_{nom}) \frac{f_{nom}}{f}. \quad (20)$$

If the standard sphere is not located on the beam axis, the measured sphere echo is a function of both the sphere and the frequency-dependent beam-directivity pattern. If the latter is known or assumed, the position of the sphere in the beam may be estimated (Lavery *et al.*, 2017). However, the split-beam measurements of off-axis angle include uncertainty due to the assumed angle sensitivity values (Demer *et al.*, 1999).

2 Investigations

To emulate EK60 for echo-integration surveys, EK80 may be operated with fast-CW pulses. Additionally, EK80 may be operated in wideband (FM) mode to provide additional information for species identification, target-size estimation, and detecting targets near one another or the seabed. Attempting to exploit the potential of EK80, some challenges are anticipated or have been experienced, e.g. larger data volumes, reduced speed of processing, changing data formats, and cross-channel interference. This section describes the motivations, methods, and results of investigations to better understand EK80 system and its performance.

2.1 Data volume and processing speed

EK80 may collect one to two orders of magnitude more data than EK60, depending on the bandwidth and other configurations. This is because EK60 outputs envelope-detected power and split-beam phase data and EK80 outputs complex waveform data for each channel, with at least twice as many samples per pulse duration. This additional EK80 data allows better detection of single targets in either CW or FM mode and analysis of backscattering spectra in FM mode. If processed and stored in the conventional manner used for EK60 data, EK80 data has greater requirements for data storage, computing power, and processing time.

Approaches to minimizing data volume and maximizing processing speed will depend on the study objectives, e.g. echo integration, echo counting, near-boundary target detection, target identification, or target size estimation. Operating in CW mode will generate less data volume than FM mode, but the latter may be useful to discriminate echoes from major taxa. Generally, all collected information should be preserved because research cruises are expensive, and the information will allow for future alternative investigations. Strategies for reducing data volume and increasing processing efficiency may be considered in terms of (i) lossless reduction during collection; (ii) lossy reduction during collection; and (iii) increased processing speed.

2.1.1 Lossless reduction during collection

To reduce data volume, the manufacturer should enable channel-dependent logging ranges (e.g. Table 2.1) and faster and programmable alternation between CW to FM and active to passive modes. The manufacturer could implement coded signals, better optimize filter bandwidth and decimation, and even implement conventional data compression algorithms (in one test, zip reduced .raw file sizes by 30%).

Table 2.1. Compared to logging all frequencies to a 500 or 1000 m range, channel-dependent logging ranges with the following settings would reduce EK80 data rates by ca. 63 and 38%, respectively (L. Andersen, pers. comm.).

Frequency (kHz)	18	38	70	120	200	333
Mode	CW	CW	FM	FM	FM	FM
Variable range (m)	2000	1500	750	500	300	150

2.1.2 Lossy reduction during collection

To store and process data for specific objectives, it may be acceptable or necessary to lose some information. In such cases, the manufacturer could (i) implement more aggressive filtering and decimation schemes, (ii) reduce the precision of complex sample representation (e.g. from 32-bit floating point to 16-bit), (iii) allow optional output of power and angle with four samples per pulse, emulating EK60 data, (iv) implement programmable data collection, e.g. mostly CW with periodic FM, and alternating active and passive, or both, (v) modulate the transmit interval to avoid multiple bottom echoes, (vi) collect passive data routinely prior to each transmit signal to continuously estimate SNR , and (vii) facilitate multiple narrowband signals within allowable bandwidth.

The minimum decimation in the stage 1 filter is 6, i.e. $1.5 \text{ MHz}/6 = 250 \text{ kHz}$ sampling. The data volume could be reduced with more aggressive decimation. The filters could be optimized for reduced data volume or the need to detect targets near one another or boundaries. Any changes to filtering which increase the data collection time will increase the transmit interval and may, therefore, reduce the performance of autonomous EK80 systems.

2.1.3 Increased processing speed

In some cases, it may be more important to reduce data processing time vs. data volume. The advantages of increased processing speed will depend on how the data are scrutinized and analysed. To rapidly visualize and utilize wideband data, EK80 data may be accessed by data subscription and written directly into an application-specific format. These data may be preprocessed and stored in a format [e.g. an application program interface (API) such as netCDF] that is optimized for processing speed.

Preprocessing could generate multiple narrowband datasets that could be analysed as EK60 data. The nominal frequencies and bandwidths of these derived datasets could be judiciously chosen to maximize SNR and the detections of single targets while minimizing the data volume and processing time. Notwithstanding the potential of this approach, it is important to recognize that FM data is not a superset of CW data. Data could be preprocessed to generate MF data with or without decimation. Preprocessed datasets could be limited by time, location, intensity, range, SNR , bandwidths, and data types or objects of interest (e.g. single targets). Preprocessed data could be analysed using multiple CPU cores, GPU processing, cluster or cloud computing, and software that anticipates requests.

2.2 Transmit power

If the transmit power p_{et} is linearly related to EK80 transmit power setting, the calibration obtained for a given p_{et} may be accurately converted to another transmit power. Deviations from a linear relationship may introduce measurement uncertainty. To evaluate this potential uncertainty, measurements of p_{et} were made for each nominal frequency for CW (18 and 38 kHz) and FM (70, 120, 200, and 333 kHz) pulses transmitted into a dummy load vs. various p_{et} settings (Table 2.2). The frequency-dependent complex impedance $z_e(f)$ was measured for the dummy load using a vector impedance analyser (Figure 2.1).

Table 2.2. Measurements were made for indicated combinations (X) of nominal transmit power and frequency.

Nominal power (W)	Nominal frequency (kHz)					
	18	38	70	120	200	333
5				X	X	X
10	X			X	X	X
15				X	X	X
20				X	X	X
25	X	X	X	X	X	
50			X	X		
60	X					
75		X	X			
100	X		X	X	X	
125		X				
140	X					
200	X	X	X	X	X	
250		X				
400			X	X	X	
600	X	X				
700			X	X	X	
1000	X	x	X	X	X	
1400	X	X				
1800	X					
2000	X	X				

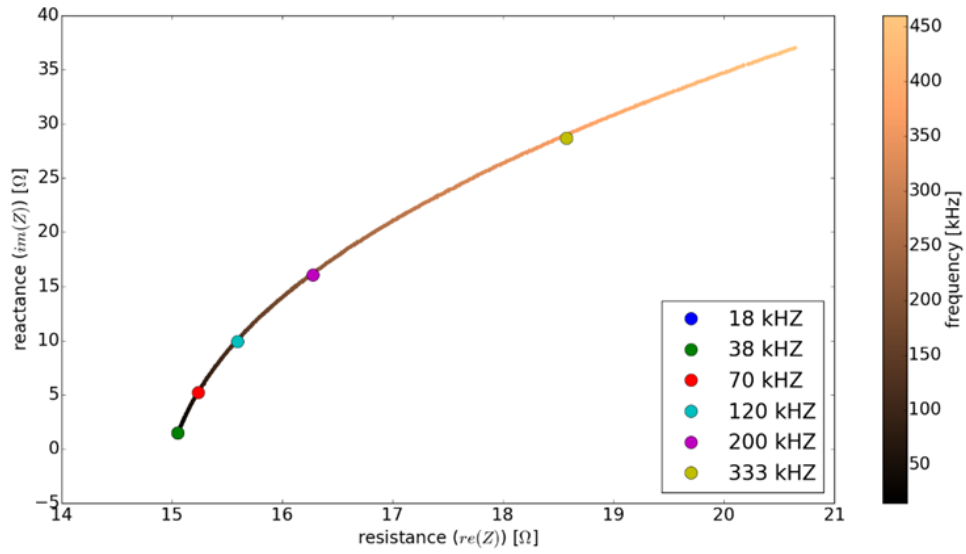


Figure 2.1. Dummy-load reactance vs. resistance and frequency.

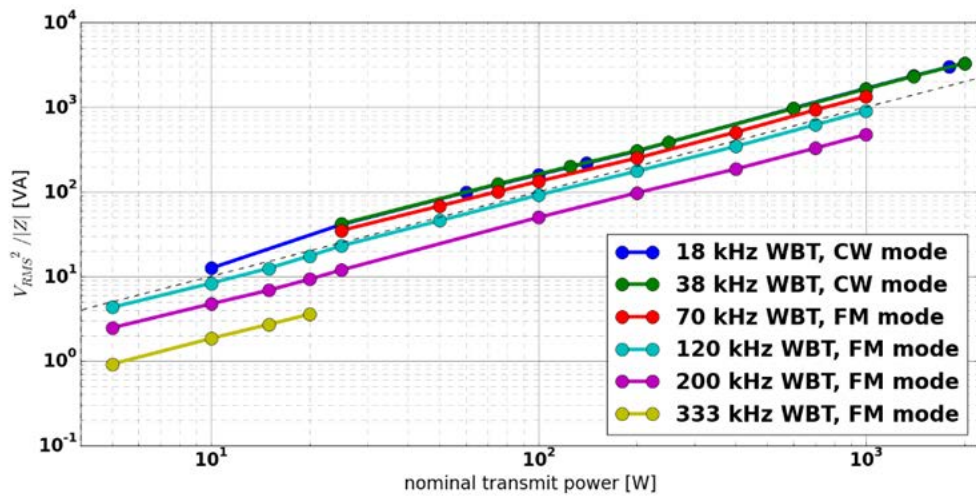


Figure 2.2. Nominal vs. measured transmit power calculated using the magnitude of the impedance. A one-to-one reference relation is shown (dashed line).

For each pulse, the root-mean-square (rms) voltage u_{et} was measured using an oscilloscope and used to compute the active power $p_{et,active} = u_{et}^2 / re(z_e)$ and apparent transmit power $p_{et,apparent} = u_{et}^2 / |z_e|$. These measured powers were compared to nominal transmit power settings in EK80 software (Figure 2.2).

The relationship between nominal and measured powers is approximately linear for each nominal frequency, but the intercept varies with frequency (Table 2.3).

Table 2.3. Intercepts of lines fit to the nominal vs. actual ($p_{et,active}$, $p_{et,apparent}$) transmit power vs. nominal frequency f_{nom} . The Pearson correlation coefficient $corr$ is the same for the actual transmit powers and the squared rms voltage u_{et}^2 because these quantities differ only by a frequency-dependent scaling factor.

f_{nom} (kHz)	$p_{et,active}$	$p_{et,apparent}$	u_{et}^2	($corr$)
18	1.67	1.66	25.13	0.99994
38	1.66	1.65	24.95	0.99992
70	1.40	1.32	21.29	0.99977
120	1.06	0.89	16.48	0.99985
200	0.66	0.47	10.80	0.99992
333	0.33	0.18	6.14	0.99983

Deviations from a linear relationship between u_{et}^2 and the nominal p_{et} setting in EK80 (Figure 2.3) will cause uncertainty in measurement if the calibration was made with a different p_{et} setting (Figure 2.4). Generally, the data are within $\pm 5\%$ of the linear relationship, irrespective of the intercept. A noticeable exception is $p_{et} = 10$ W (a low, non-standard setting) at 18 kHz, where u_{et}^2 lies $\sim 25\%$ below the line (Figure 2.4).

The following equation assesses bias in measurements of S_v due to deviations of the measured rms voltage u_{et} from that estimated from the linear relationship at the nominal p_{et} setting (Figure 2.4),

$$S_v - \hat{S}_v = 20 \log_{10} \frac{u_{et}}{u_{et,linear}}. \quad (21)$$

For the tested EK80, the results of these calculations (Figure 2.5 and Table 2.4) indicate that the bias is generally less than 0.5 dB. To avoid this potential bias, calibrations should be conducted at the transmit power used for data acquisitions.

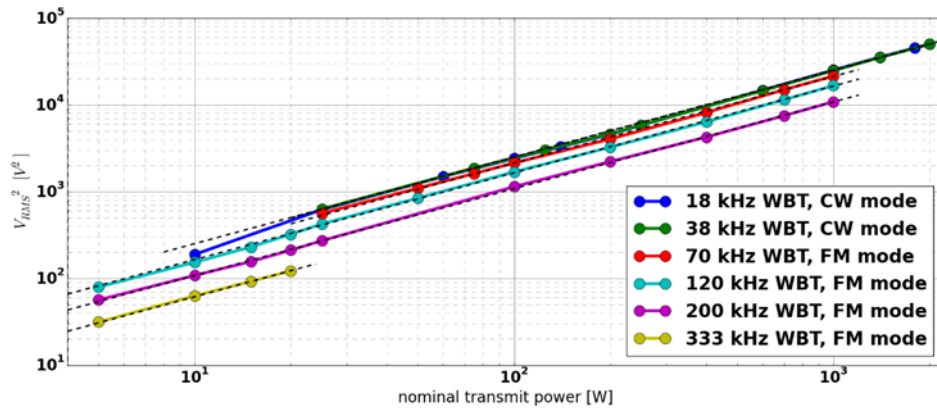


Figure 2.3. Nominal transmit power vs. the root-mean-square (rms) transmit voltage squared.

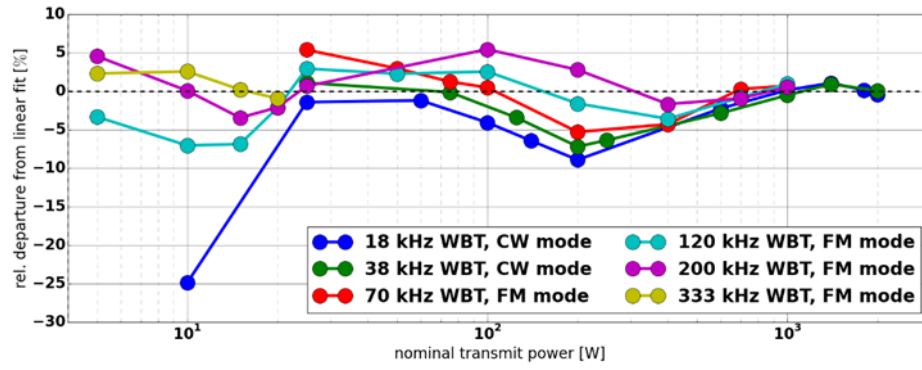


Figure 2.4. Deviation from the linear fit of transmit power vs. nominal transmit power.

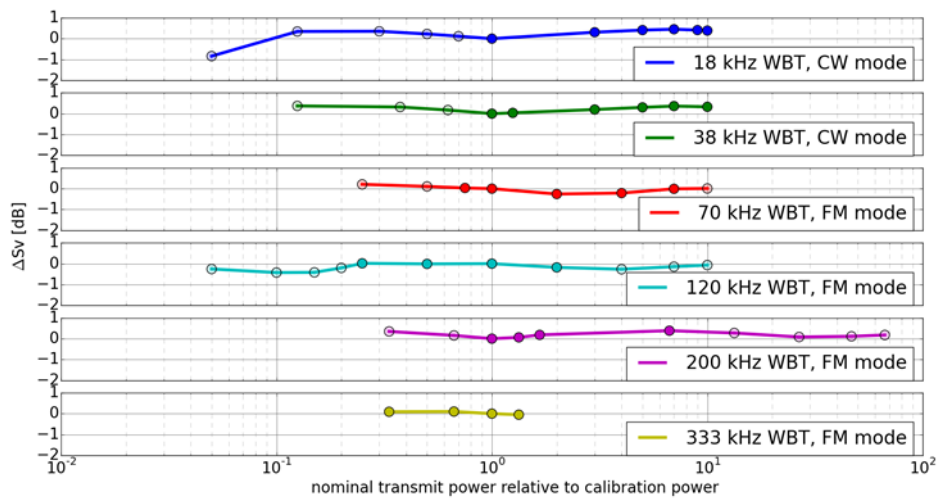


Figure 2.5. Bias in S_v due to non-linearity in the transmit-power setting for different nominal frequencies. Indicated are the default nominal transmit powers (solid circles) and non-default settings (open circles).

Table 2.4. Bias in S_v (dB) because of non-linearity in the transmit-power setting vs. nominal frequency.

f_{nom} (kHz)	Default p_{et}	All p_{et}
18	0.45	0.84
38	0.36	0.37
70	0.26	0.26
120	0.18	0.43
200	0.38	0.38
333	0.10	0.10

2.2.1 Voltage droop

The shapes of transmit pulses into a dummy load (see Section 2.2, Transmit power) were analysed. The envelope of each voltage waveform was computed using the Hilbert transform and high-frequency oscillations were smoothed using a 71-point, order-1 polynomial Savitzky–Golay filter (Orfanidis, 1996) (Figure 2.6).

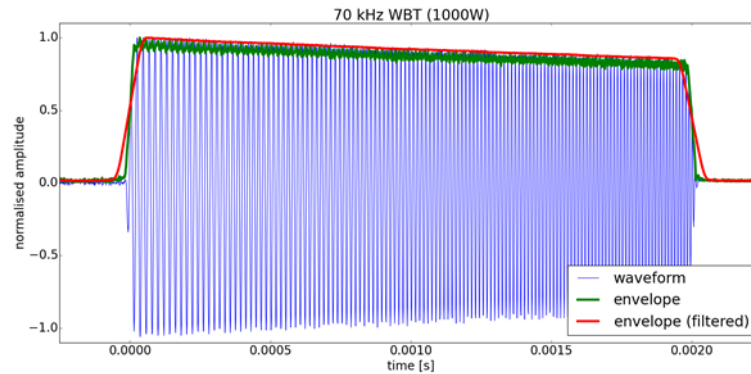


Figure 2.6. The normalized voltage of a 2.048 ms 1000 W 70 kHz pulse transmitted into a dummy load (blue); the envelope of the signal (green); and the smoothed envelope of the signal (red).

Filtered envelopes were evaluated for pulses into a dummy load vs. transmit power and frequency (Figure 2.7). The voltage droop across the pulse increases with power and frequency, from a few percent for 10 W at 18 kHz to almost 25% for all transmit powers at 333 kHz.

To evaluate if the shapes of transmit pulses into a dummy load are indicative of those into real transducers, the shape of a fast-FM 2.048 ms, 100 W pulse into an ES200-7C transducer was recorded (Figure 2.8). The pulse shape is peaked at each end, droops in the middle, and is different than both the pulse into the dummy load and the ideal rectangular-envelope pulse. However, both the pulses into the dummy load and the 200 kHz transducer suggest that the EK80 transmitter may not have sufficiently low output impedance to consistently produce a rectangular-envelope pulse for all transmit-signal parameters. (Note, these measurements were not made for EK60 transmitters, so it is presently unknown if this concern is unique to EK80.) Additional study is warranted.

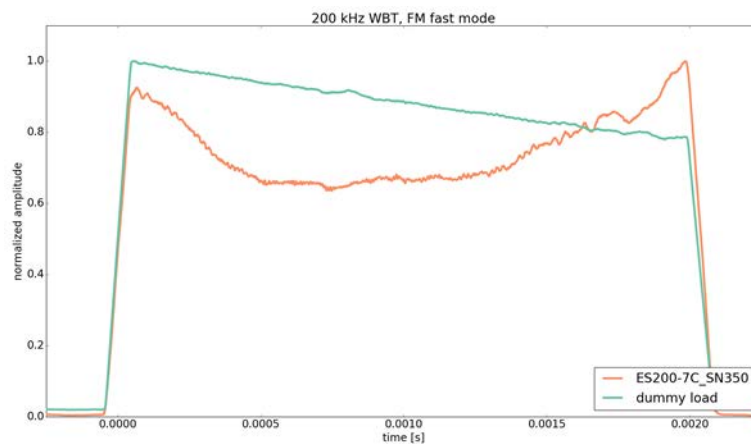


Figure 2.7. Filtered envelopes of pulses into a dummy load and an ES200-7C transducer.

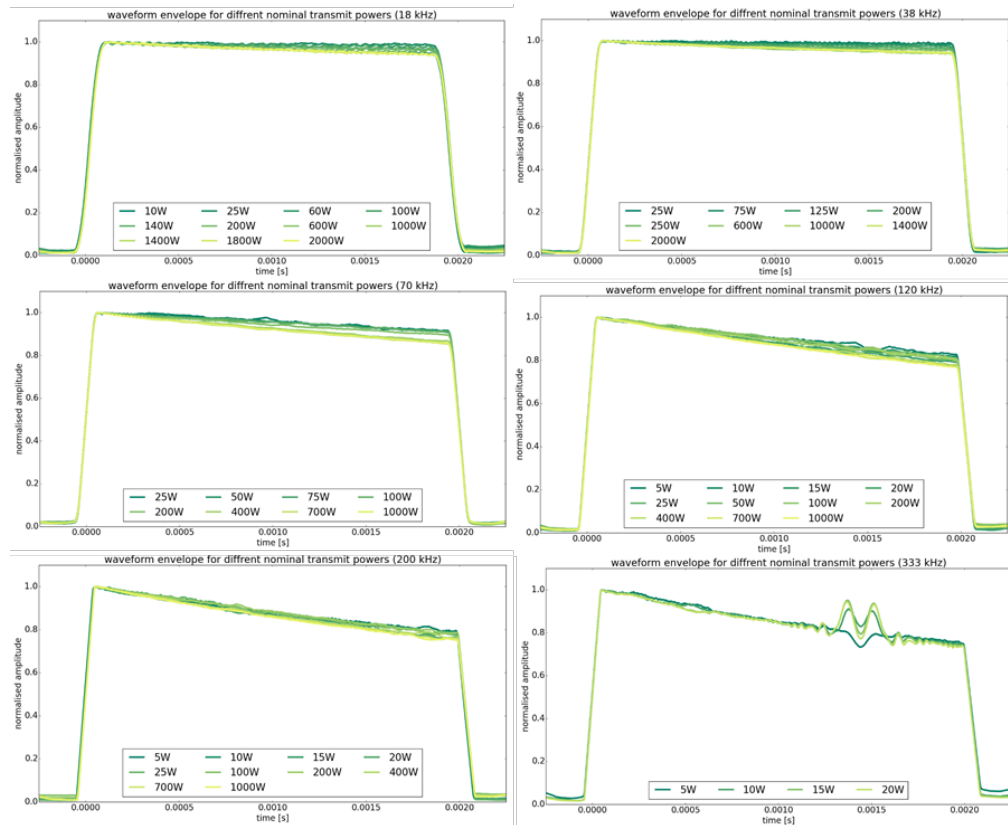


Figure 2.8. Filtered envelopes of pulses into a dummy load vs. transmit power and nominal centre frequency.

2.2.2 Non-linear effects

Sound is a pressure wave, and sound speed is dependent on pressure. Therefore, in a lossless medium, the peaks of a pressure wave propagate faster than the troughs, the wave distorts, and energy is transferred from the fundamental frequencies to higher harmonics, which are integer multiples of the fundamental frequencies. These non-linear effects increase with sound pressure and frequency and are largest near the transducer-beam axis, where sound pressure is largest.

In a lossy medium, sound energy is attenuated by absorption, which is the conversion of sound energy to heat, and geometric spreading. Sound absorption increases with frequency, so the higher harmonics are attenuated more rapidly than the fundamental frequencies. Non-linear effects decrease with increased range.

Non-linear propagation may cause measurement uncertainty because lower-frequency bands may have less energy than expected from linear theory, higher-frequency bands may have more energy than expected, and the shape of the main lobe of the transducer directivity pattern may be flatter than expected (Figure 2.9).

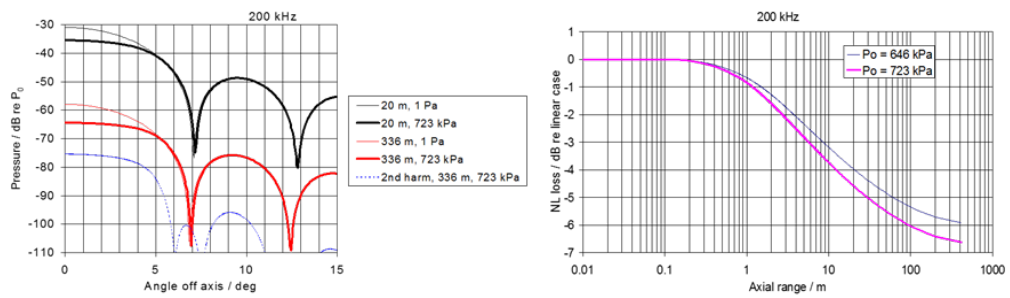


Figure 2.9. Theoretical non-linear loss across (left) and along (right) a 200 kHz beam axis for two power settings. 723 kPa is similar to $p_{et} = 1000 W$.

To mitigate non-linear effects, assure that the transmit power for fast-CW is $< 25 \text{ kW m}^{-2}$ for Tonpiliz transducers with 60% efficiency, or $< 20 \text{ kW m}^{-2}$ for composite transducers with 75% efficiency (Table 2.5; Korneliussen *et al.*, 2008). Measurements should not be made with higher transmit power. However, in such cases, calibrations should be performed with the sphere at 20 m range, beyond the range where most of the non-linear effects occur. Then, a range-dependent correction may be applied if the range to the calibration sphere is known (Pedersen, 2006).

Table 2.5. Recommended transmit power to mitigate non-linear effects (Korneliussen *et al.*, 2008).

	18 kHz	38 kHz	70 kHz	120 kHz	200 kHz	333 kHz
Approximate transducer area (10^{-3} m^2)	200	100	30	10	4.4	1.6
Approximate 3 dB beamwidth ($^\circ$)	11	7	7	7	7	7
Recommended maximum input power for 75% electro-acoustic efficiency (W)	4000	2000	600	200	90	30

To investigate non-linear effects in an EK80 system, a WC38.1 sphere was placed on transducer axes at $\sim 10 \text{ m}$ range, and CW and FM pulses were transmitted with p_{et} ranging from 25 to 200 W for 333 kHz and 1000 W for 70, 120, and 200 kHz. Although the measurements are variable, the decrease in signal with increasing p_{et} approximates theoretical predictions (Pedersen, 2006) (Figure 2.10). Therefore, the magnitudes of non-linear effects appear to be predictable and the same for the EK80 as for EK60.

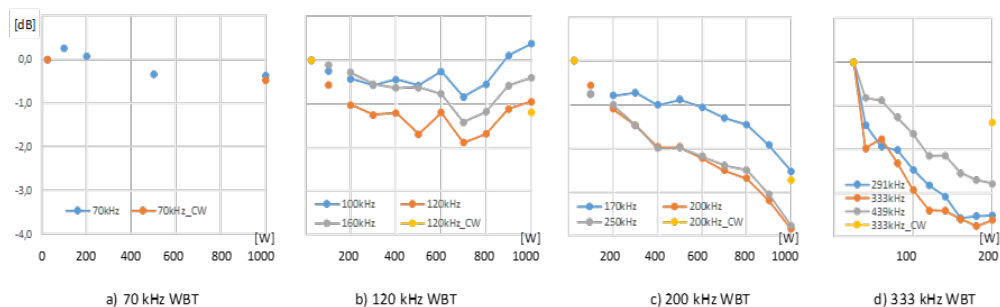


Figure 2.10. MF data averaged over 20 kHz bandwidths, normalized to that for $p_{et} = 25 W$, measured on the transducer axis at $\sim 10 \text{ m}$ range. Note that the measurements at $p_{et} = 25 W$ had higher noise than those for the higher p_{et} settings.

Table 2.6. Settings for cross-channel interference characterization. Pulse durations were 2.048 ms.

Sphere on axis	Active	Ramping	Passive
70 kHz	70 kHz	Fast	120, 200, 333 kHz
	70 kHz	Slow	120, 200, 333 kHz
	All channels	Fast	-
	All channels	Slow	-
120 kHz	120 kHz	Fast	70, 200, 333 kHz
	120 kHz	Slow	70, 200, 333 kHz
	All channels	Fast	-
	All channels	Slow	-
200 kHz	200 kHz	Fast	70, 120, 333 kHz
	200 kHz	Slow	70, 120, 333 kHz
	All channels	Fast	-
	All channels	Slow	-
333 kHz	333 kHz	Fast	70, 120, 200 kHz
	333 kHz	Slow	70, 120, 200 kHz
	All channels	Fast	-
	All channels	Slow	-

Ideally, the sphere should have been placed in the centre of all beams, but the Technology Tank was not large enough. Consequently, when the sphere was in the centre of the 70 kHz beam, it was off axis in the 120, 200, and 333 kHz beams, and the measurements were compensated for transducer directivity (Table 2.7). The uncalibrated measures are compared within each band.

Table 2.7. For the transducer configuration in Figure 2.11, the following factors are used to compensate off-axis measurements for transducer directivity. For example, if the sphere was positioned on the axis of the 70 kHz transducer, the 120 and 200 kHz measurements are multiplied by 1.25 and 1.45.

	Adjust to 70 kHz axis	Adjust to 120 kHz axis	Adjust to 200 kHz axis
Sphere on 70 kHz axis	1	1.25	1.45
Sphere on 120 kHz axis	1.24	1	2.8
Sphere on 200 kHz axis	1.37	2.8	1

Table 2.8. Uncalibrated nautical area backscattering coefficients (s_A ; m^2 nautical mile⁻²) measured with the sphere on the axis of the active system and the others passive.

Active system	70 kHz	120 kHz	200 kHz
70 kHz	2335	263	156
120 kHz	0	4654	40
200 kHz	0	0	4507

These measures indicate that 7% ($263 \times 1.24/4654$) of the S_A measured by a 120 kHz EK80 is due to harmonic energy from a synchronous 70 kHz EK80, and 7% ($(156 \times 1.37 + 40 \times 2.8)/4507$) of the S_A measured by a 200 kHz EK80 is due to harmonic energy from synchronous 70 and 120 kHz EK80. To mitigate cross-channel interference (Figure 2.12), reduce p_{et} to minimize non-linear effects (Table 2.5), transmit sequentially, not simultaneously, and perhaps use different pulse shapes for each frequency band, e.g. up-sweep 70 kHz FM, down-sweep 120 kHz FM, up-sweep 200 kHz hyperbolic, and up-sweep 333 kHz FM.

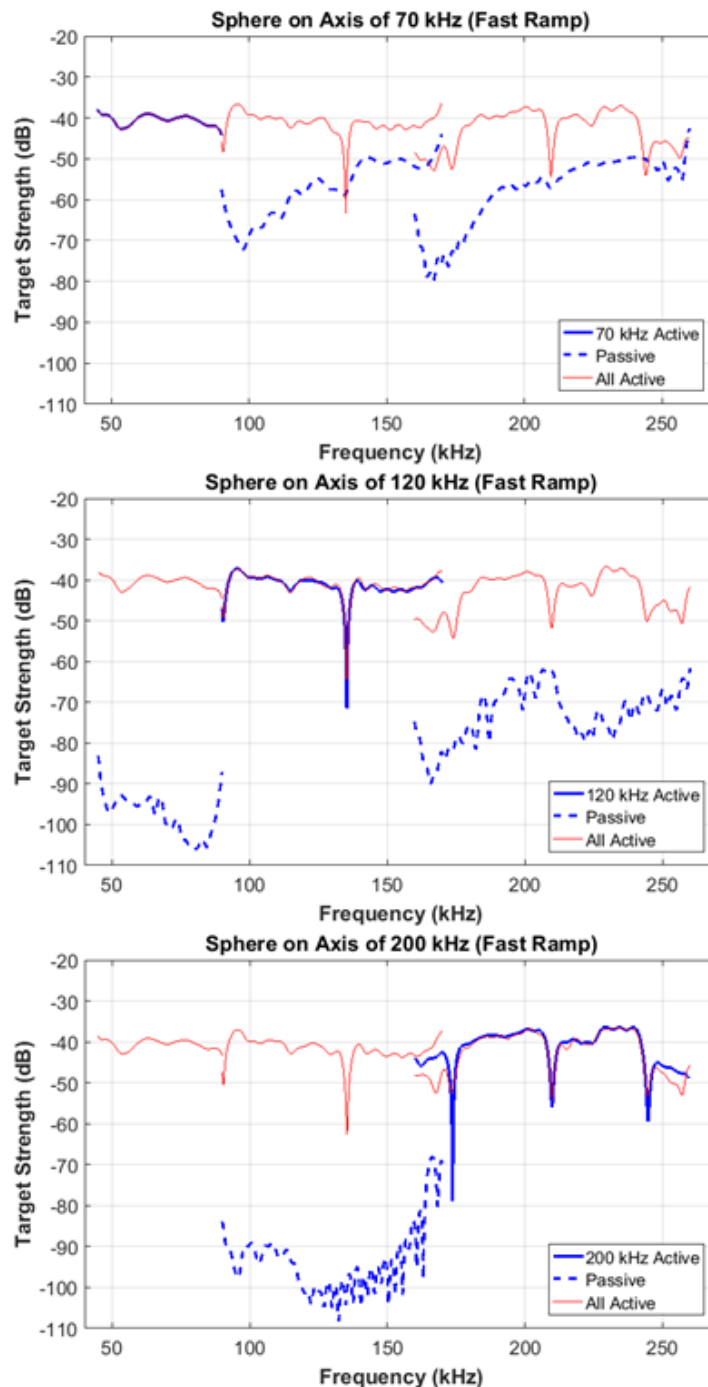


Figure 2.12. Target strength measured from a sphere by one active channel (solid blue line) and others passive (dashed blue lines), and all active (solid red line), for the WC38.1 sphere on the axis of the 70, 120, and 200 kHz transducer (top to bottom, respectively), and a fast-FM pulse with 2.048 ms duration. All spectra are twenty-pulse averages.

When all channels are active, the echoes from the sphere received by one channel are the coherent addition of signals within the receiver bandwidth generated by all channels. Since the frequencies are relatively large, small perturbations in sound speed stemming from possible time-varying heterogeneity in the tank water cause differences in travel time and phase among echoes from different ray-paths. This results in between-transmission variation in $TS(f)$ (Figure 2.13).

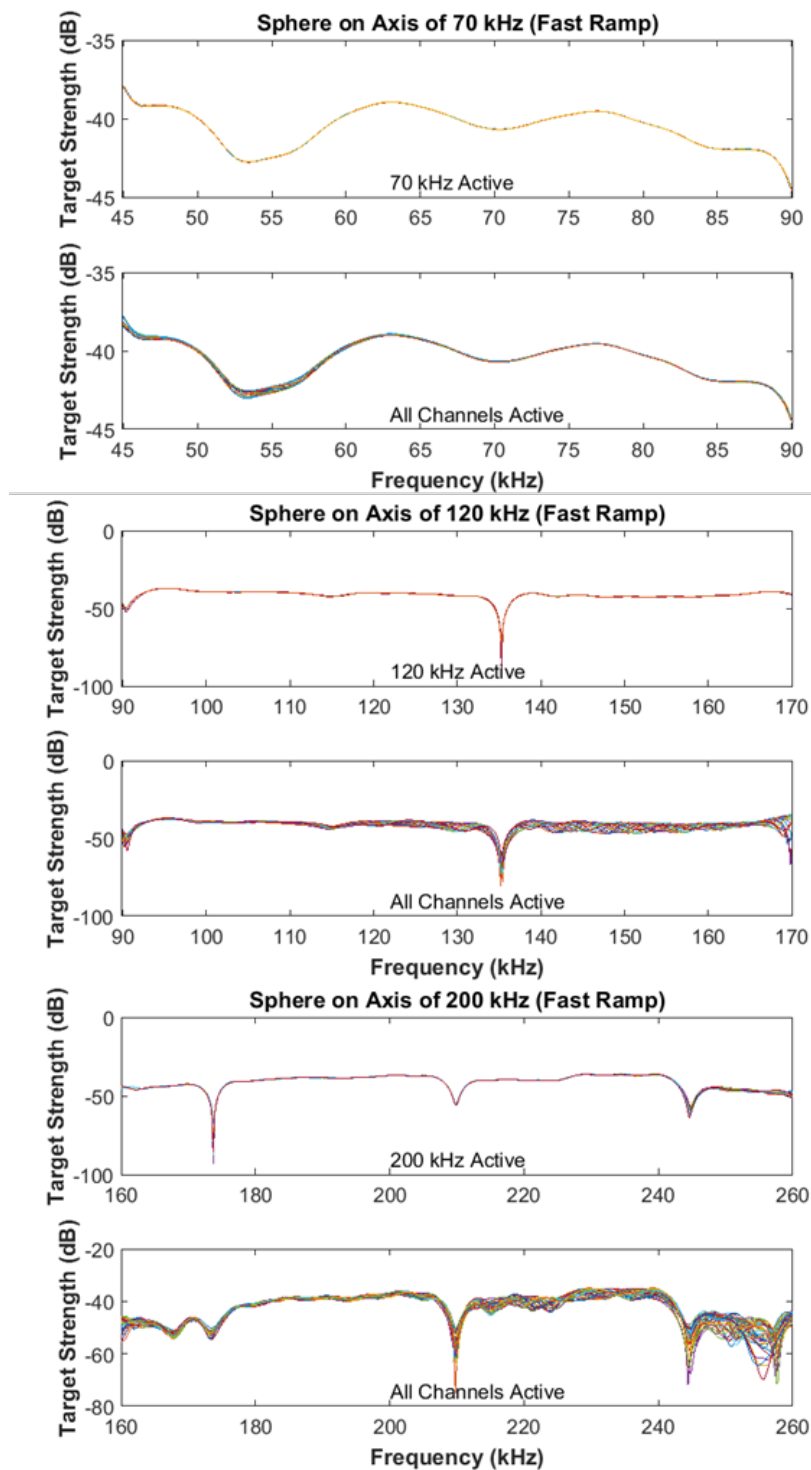


Figure 2.13. Comparison of WC38.1 sphere $TS(f)$ for 70, 120, and 200 kHz EK80, averaged over twenty 2.048 ms fast-FM pulses.

Between-transmission variability in $TS(f)$ (Table 2.9) was also evaluated with one channel active and all channels active for a WC38.1 sphere placed sequentially on the axis of the 70, 120, and 200 kHz transducer (Figure 2.14). The cross-channel interference is lowest for the 70 kHz channel, since the energy from sub-harmonics is low; and the 200 kHz channel has the largest cross-channel interference.

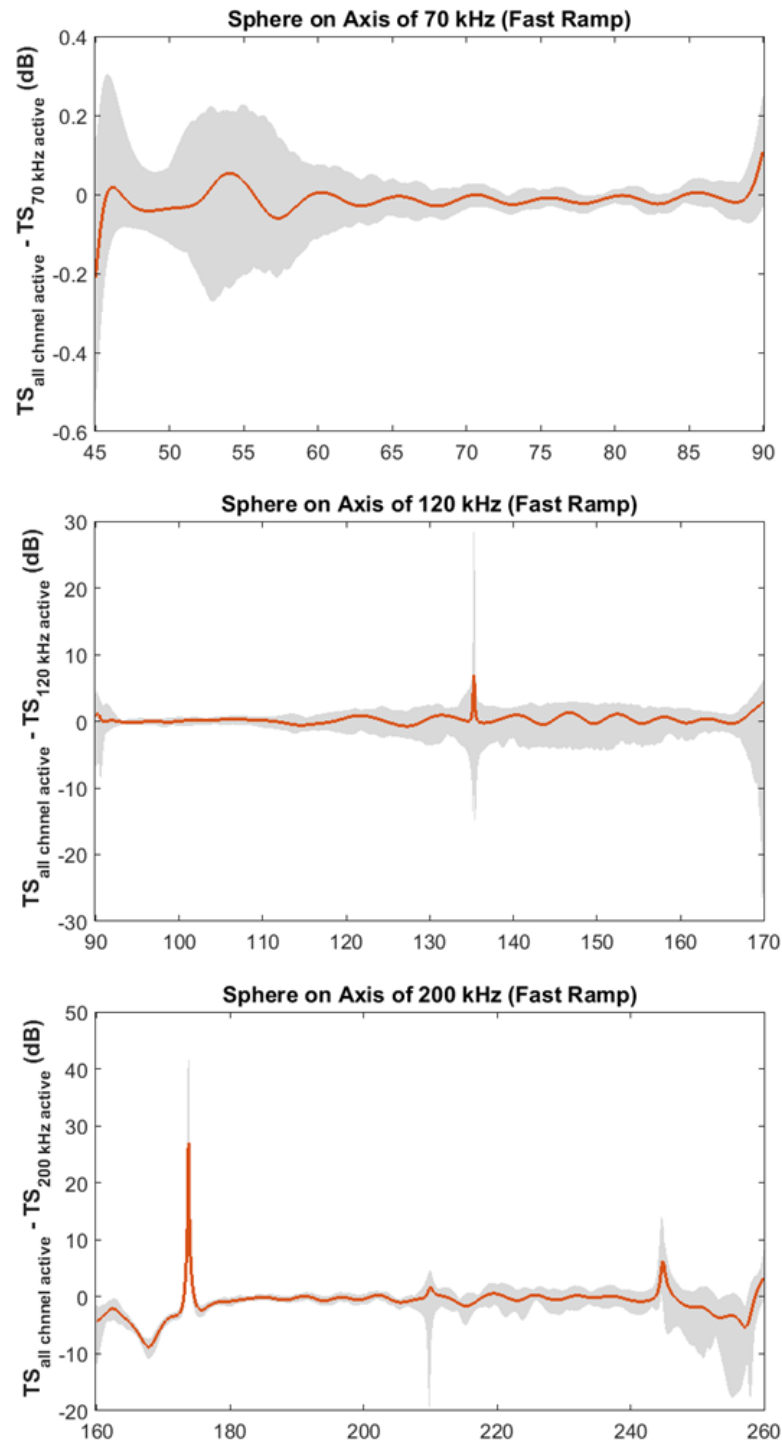


Figure 2.14. Between-transmission variability (grey) of $TS(f)$ for a WC38.1 sphere positioned sequentially on the beam axis of the 70, 120, and 200 kHz transducer. The solid line is the average of twenty 2.048 ms fast-FM pulses. Note the different y -axis scales.

If EK80 is calibrated with sequential transmissions, but the survey is conducted with simultaneous transmissions, cross-channel interference may bias the data from higher frequencies (e.g. Table 2.9). Furthermore, if EK80 is calibrated with simultaneous transmissions, stochastic variability in the cross-channel interference may bias the data from higher frequencies.

Table 2.9. Standard deviation difference in averaged TS between one channel active and all channels active.

Channel	70 kHz	120 kHz	200 kHz
$\sigma_{\Delta TS}$ (dB)	0.03	0.6	2.45

Cross-channel interference should be further investigated for all survey frequencies and as a function of range. Since the interference results from a coherent summation of echoes from different ray paths, cross-channel interference may differ by range, particularly for higher-frequency channels. Resonance may cause cross-channel interference that is not relative, possibly causing bias.

2.3 Trigger stability

In some installations, it is desirable to accurately and precisely synchronize the transmit pulses from the EK80 with signals from other instruments. EK80 may input or output trigger signals via its auxiliary connector or via a serial port on the computer running the EK80 software. The communication port and synchronization mode, e.g. master or slave, may be selected in EK80 software (in the Installation dialog box, select Synchronization, then select Synchronization Port).

Variability in latency between trigger and transmit signals was measured for EK80 and EK60 using a two-channel oscilloscope. The echosounders were triggered via the auxiliary port, a serial (RS232) port on the motherboard, and a USB-to-serial port converter device. Delays were measured between the input trigger time $t_{trig-in}$ and the first peak of the pulse waveform $t_{pulse-p1}$, and between $t_{trig-in}$ and the time of the output trigger $t_{trig-out}$ (Figure 2.15). The duration of the CW pulse was 1024 μs . Measurements of $t_{pulse-p1}$ were made using the oscilloscope's "time at max" function.

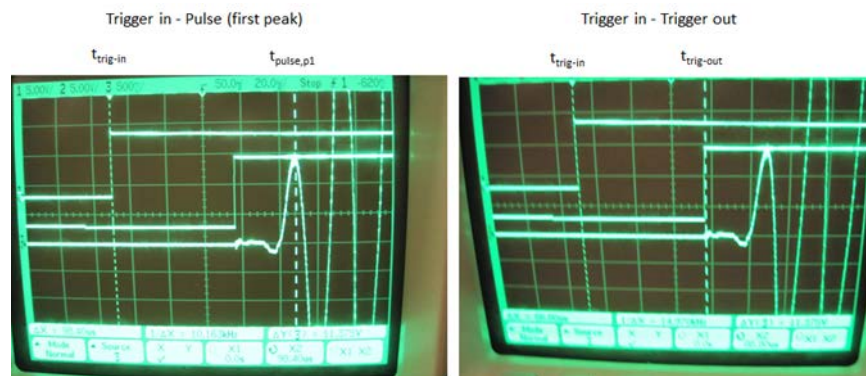


Figure 2.15. Oscilloscope displays of EK80 triggers. Delays were measured between the input trigger time, $t_{trig-in}$, and the first peak of the pulse waveform $t_{pulse-p1}$ (left); and between $t_{trig-in}$ and the time of the output trigger $t_{trig-out}$ (right).

When triggered via the auxiliary port, the mean delay $t_{pulse-p1} - t_{trig-in}$ was 98.1 μs (s.d. = 0.67 μs) for EK80 and 54.5 μs (s.d. = 0.50 μs) for EK60 (Table 2.10). Assuming $c_w = 1500 \text{ m s}^{-1}$, these latencies correspond to mean distances of 147 mm (s.d. =

0.6 mm) and 81.8 mm (s.d. = 0.8 mm). The mean delay between $t_{trig-out} - t_{trig-in}$ was 66.3 μs (s.d. = 0.18 μs) for EK80 and 0.0 μs (s.d. = 0.0 μs) for EK60.

Table 2.10. EK80 and EK60 trigger stability measurements when triggered via the auxiliary port.

Measurement	EK80		EK60			
	$t_{pulse-p1} - t_{trig-in}$	$t_{trig-out} - t_{trig-in}$	$t_{pulse-p1} - t_{trig-out}$	$t_{pulse-p1} - t_{trig-in}$	$t_{trig-out} - t_{trig-in}$	$t_{pulse-p1} - t_{trig-out}$
	(μs)	(μs)	(μs)	(μs)	(μs)	(μs)
1	97.3	66.4	30.9	53.9	0.0	53.9
2	99.1	66.4	32.7	54.2	0.0	54.2
3	97.2	66.0	31.2	54.8	0.0	54.8
4	97.8	66.0	31.8	55.0	0.0	55.0
5	98.6	66.1	32.5	54.8	0.0	54.8
6	98.8	66.4	32.4	53.9	0.0	53.9
7	98.3	66.4	31.9	54.3	0.0	54.3
8	97.5	66.4	31.1	55.2	0.0	55.2
9	98.5	66.4	32.1	55.0	0.0	55.0
10	98.4	66.4	32.0	54.0	0.0	54.0
Mean (μs)	98.1	66.3	31.8	54.5	0.0	54.5
Variance	0.5	0.03	0.4	0.3	0.0	0.3
s.d. (μs)	0.7	0.2	0.6	0.5	0.0	0.5
Mean (mm)	147.2	99.4	47.7	81.8	0.0	81.8
Variance (mm)	0.7	0.05	0.6	0.4	0.0	0.4

When EK80 was triggered via a USB serial port, the mean delay $t_{pulse-p1} - t_{trig-in}$ was 5.4 ms (s.d. = 0.3 ms) and when triggered via an internal serial port, the mean delay was 2.2 ms (s.d. = 0.04 ms) (Table 2.11). In terms of range, for $c = 1500 \text{ m s}^{-1}$, these mean delays correspond to 8.1 and 3.3 m, respectively. Therefore, because triggering via a serial port has large and variable latency, the auxiliary port should be used to obtain a stable trigger with low latency.

Table 2.11. EK80 trigger latencies $t_{pulse-p1} - t_{trig-in}$ when triggered via USB and internal serial ports.

Measurement	USB-serial (μs)	Internal serial (μs)
1	5 520.7	2 162.6
2	5 117.4	2 163.0
3	5 241.2	2 158.5
4	5 610.3	2 208.4
5	5 499.1	2 162.1
6	5 575.1	2 116.5
7	5 777.4	2 085.9
8	5 333.2	2 186.3
9	4 804.9	2 193.5
10	5 400.0	2 225.9
Mean (μs)	5 387.9	2 166.3
Variance (μs^2)	78 215.1	1 723.5

2.4 Noise measurements

Background noise level affects *SNR* and, therefore, the usefulness of EK80 measurements. EK80 can measure both signals and noise over wide-bandwidths, so the measurements have higher cumulative noise (assuming equal noise per frequency band) compared to narrowband EK60 measurements. In this section, we evaluate and compare noise received by EK60 and EK80 vs. frequency.

Noise was measured in passive and active modes when the transceivers were connected to a dummy load. First, EK60 and EK80 were equivalently grounded to earth. Then, the transceivers were connected, in turn, to a Simrad dummy load, and noise power was recorded in .raw format. For three echosounder configurations (EK60 and EK80 configured in CW mode and EK80 configured in FM mode), five frequencies (18, 38, 70, 120, and 333 kHz), up to three pulse durations (0.512, 1.024, and 2.048 ms), and two ramps (fast and slow), a total of 146 raw files were recorded, each including data to 100 m range for 10–15 trigger pulses, with a 1 s interval. EK60 and EK80 were controlled by ER60 and EK80 software, respectively. FM mode was not available for 18 and 38 kHz, and the 2.048 ms pulse duration was not available for $f > 120$ kHz.

Recorded data files were analysed in Echoview to determine the median received power (dB *re* 1 W) for each configuration. Data that included the trigger or pulse and the transition from transmit-to-receive periods were excluded from the analysis. For each configuration, the median power was calculated for data in a 30 to 90 m range and for all 10–15 triggers.

2.4.1 EK60 CW

For the various EK60 configurations, noise was estimated for active and passive modes (Figure 2.16). Among all configurations, the maximum variation in the median noise estimate was 8.2 dB. Differences between active and passive modes for otherwise identical configurations were generally less than 0.5 dB, except at 200 kHz, where passive mode noise was 0.8 dB lower than active mode for 512 μs pulses and 1.2 dB lower for 1024 μs pulses. Noise decreased with increasing pulse duration.

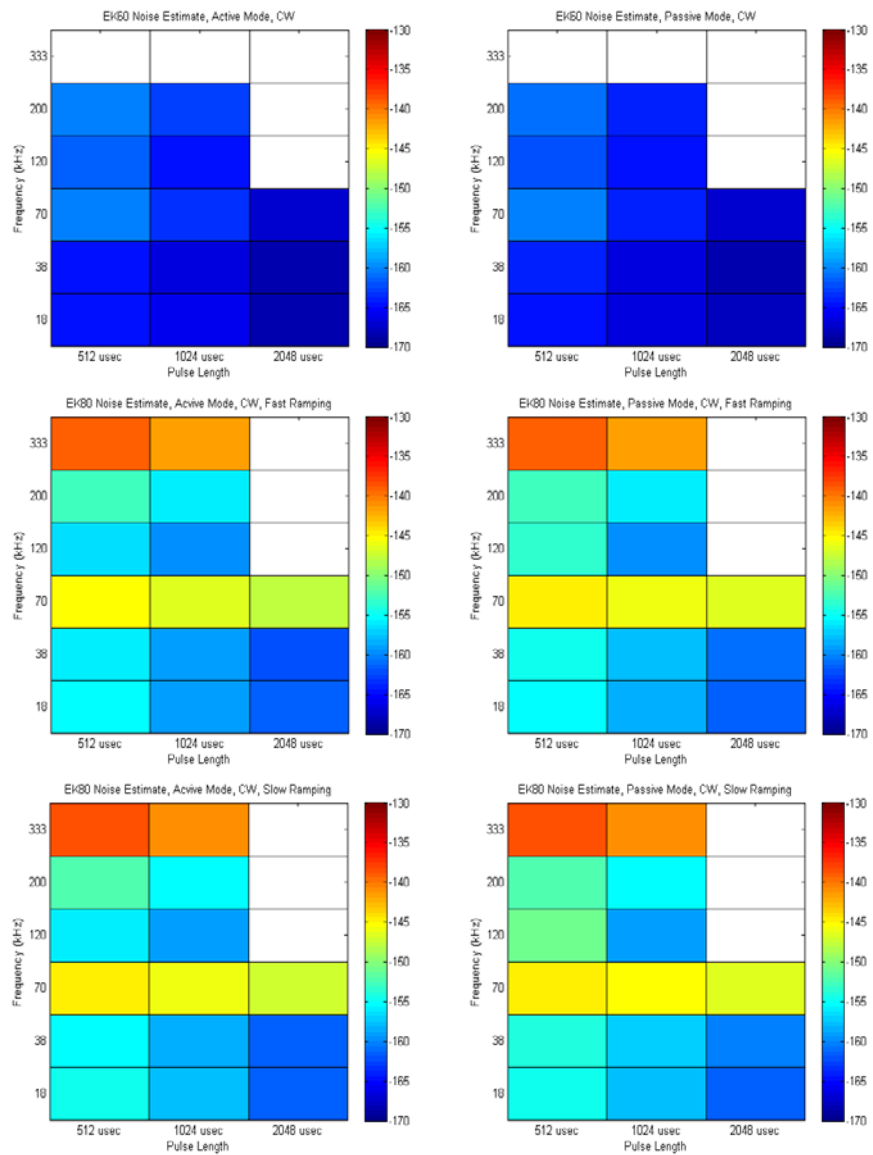


Figure 2.16. Background noise levels (dB re 1 W) for EK60 (top row), EK80 fast-CW (middle row), and EK80 slow-CW (bottom row) in active (left column) and passive modes (right column) by pulse duration and frequency.

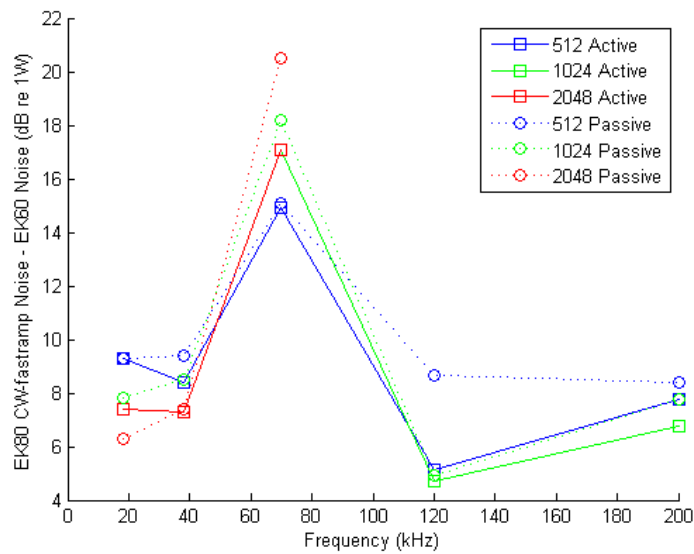


Figure 2.17. Mean differences between EK80 and EK60 noise for fast-CW.

2.4.2 EK80 CW

Noise was also estimated for EK80 CW (Figure 2.16). Noise levels were highest in 333 and 70 kHz data. Differences between passive and active modes were less than 1.4 dB, except for 120 kHz, which had noticeably higher noise in passive mode than active. For both active and passive modes, noise decreased with increasing pulse duration, and fast-ramp had less noise than slow-ramp configurations.

Due to wider receiver bandwidths, noise was higher and more variable vs. pulse duration and frequency in EK80 data than in EK60 (Figure 2.17). Comparing measures with fast-CW, noise was ~4–20 dB higher for EK80 vs. EK60, with the highest differences observed for 70 kHz.

2.4.3 EK80 FM

Noise was measured for fast-FM and slow-FM pulses (bandwidths from Table 1.2), with EK80 in both active and passive modes (Figure 2.18). Noise was highest for FM in the EK80 70 and 333 kHz channels; however, these values were lower than for EK80 CW. Noise decreased with increased pulse duration and was lower for fast-ramping vs. slow. Noise was lower for received power with MF processing, depending on the impedance used for conversion from complex samples to received power (see Section 1.3.4.6.1, Transducer and receiver impedances).

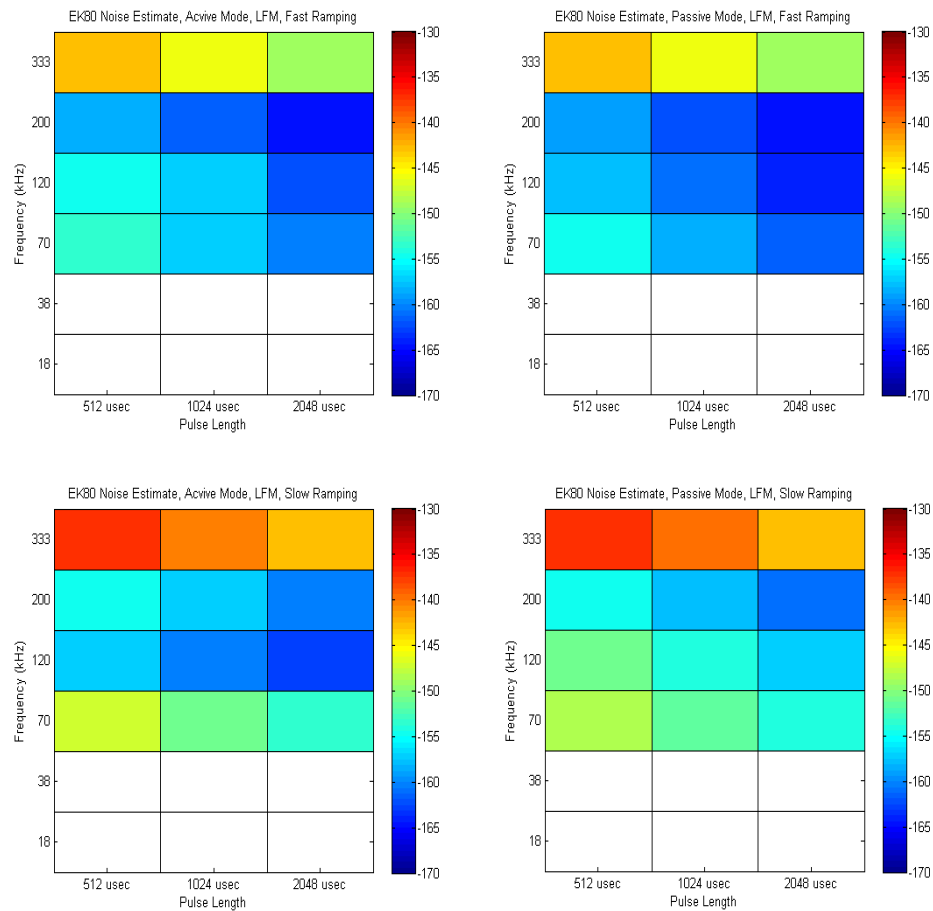


Figure 2.18. Background noise levels for EK80 fast-FM (top row), and EK80 slow-FM (bottom row), in active (left column) and passive (right column) modes, by pulse duration and frequency.

2.4.4 EK60 and EK80 on board FSV “Reuben Lasker”

Passive-mode noise measurements were also conducted with the EK60 and EK80 connected, via a multiplexer, to six transducers (ES18, ES38B, ES70-7C, ES120-7C, ES200-7C, and ES333-7C) in the centreboard of the NOAA FSV “Reuben Lasker” on 23 September 2016 between 1720 and 1800 GMT. The ship was drifting, and the water depth was 550 m. Received noise was converted to equivalent ambient noise ($\text{dB re } 1 \mu \text{Pa}/\sqrt{\text{Hz}}$), and averaged for periods corresponding to a 10–650 m range, following 14 trigger pulses (Figure 2.19).

The noise measured by EK80 is higher than on EK60, especially at 70, 120, and 200 kHz. For 18 and 38 kHz, but not for 70 kHz, the noise on EK80 varies less with pulse length and bandwidth than on EK60. Noise differs for each installation.

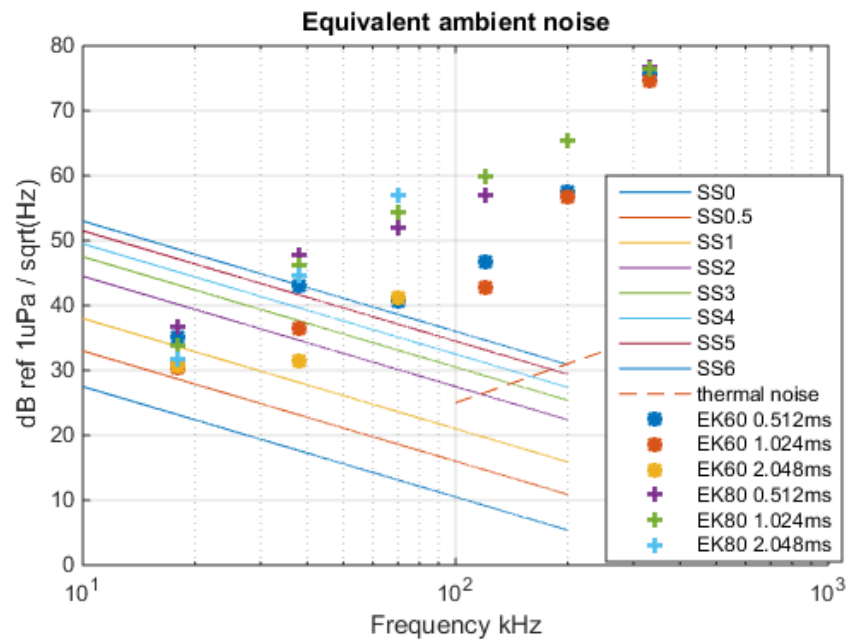


Figure 2.19. Ambient noise measured by EK60 and EK80 on board NOAA's FSV "Reuben Lasker", operating in passive mode, compared to Knudsen sea states (SS) 0 to 6 (Knudsen *et al.*, 1948).

2.5 Target-spectra measurements

When computing frequency spectra with an FFT, there is a trade-off between temporal and frequency resolution. For accurate and precise measurement of echo spectra, the FFT length should include as much of the backscattered energy from the target as possible without including echoes from nearby scatterers. Capturing too little of the target echo or too much non-target echo will degrade the measurements. The FFT length and location may be optimized based on *a priori* knowledge of the duration and symmetry of the target backscatter and the proximity of the target echo to that of other scatterers.

To explore the effects of FFT length and location on the resolution of backscatter spectra, a WC38.1 sphere was positioned in the Technology Tank at ~9.5 m range on the axis of an ES70-7C transducer. ES120-7C and ES200-7C transducers were positioned adjacent to the 70 kHz transducer (see Figure 2.11) such that the sphere was within the main lobe of all three transducer beams. While transmitting sequentially, the sphere was moved slowly through the beams.

2.5.1 FFT length

Angle-compensated $TS(f)$ data were derived with a 0.4 m FFT length (0.1 m before and 0.3 m after the temporal-domain peak) for three pulse durations (512, 1024, and 4096 μ s) and compared to theory (Figure 2.20). Because the SNR was consistently high for $f > 100$ kHz, the nulls were resolved for all pulse durations. However, fine-spectral detail was modulated by the amount of sphere backscatter spanned by the FFT.

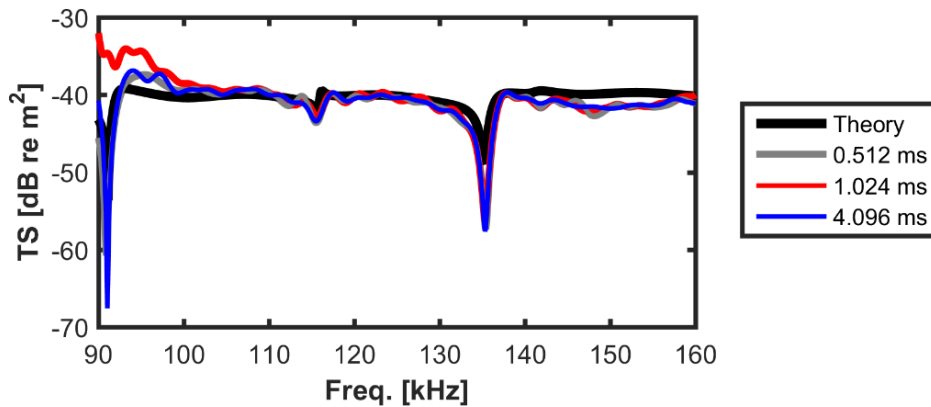


Figure 2.20. Theoretical TS for a WC38.1 sphere (black) and average measurements of TS spectra for three transmit-pulse durations (90–160 kHz), using a 0.4 m FFT length extending 0.1 m before the target and 0.3 m after.

2.5.2 FFT position

For an ideal point scatterer, an MF time-series is approximately the same duration as the transmit pulse and is symmetric about the peak. However, for scatterers supporting circumferential waves, e.g. metal spheres, an MF time-series is longer than the transmit pulse and is asymmetrical. In this case, the data used in the FFT should capture wave interferences following the peak echo, which result in the nulls of the sphere $TS(f)$ (Figure 2.21).

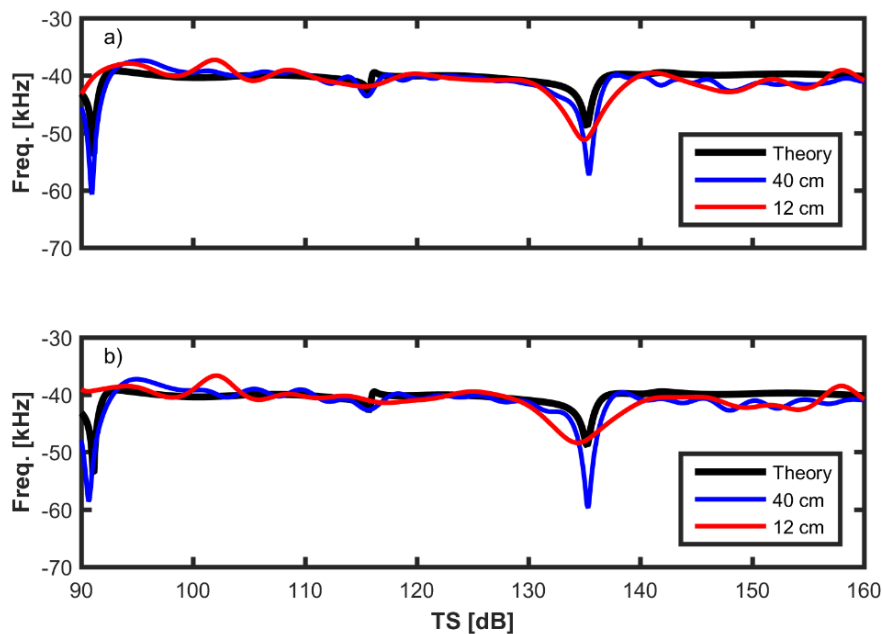


Figure 2.21. $TS(f)$ for a WC38.1 sphere measured with a 1.024 ms, 90–160 kHz transmit pulse and processed with 40 cm (blue) and 12 cm (red) FFT lengths. The FFTs are (a) 25% before and 75% after the first echo and (b) centred on the first echo. These plots show that the spectrum is more accurately measured, compared to theory (black), if the FFT includes more backscatter from the sphere.

2.5.3 Target separation

When the target is separated from other scatterers by $c\tau/2$, and there is little or no overlap between the sidelobes of the MF time-series, then the FFT may span the entire target echo. If the FFT is longer than the echo and if the SNR is high, the spectral resolution

will be improved, but no additional spectral features will be resolved. For closer scatterers, the FFT must be short enough to avoid mixing scattering spectra, but then the target spectra may be inaccurate (see Figure 2.22).

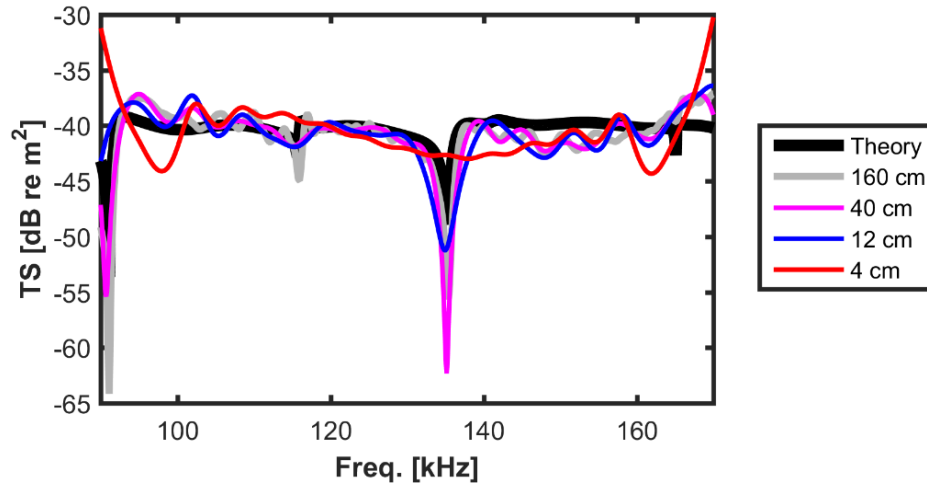


Figure 2.22. Average $TS(f)$ from a WC38.1 sphere, measured with 1.024 ms, 90–160 kHz transmit pulses and processed using FFT lengths of 4, 12, 40, and 160 cm positioned 25% before and 75% after the temporal-domain peak echo. The theoretical spectrum (black) is increasingly resolved for longer FFT lengths.

2.5.4 Calibration

During calibration, it is important to resolve the nulls in $TS(f)$ from spheres to assure a match between actual and assumed sphere properties (see Section 1.4, Calibration). As previously discussed, choice of FFT length (see Section 2.5.1, FFT length) and location (see Section 2.5.2, FFT location) can cause differences, some subtle, in measurements of sphere $TS(f)$ (Figure 2.23).

Too short an FFT will decrease the accuracy and precision of the beamwidth and gain measurements because the observed nulls will be wider than predicted by theory. Therefore, if the sphere is separated from other scatterers by $c\tau/2$ and there is little or no overlap between the sidelobes of the MF time-series (see Section 2.5.3, Target separation), then the FFT should span the entire target echo. This will resolve the nulls in $TS(f)$ and allow more of the EK80 bandwidth to be calibrated, requiring less interpolation.

2.5.5 Effective pulse duration

For fast- and slow-FM pulses with τ ranging from 512 to 4096 μs , $TS(f)$ did not vary significantly (Figure 2.24). These results suggest that calibrated gain values may not vary with τ . However, this may not be true for low SNR , particularly for frequencies in the pulse ramping. For example, for 512 and 4096 μs fast-FM pulses, each with a starting frequency of 90 kHz, the ramping will occur over 4 and 0.5% of the signal, respectively. Slow-FM pulses will have further decreased the τ_{eff} and usable measurement bandwidths.

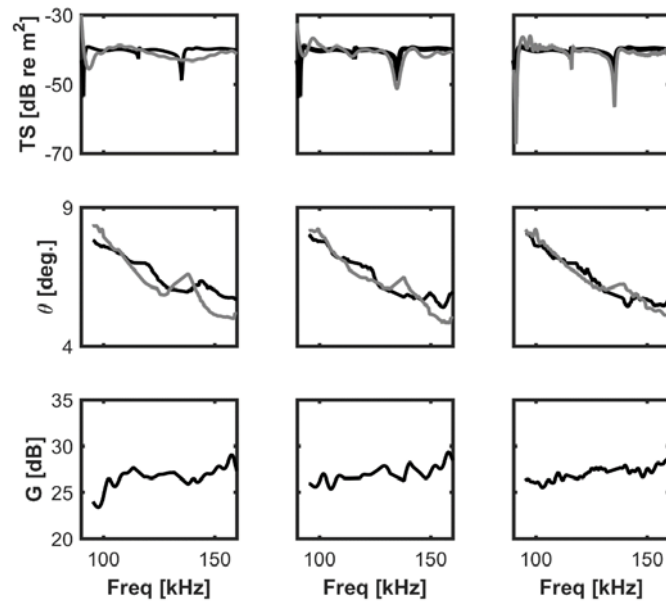


Figure 2.23. Measurements of $TS(f)$ (grey) from a WC38.1 sphere, compared to theory (black) (row 1), alongships (black) and athwartships (grey) beamwidths (row 2), and $G(f)$ (row 3) obtained using 4 cm (column 1), 12 cm (column 2), and 40 cm (column 3) FFT lengths for a 1.024 ms, 90 to 160 kHz, fast-FM transmit pulse.

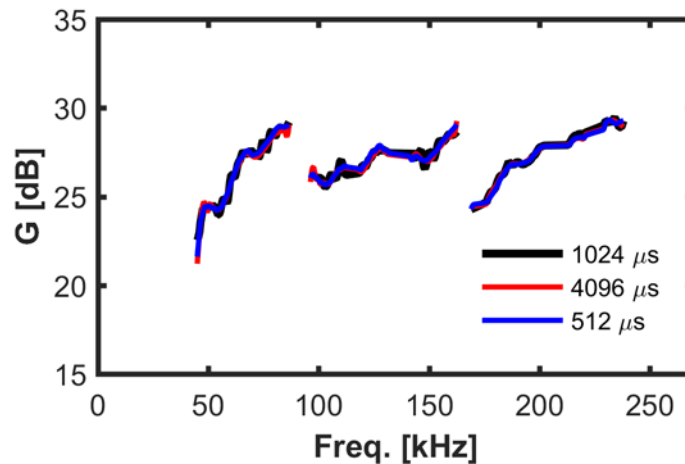


Figure 2.24. Calibration curves generated using data from a WC38.1 sphere and processed using EK80 software for 45–90, 90–170, and 160–260 kHz fast-FM signals with three pulse durations.

2.5.6 Single-target detection

Individual targets are detected as resolved peaks in the matched-filter output. Detection of individual targets is dependent on Δr , which is inversely related to b_f (see Section 1.1.1, Advantages).

To test the minimum range for targets to be spatially and spectrally resolved, a 23 mm diameter copper sphere (Cu23) and a WC38.1 sphere were placed adjacent to each other (touching) in the Technology Tank on the axis of the 70 kHz transducer (Figure 2.25). The Cu23 was then moved sequentially along the beam axis 1, 3, 5, 8, 10, 15, 20, 40, 80, and 120 cm away from the WC38.1. For each separation, measurements were made with 70, 120, and 200 kHz EK80 (sequential transmit) using 512, 1024, and 4096 μs pulse durations and fast- and slow-FM. The measurements were compared with *a priori* knowledge of the sphere spectra and locations.

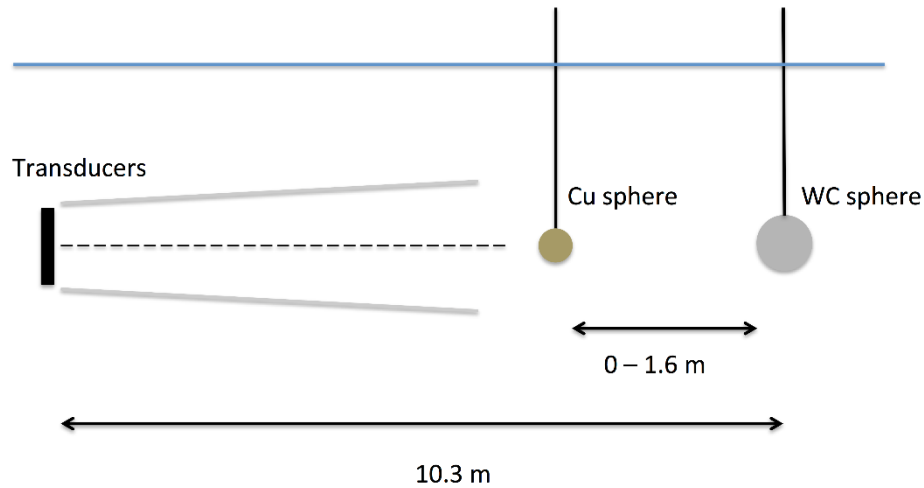


Figure 2.25. The geometry for the target separation experiment. The range to the WC38.1 was constant, while the Cu23 was moved towards the transducers in small increments.

Results of $S_p(t)$ are shown for the 120 kHz channel and 5, 15, and 40 cm separations (Figure 2.26). Echoes from the two spheres are consistently resolved using fast-FM pulses. In contrast, slow-FM pulses did not resolve the sphere with 5 cm separation. However, the slow-FM suppresses the side lobes causing the amplitude preceding the peak to decrease more rapidly. Following the peak, the amplitude drops slowly because of the echo coda.

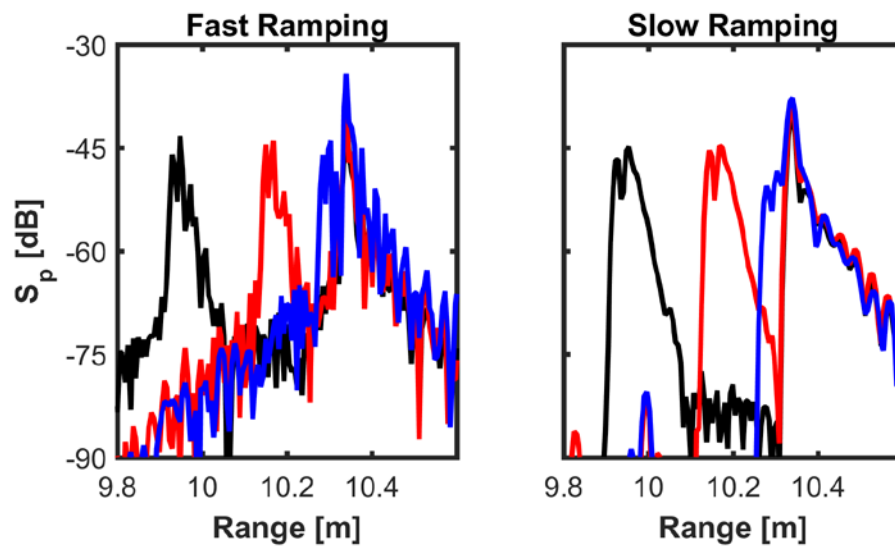


Figure 2.26. $S_p(t)$ data for the 120 kHz EK80 channel for 5 (blue), 15 (red), and 40 cm (black) separations between Cu23 and WC38.1. For fast-FM pulses (left), the spheres are resolved for each separation. For slow-FM pulses (right), the spheres with a 5 cm separation are not resolved.

Results of $S_p(t)$ are shown for a 5 cm sphere separation for the 70, 120, and 200 kHz channels (Figure 2.27). The MF output includes multiple peaks that could be misinterpreted as separate targets. However, with *a priori* knowledge of the number and locations of spheres, the two sphere echoes are consistently resolved using fast-FM pulses. The resolution improves with increasing f caused by increasing b_f and decreasing Δr . For the slow-FM pulses, only the 200 kHz channel had a sufficiently large b_f and small Δr to resolve the sphere echoes.

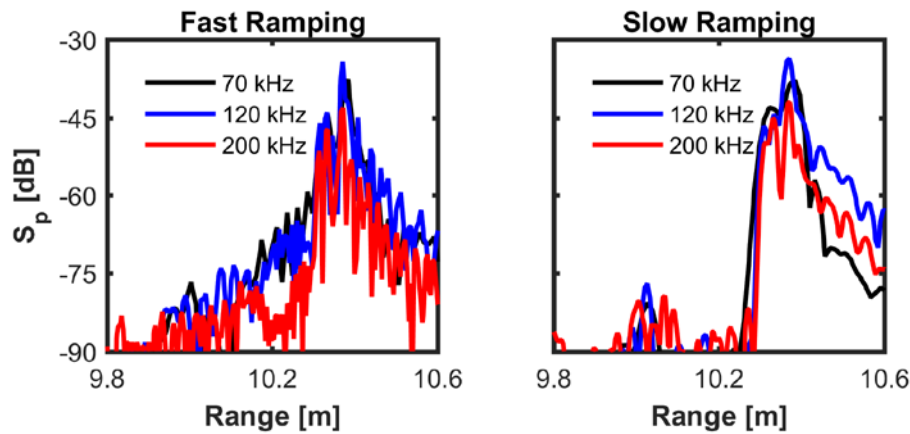


Figure 2.27. Fast-ramped and slow-ramped $S_p(t)$ data for the 70, 120, and 200 kHz channels. The targets are separated by 5 cm. Both echoes are identifiable for all three channels using the fast ramping. With slow ramping, the unique echoes are only identifiable using the 200 kHz channel.

For a 40 cm sphere separation, $S_p(t)$ and $TS(f)$ were calculated using 6, 12, 25, and 75 cm FFT lengths for fast- and slow-FM, 1024 μ s duration pulses (Figure 2.28). The measured $TS(f)$ are consistent with theory, except for the fast-FM pulses processed with a 6 cm FFT length and the slow-FM pulses near the edges of the bandwidths. The overlapping MF sidelobes do not include sufficient energy to significantly affect the $TS(f)$ measurements from the two spheres. However, when the FFT includes echoes from both spheres, the echo spectra include nulls associated with their separation.

For the 5 cm sphere separation, measured $TS(f)$ for the Cu23 approaches theory for the fast-FM, but not the slow-FM pulses (Figure 2.29). For fast-FM, the overlapping MF sidelobes do not include sufficient energy to significantly affect the $TS(f)$ over most of the bandwidth. For slow-FM, the SNR is too low at the edges of the band to accurately replicate the theoretical $TS(f)$.

The $TS(f)$ values for the WC38.1 include some of the theoretical structure, but are positively offset due to additional energy from the Cu23. Note, while close targets may be resolved, measurements of their $TS(f)$ may not be accurate. Again, when the FFT spans both sphere echoes, the spectra include nulls indicative of their separation.

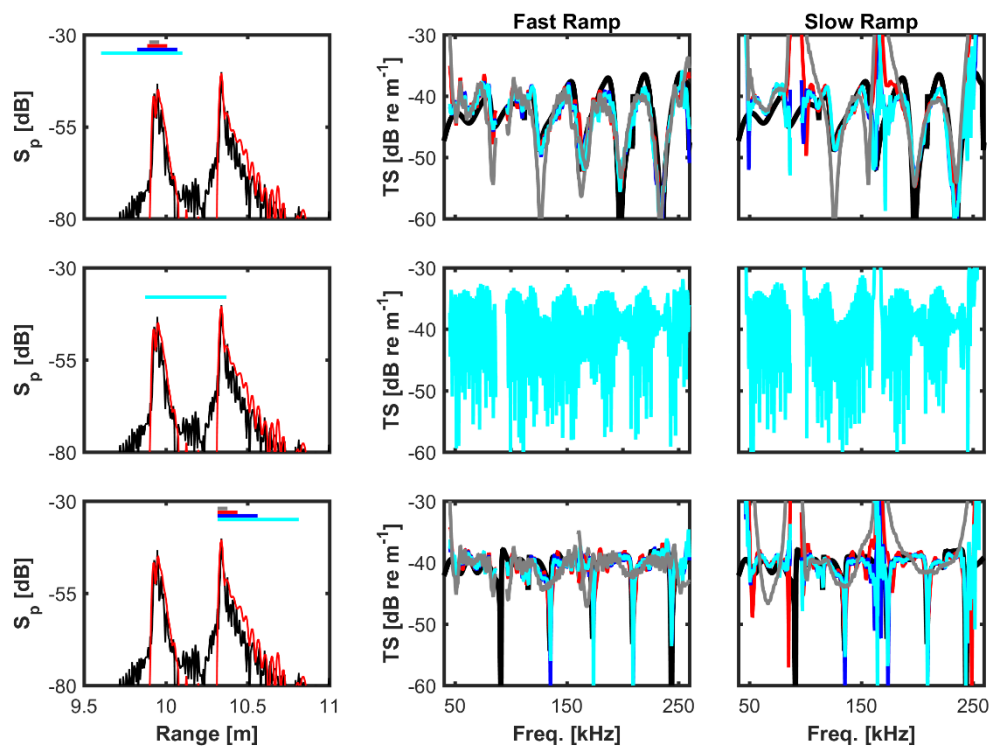


Figure 2.28. $S_p(t)$ (left column) and $TS(f)$ (middle and right columns) for Cu23 (~9.9 m range) and WC38.1 (~10.3 m range) spheres separated by 40 cm. $S_p(t)$ is for the 120 kHz channel with fast-FM (black) and slow-FM (red) pulses. The FFT lengths used to calculate $TS(f)$ are indicated by horizontal bars with corresponding colours (left column). Results are shown for the Cu23 (top row) and the WC38.1 (bottom row) using fast- (middle column) and slow-FM (right column) pulses. The amplitudes and shapes of the curves agree well with theory (black), except for data from the slow-FM pulse processed with a 6 cm FFT length where the edges of the band diverge. The combined spectra from both spheres (middle row) include nulls indicative of the sphere separation.

These experiments indicate that EK80 data can be used to spatially resolve and spectrally characterize metal spheres with similar TS that are separated by a few centimetres. However, unless the nature of their echoes is known *a priori*, measures of *in situ* biological targets will be more challenging. More work is needed to understand the structure of broadband echoes from biological targets, and to determine the minimum separation necessary to accurately measure their $TS(f)$. The information will inform protocols and algorithms for broadband detection and characterization of animals.

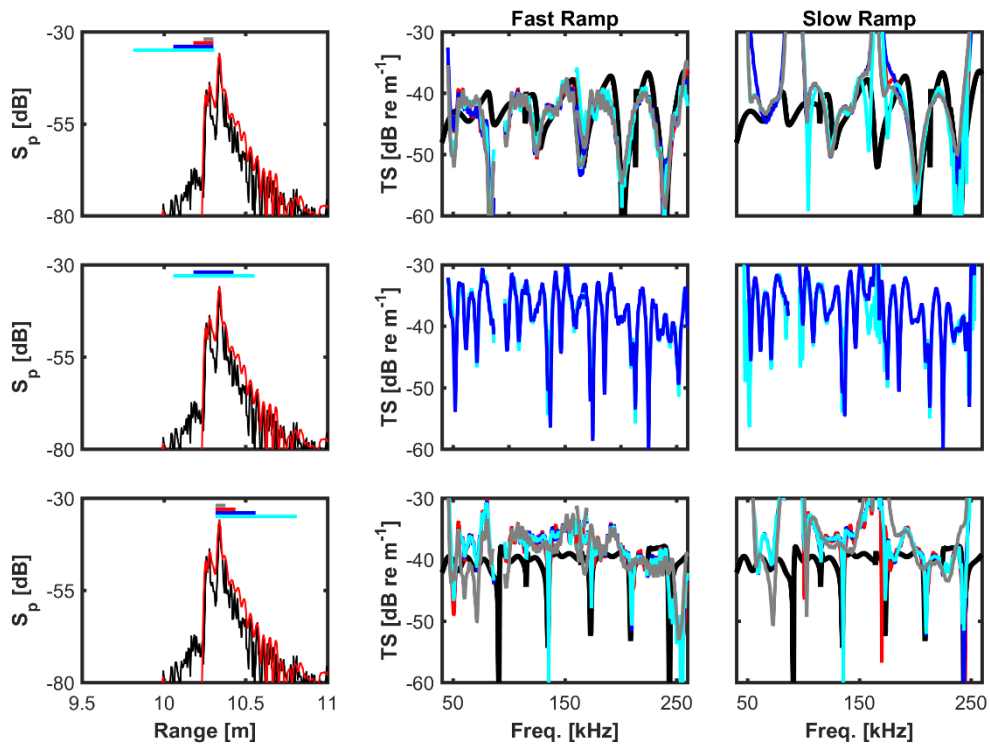


Figure 2.29. $S_p(t)$ (left column) and $TS(f)$ (middle and right columns) for Cu23 (~10.25 m range) and WC38.1 (~10.30 m range) spheres separated by 5 cm. $S_p(t)$ is for the 120 kHz channel with fast-FM (black) and slow-FM (red) pulses. The FFT lengths used to calculate $TS(f)$ are indicated by horizontal bars with corresponding colours (left column). Results are shown for the Cu23 (top row) and the WC38.1 (bottom row) using fast- (middle column) and slow-FM (right column) pulses. Results for the WC38.1 include some of the theoretical structure, but positively offset because of energy from the CU23. The combined spectra from both spheres (middle row) include nulls associated with the sphere separation.

2.6 Nautical area backscattering coefficients

When transitioning survey operations to the new echosounder, EK80 may be configured in CW mode to emulate EK60. To learn if EK80 fast-CW data is equivalent to EK60 data, the Institute of Marine Research in Bergen, Norway conducted surveys prior to the workshop using EK60 and EK80 multiplexed to the same transducers. Conventional processing and echo integration of these datasets with 10 m vertical by 100 transmission horizontal cells indicated linear relationships between s_A measured with the two systems. However, for all frequencies, the linear relationships had frequency-dependent offsets up to 6 dB. This result led to the discovery of some errors related to transducer depth in early versions of EK80 firmware and related to τ_{eff} in early versions of data processing software (LSSS). After correcting these errors and ensuring identical system and environmental parameters were used by both EK60 and EK80, the differences were < 0.5 dB. During the EK80 workshop, EK60 and EK80 data were collected in the Technology Tank to resolve the residual differences.

First, a simulated echo signal was input to both EK60 and EK80 transceivers. Then, using the same transducer, echoes from a WC38.1 sphere were measured by EK60 and EK80 transceivers. The pulses generated by EK60 and EK80 were measured using a hydrophone. Finally, the multiplexed data described above were reanalysed.

2.6.1 Simulated echo

A Depth Sounder Test Set (DSTS, model DSTS4A-3, Electronic Devices, Inc., USA, S.N. 003H03-306), was connected, in turn, to a 38 kHz GPT (S.N. 102-202585) or 38 kHz WBT (S.N. 582207, EK80 software version 1.10.6088.15664), with the four quadrants connected in parallel to simulate a single-beam transducer. The DSTS sensed the echosounder transmit pulse and replied with a simulated echo of the same duration (via “Auto-width mode”). This appeared in the echosounder display as a target at a constant range and was detected as a single, on-axis target by both echosounders. The DSTS load impedance was set to “Low”, the sound speed to 1500 m s⁻¹, the reply delay to 5 m, the reply level to 50 mV, and the “AMPL VERNIER” control to the maximum of 3x for a reply level of ca. 150 mV. The EK80 receiver saturates for input voltages > 1.5 V peak-to-peak. Data were recorded for ca. 100 transmissions on both systems. Measurements were repeated for various receive-pulse durations (Table 2.12). Data were recorded in EK60 and EK80 .raw files.

Table 2.12. Parameters for comparing s_A in EK60 and EK80.

Parameter	EK60	EK80
Transmit power (W)	200	200
Pulse durations (ms)	0.512, 1.024, 2.048	0.512, 1.024, 2.048
Receiver bandwidth (kHz)	3.28 (0.512), 2.43 (1.024), 1.45 (2.048)	Not reported by EK80 software
Pulse ramping (proportion of transmit pulse)	Not configurable	0.103 (0.512), 0.051 (1.024), 0.026 (2.048)

The simulated signal was arbitrarily assumed to have a $TS = -50$ dB, and the calibration programs provided by EK60 and EK80 were used to derive the respective calibration parameters (Table 2.13). Because EK60 and EK80 loads were different and the voltage measured by EK80 was about 20 dB lower than that measured by EK60, the calibrated gains differed by roughly 10 dB (Table 2.13). Note that when the data were further analysed, the large differences in gains cast some doubt on the results.

Table 2.13. EK60 and EK80 calibration results vs. pulse duration. Note that the gain values are nominally 10 dB different between EK60 and EK80.

Pulse duration (ms)	EK60 G (dB)	EK80 G (dB)	EK60 $S_{A,corr}$ (dB)	EK80 $S_{A,corr}$ (dB)
0.512	21.10	33.60	-0.31	-0.59
1.024	23.58	33.83	-0.13	-0.43
2.048	23.65	34.32	-0.18	-0.28

The echo signal was integrated, the calibration values applied, and estimates of mean S_A were derived. The integration was repeated with multiple software systems. First, EK60 and EK80 software was used to replay the .raw files and manually record s_A for a layer. This S_A was adjusted for calibration using

$$S_{A,cal} = S_{A,uncal} + 2(G_{old} + S_{A,corr,old}) - 2(G_{new} + S_{A,corr,new}) . \quad (22)$$

Echoview was used to output s_A , calibrated using an .ecs file. LSSS was used to output S_A , calibrated using a calibration.xml file. In all cases, the mean S_A was calculated for a layer around the echo.

Values of S_A from EK60 were less than 1 dB different from those in EK80 (Table 2.14). Values of S_A from Echoview matched the ER60 and EK80 values to within 0.04 dB.

Table 2.14. Values of s_A vs. pulse duration for EK60 and EK80 operated in CW mode.

Pulse duration (ms)	S_A (EK60)	S_A (EK80)	S_A (EK60) – S_A (EK80) (dB)
0.512	-43.69	-43.56	-0.13
1.024	-44.54	-43.79	-0.74
2.048	-44.59	-44.34	-0.24

2.6.2 Sphere echo

A WC38.1 sphere was placed, in turn, at ~6 m range on the axis of a 38 and a 200 kHz transducer, both oriented horizontally in the Technology Tank. Using EK80 or ER60 software, data were recorded following 100 transmissions for each of multiple combinations of p_{et} and τ (Table 2.15).

Table 2.15. Parameters for measurements of a WC38.1 sphere.

Recording software	Hardware	Frequency (kHz)	Pulse duration (ms)	Transmit power (W)
EK80	GPT	38	0.512, 1.024, 2.048	1 000
EK80	WBT	38	0.512, 1.024, 2.048	1 000
ER60	GPT	38	0.512, 1.024, 2.048	2 000
EK80	WBT	38	0.512, 1.024, 2.048	2 000
ER60	GPT	200	0.512, 1.024	110
EK80	WBT	200	0.512, 1.024	110

Using EK80 software, the on-axis sphere echoes were used to estimate calibrated gain values for each combination of echosounder p_{et} and τ .

Using both ER60 and EK80 software, calibrated S_A values were calculated for a layer including the sphere. Using both Echoview and LSSS software, calibrated S_A values was calculated for a region including the sphere. All of these S_A values were compared (Table 2.16). Results indicate that EK80 hardware and software, EK60 hardware and ER60 software, and EK60 or EK80 hardware and Echoview software produce virtually equivalent values of S_A for measurements of a WC38.1 sphere in a tank.

Table 2.16. Differences in sphere- S_A (a) measured with GPT and processed with ER60 vs. measured with WBT and processed with EK80 (ER60–EK80), (b) measured with GPT and processed with EK80 vs. measured with WBT and processed with EK80 (EK80–EK80), and (c) measured with GPT and recorded with EK80 for $p_{et} = 1000$ W, else ER60, and processed with Echoview vs. measured with WBT and processed with Echoview (Echoview). Note that some differences (grey values) are anomalously large, resulting from too few single targets, noise, or both.

Frequency (kHz)	Transmit power (W)	Pulse duration (ms)	S_A difference (dB)		
			ER60–EK80	EK80–EK80	Echoview
38	1 000	0.512	-	0.00	0.04
		1.024	-	-0.08	-0.05
		2.048	-	0.78	0.80
	2 000	0.512	-0.13	0.02	-0.12
		1.024	-0.03	0.00	-0.01
		2.048	0.33	0.10	0.27
200	110	0.512	-0.04	-0.01	-0.02
		1.024	0.14	-0.01	0.16

2.6.3 Transmit pulses

A Reson TC4013 hydrophone (S.N. 0203086) was placed on the axis of a vertically-oriented Simrad ES38B transducer (S.N. 30472) at a range of approximately 5.5 m. A Stanford Research Systems SR560 low noise preamplifier (S.N. 69041) amplified the hydrophone output signal (preamplifier configuration was; DC filter, DC coupling, source A, gain mode low noise, gain x10, power line). The signal was viewed and digitized using an Agilent 54624A oscilloscope (S.N. MY40003344) and saved into Matlab formatted files.

EK60 GPT (S.N. 102-202585) and EK80 WBT (S.N. 582207, EK80 software version 1.10.6088.15664, 1 September 2016) generated, in turn, 38 kHz CW pulses of duration 0.512, 1.024, and 2.048 ms with a requested transmit power of 200 W. EK80 ramping was set to fast. One transmitted waveform was recorded for each setting.

The rms voltage over the duration of the transmitted pulse, the maximum peak-to-peak voltage, and the integral were estimated from the waveforms (Table 2.17). The envelopes of the waveforms, required for the integration, were estimated using a Hilbert transform.

The start ramping is slower on EK60 vs. EK80, post-transmit ringing is more consistent on EK60, and the pulse-envelope amplitude was consistently lower on EK60 (Figure 2.30). The pulses from both systems decreased in amplitude during the pulse, but the decrease was larger for EK80. EK80 pulses have a small overshoot after the start of the ramp, which was not present in EK60 pulses. The maximum peak-to-peak amplitude of the waveforms increased markedly with pulse duration for EK60, but remained almost constant for EK80.

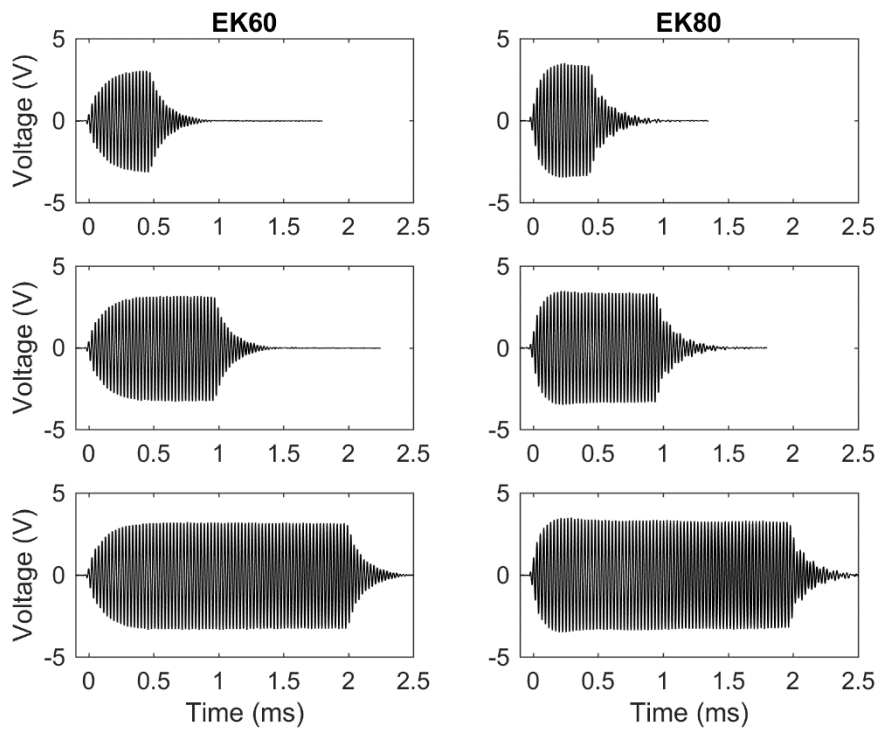


Figure 2.30. 38 kHz CW waveforms generated by an EK60 (left column) and EK80 (right column). Pulse duration settings were 512 μ s (upper row), 1024 μ s (middle row), and 2048 μ s (lower row).

The power-spectral densities, calculated for the durations of the pulses, peaked at 38.0 kHz for EK80 and 38.1 kHz for EK60 (Figure 2.31). Compared to EK60 pulses, EK80 pulses have higher V_{P-P} (Figure 2.30) and higher power, notably in the spectral peaks at \sim 27.5 and \sim 76 kHz (Figure 2.31). The peak at \sim 27.5 kHz should be investigated.

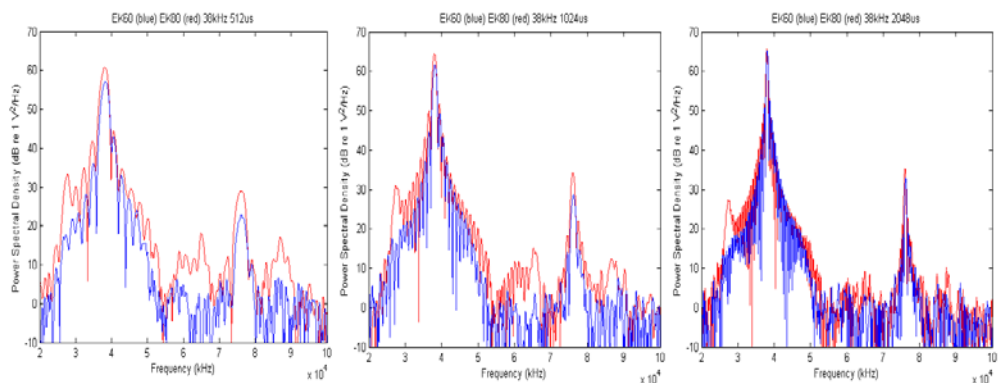


Figure 2.31. Power spectral densities of EK60 (blue) and EK80 (red) 38 kHz CW pulses with 512, 1024, and 2048 μ s duration (left to right; see Figure 2.30).

Table 2.17. Estimates of hydrophone-recorded pulse amplitude.

Pulse duration (ms)	EK60 V_{rms}	EK80 V_{rms}	EK60 V_{P-P}	EK80 V_{P-P}
0.512	1.02	1.36	6.19	6.97
1.024	1.42	1.74	6.47	6.97
2.048	1.79	1.88	6.56	7.00

The shapes of CW pulses transmitted by EK60 and EK80 are different, particularly at the start of the pulse. However, these differences do not affect echo integration, which relies on the ratio of the echo and transmitted energies. Nevertheless, different sampling rates may affect accurate characterizations of echo energy.

2.7 Targets near one another or boundaries

Acoustic surveys may require targets to be resolved close to one another or near a boundary, e.g. the seabed. FM signals and MF processing may be used to increase Δr , but MF processing introduces side lobes related to the length of the transmitted pulse and the frequency content of the signal. If the echo from one target is much weaker than the other, e.g. for a fish near the seabed, the side lobes may not allow the targets to be resolved. Even if the targets are resolved, $TS(f)$ from each target may not be separable. These considerations may limit the use of wideband systems for characterizing the scattering spectra of individual targets within aggregations or near a boundary.

The temporal extent of processing side lobes is described by $c_w\tau/2$ or the range resolution of a narrowband signal, although most of the energy is contained within the main lobe whose temporal extent is ca. $\Delta r = 1/2b_f$. While the main lobe is significantly higher in amplitude than the side lobes, a strong target can easily result in side lobes that exceed the primary peak associated with an adjacent weaker target, effectively masking it in the temporal domain despite the improved range resolution.

A slow ramp signal suppresses the processing side lobes, but also reduces the bandwidth. It may also be possible to process fast-ramp signal to reduce side lobes and thereby improve the detection of targets near boundaries (Lavery *et al.*, 2017).

The effects of processing side lobes on near-boundary target detection and spectral characterization are illustrated through temporal domain, MF processing of the filtered and decimated transmit signals from a smooth, rigid boundary. The reflected waves perfectly reproduce the incident signal so the autocorrelation of the transmit signal represents the amplitude and temporal extent of the side lobes from an ideal scatterer. For example, autocorrelations are shown for fast- and slow-ramped signals (45–95 kHz) with two transmit pulse durations (1.024 ms and 4.096 ms; Figure 2.32). For fast-ramped signals, the autocorrelations decrease slowly to a range related to the pulse length. For slow-ramped signals, the side lobes are smaller, except for the side lobe associated with the current EK80 stage 2 filter, which could be better suppressed by changing the software filter parameters.

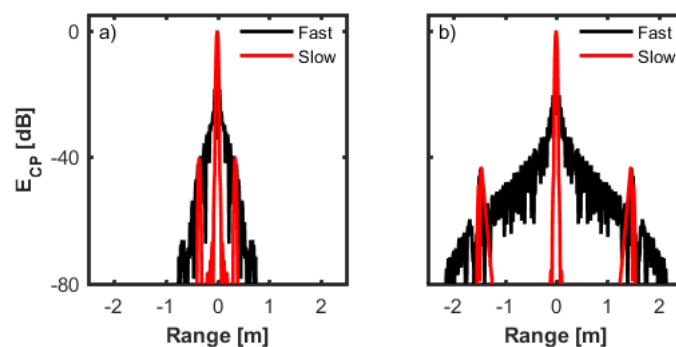


Figure 2.32. Normalized autocorrelation envelopes for filtered, decimated, fast (black), and slow (red) 45–90 kHz transmit signals with 1.024 ms (a) and 4.096 ms (b) pulse durations. To show the spatial extents of the side lobes, time is converted to range assuming a sound speed of 1500 m s⁻¹.

For comparison, transmit signals and autocorrelations of the ramped, but full sampling rate (1.5 MHz), signals generated by EK80 are shown for a 1.024 ms, 45–90 kHz pulse (Figure 2.33). The side lobes quickly drop -30 dB relative to the main lobe.

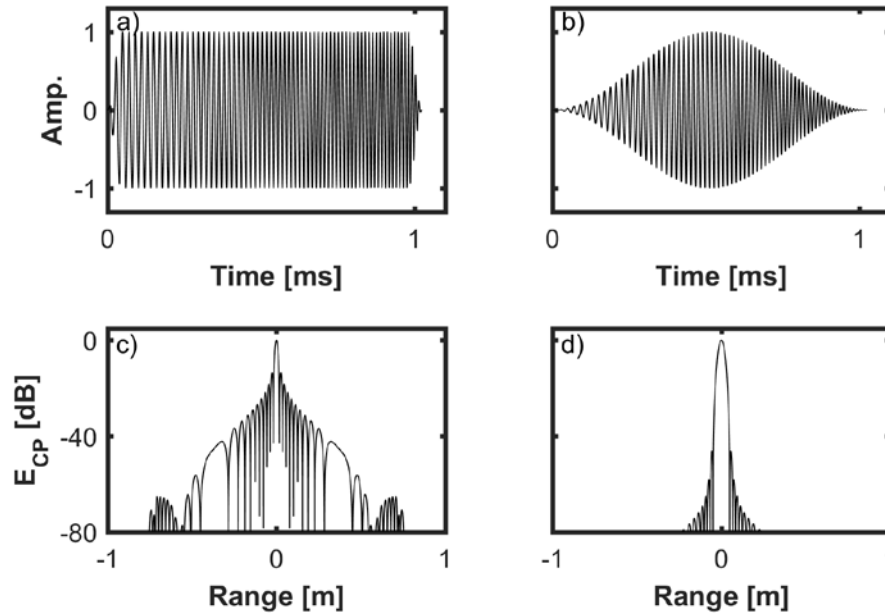


Figure 2.33. Simulated, fast- (a) and slow-ramp (b) 45–90 kHz transmit pulses sampled at 1.5 MHz. The autocorrelation envelopes of the fast- (c) and slow-ramped pulse (d) show the theoretical side lobes without artefacts associated with the stage 2 filter.

Slow ramping suppresses the side lobes by reducing the bandwidth of the transmitted signal, which decreases range resolution and reduces spectral characterization. The loss of spectral information may be important, e.g. when aiming to measure a resonance peak. If the stage 2 filter is improved to suppress the side lobes, a fast-FM signal may be used to characterize the scattering spectra of pelagic targets, and then a slow ramp may be applied in post-processing for improved detection of targets near the seabed (Lavery *et al.*, 2017). However, this approach may need further study as the temporal extent of the side lobe echo may be longer than that for the theoretical slow-FM echo.

2.7.1 Targets near the seabed

To quantify the resolution of targets near the seabed, ten ~ 4 cm diameter spherical lead targets were spaced 1 m apart in a vertical array deployed on the rocky area of Forty-Three Fathom Bank (32 39.48'N 117 58.39'W, ~ 89 m depth; Figure 2.34). EK80 and ME70 aboard the NOAA FSV "Reuben Lasker" were used to observe the targets.

Targets near the rocky seabed were studied using an EK80 configured with an ES120-7C transducer with a 7° beamwidth operating in FM and CW modes with various pulse ramp and duration settings. The array was centred in the beam using the ship's dynamic positioning system. These results were compared with measures from a Simrad ME70 multibeam configured with 21 beams. The vertical array was positioned in a 116 kHz beam with a 3.1° beamwidth, steered 3.6° athwartships.

The EK80 operating in FM mode clearly resolves eight of the ten targets (Figure 2.35). The echo from the ninth is mixed with that from the seabed. With a 2.048 ms slow-FM pulse, the EK80 resolution improved periodically, presumably when vessel movement

moved rocky outcrops out of the transducer beam (Figure 2.35). With a 0.064 ms CW pulse, the ninth target is partially resolved. In contrast, the ME70 clearly resolves nine of the ten targets. This is because the ME70 has a narrower beamwidth compared to the EK80 transducer (Ona and Mitson, 1996).

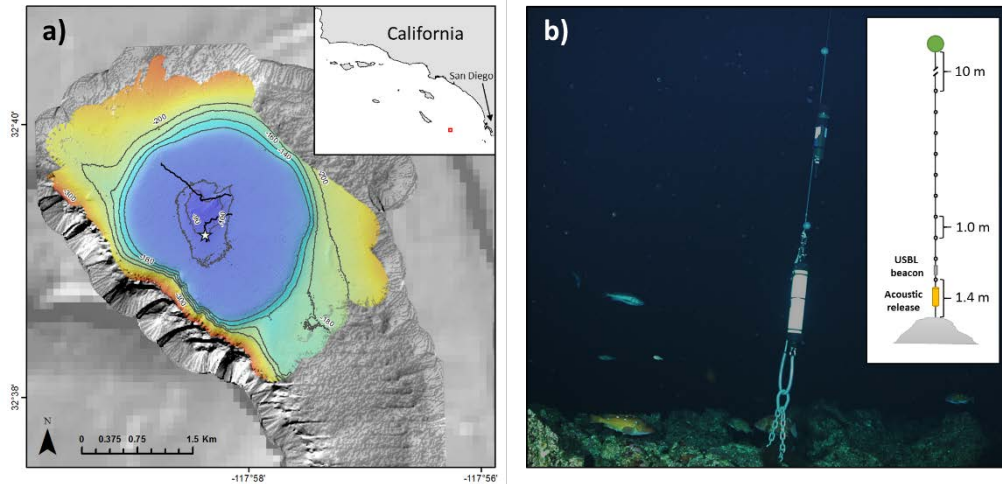
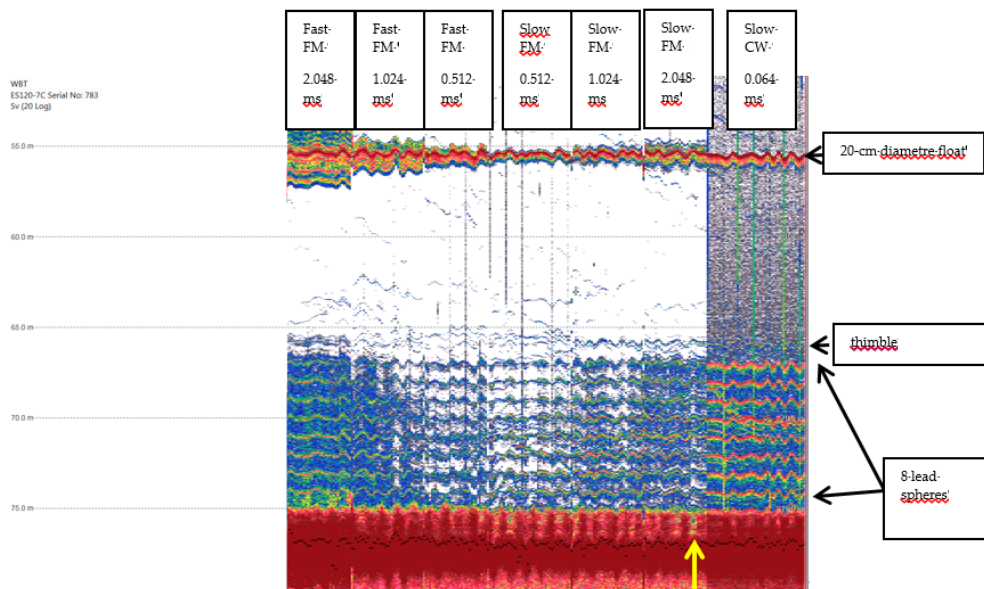


Figure 2.34. Forty-Three Fathom Bank located ~40 nautical miles west of San Diego, California, USA (a), and a vertical array of targets (b) deployed on the rocky reef near the centre of the bank (star on map). From the seabed to 20 m above, the vertical array was comprised of a chain ballast, an acoustic release (yellow cylinder), a lead sphere at ~1.4 m, an acoustic transponder at ~1.9 m, lead spheres at ~2.4, 3.4, 4.4, 5.4, 6.4, 7.4, 8.4, 9.4, and 10.4 m, and a ~20 cm float at ~20.4 m. The array was imaged using a camera on a remotely operated vehicle during the first of two transects (black lines).

From these measurements, it appears that the EK80 with short fast-CW pulses better resolves targets near the seabed, compared to fast- or slow-FM pulses with longer durations, even with MF processing. Narrower beamwidths, e.g. using the ME70, further improve the resolution of targets near the seabed.



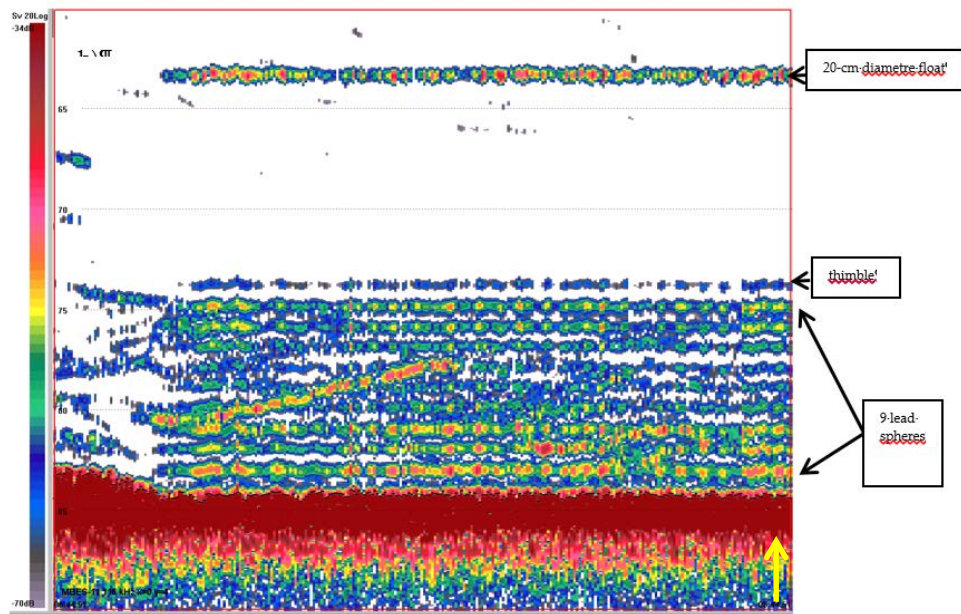


Figure 2.35. Pulse-compressed EK80 echogram for a 120 kHz beam at 7° beamwidth with various FM and CW pulses (top), and an ME70 echogram for a 116 kHz beam at 3.1° beamwidth steered 3.6° athwartships (bottom). Arrows indicate components of the vertical target array. Diagonal echo tracks are likely from fish in the study area.

3 Discussion

Conventional narrow-bandwidth echosounders, such as EK60, transmit pulses containing a single-frequency sinusoidal, continuous wave (CW) signal. Wide-bandwidth echosounders, such as EK80, transmit pulses containing a range of frequencies, often a linear low-to-high frequency modulated (FM) signal. FM signals with MF processing provide numerous new capabilities for detecting and tracking single targets and evaluating their backscattering spectra.

EK80 may be configured to closely emulate EK60 by transmitting CW pulses simultaneously at multiple frequencies, e.g. $f = 18, 38, 70, 120, 200,$ and 333 kHz. Even when similarly configured, however, there are some inherent differences between the two systems. For example, EK80 has wider bandwidth receiver filters, and it outputs complex waveform data from each transducer quadrant or section at higher decimated sampling rates than EK60.

EK80 can also be configured to transmit wideband FM pulses sequentially or simultaneously from the same array of transducers, potentially spanning large portions of the frequency range from 10 to 500 kHz. This feature offers the potential for improved range resolution, signal-to-noise ratio, and characterizations of the frequency responses of target strength and volume backscattering strength. The latter may be used to improve target identification, thereby reducing uncertainty in estimates of target abundance.

The many advantages of wideband vs. narrowband echosounders come with additional complexities associated with system calibrations, data storage, processing speed, signal processing and analyses, and interpretation. This stems largely from the necessity of having wider receiver bandwidths, from higher sampling rates, and from the frequency dependence of many environmental and system parameters, e.g. acoustic absorption, transducer efficiency and beamwidths, and scatterer reflectivity and directivity. For example, compared to narrowband data, wideband data may be inherently more susceptible to noise and more voluminous.

3.1 Research findings

During this workshop, experiments were conducted which confirm, for the first time, that EK60 and EK80, operating in CW mode, and ER60, EK80, Echoview, and LSSS software, provide equivalent measures of nautical-area backscattering coefficients for echoes from a metal sphere in a tank (see Section 1.1.1, Sphere echo and Table 2.16).

If processed and stored in the conventional manner used for EK60 data, EK80 data has greater requirements for data storage, computing power, and processing time.

It is important to preserve all of the information contained in wideband data to allow future alternative investigations. To facilitate lossless reduction of data volume during collection, Simrad should enable channel-dependent logging ranges and faster and programmable alternation between CW to FM and active to passive modes. Simrad could also better optimize filter bandwidth and decimation and implement conventional data compression algorithms.

To store and process less data for specific objectives, Simrad could (i) emulate EK60 data output, i.e. power and angle with four samples per pulse; (ii) use more aggressive filtering and decimation schemes; (iii) implement programmable data collection, e.g. mostly CW with periodic FM, and alternating active and passive, or both; (iv) collect passive data routinely prior to each transmit signal and optionally only log data with

acceptable *SNR*; and (v) facilitate multiple narrowband signals within allowable bandwidths.

Multiple narrowband datasets could be analysed as for EK60 data. Preprocessing may be used to generate MF data, with or without decimation. Preprocessed datasets could be limited by time, location, intensity, range, *SNR*, bandwidths, and data types or objects of interest (e.g. single targets).

The EK80 transmitter may not have sufficiently low output impedance to consistently produce a rectangular-envelope pulse. This may have ramifications for accurate measurements of volume backscattering strength spectra. Further investigation is warranted.

EK80 may transmit pulses from each channel simultaneously or synchronously. When transmitting simultaneously, cross-channel interference may bias the higher-frequency measurements. To mitigate cross-channel interference, set the transmit power to minimize non-linear effects; use orthogonal pulse-shapes for each channel, or both. To avoid cross-channel interference, transmit sequentially.

The EK80 transmit trigger may be input or output for synchronization with other instruments. To obtain stable triggering with low latency, the EK80 auxiliary port should be used. Triggering via the computer serial port, with or without a USB converter, causes large and variable latency.

Noise is higher and more variable in EK80 data than in EK60. For both active and passive modes, noise decreases with increasing pulse duration, and fast-ramp has less noise than slow-ramp configurations. Noise levels depend on the instrument platform and the environment.

Acoustic surveys may require targets to be resolved close to one another or near a boundary, e.g. the seabed. Theoretically, EK80 operating in FM mode has higher range resolution compared to EK60 in CW mode. However, MF processing introduces side lobes related to the length of the transmitted pulse and the frequency content of the signal. If the echo from one target is much weaker than another, e.g. a fish near the seabed, the side lobes from the seabed echo may eclipse the fish echo. Therefore, even if echoes from nearby targets are resolved, their backscattering spectra may not be separable. Additional work is needed to learn the potential for wideband systems to characterize scattering spectra of individual targets within aggregations or near a boundary.

Slow ramping suppresses MF side lobes and reduces the bandwidth of the transmitted signal, so FM-mode measurements with improved range resolution may have reduced spectral information. One solution may be to use a fast-FM signal with a wide bandwidth to measure scattering spectra of pelagic targets, and then post-process the data with a slow ramp to improve detections of targets near the seabed. However, this approach will require changes to the current stage 2 filter.

EK80 with short-CW pulses better resolved targets near the seabed, compared to fast- or slow-FM pulses with longer durations, even with MF processing. Narrower beamwidths, e.g. using the ME70, further improved the resolution of targets near the seabed.

3.2 Future EK80 research

Although significant progress was made by participants of the USA–Norway EK80 Workshop, research on EK80 and its use will likely continue for the next decade and beyond. To gain the most information from this wideband echosounder and to learn how the FM signals may be used in standard survey operations, numerous additional studies should be conducted soon. For example, experiments should be conducted to characterize (i) any frequency dependence of target-range estimates; (ii) effects of matched filter processing on incoherent volume scattering; (iii) effects of pulse duration on *SNR*, and range and spectral resolutions; (iv) effects of pulse signal (CW, FM, hyperbolic, arbitrary waveform) on *SNR*, and range and spectral resolutions; and (v) how the independent measurements of receiver and transducer impedance compare to those measured internally by EK80. Also, procedures for calibrating wideband echosounders should be standardized, and the accuracies and precisions of wideband measurements should be quantified. Software should be developed to plot spectrograms for each transmission and stack them by transmission. Low-frequency (< 15 kHz) measurements should be explored for resonance scattering, and any relevant regulations should be considered. This example list of EK80 research will continue to expand as more is learned about this powerful new instrument.

4 Acknowledgements

We thank Scott Mau and Dan Palance from the Advanced Survey Technologies group for their support of the shipboard data collections, particularly regarding underwater imaging with the remotely operated vehicle, and seabed mapping with the ME70, respectively. We give special thanks to Richard O'Driscoll, Mike Jech, Andone Lavery, and Gareth Lawson for their thorough, insightful, and constructive critiques of this work.

5 References

- Bodholt, H. 2002. The effect of water temperature and salinity on echosounder measurements. In ICES Symposium on Acoustics in Fisheries. Montpellier, June 2002. Presentation No. 123. 7 pp.
- Chu, D. Z., and Stanton, T. K. 1998. Application of pulse compression techniques to broadband acoustic scattering by live individual zooplankton. *Journal of the Acoustical Society of America*, 104: 39–55.
- Demer, D. A., Soule, M. A., and Hewitt, R. P. 1999. A multiple-frequency method for potentially improving the accuracy and precision of in situ target strength measurements. *Journal of the Acoustical Society of America*, 105: 2359–2376.
- Demer, D. A., Cutter, G. R., Renfree, J. S., and Butler, J. L. 2009. A statistical-spectral method for echo classification. *ICES Journal of Marine Science*, 66: 1081–1090.
- Demer, D. A., Berger, L., Bernasconi, M., Bethke, E., Boswell, K. M., Chu, D., Domokos, R., et al. 2015. Calibration of acoustic instruments. ICES Cooperative Research Report No. 326. 130 pp.
- Dragonette, L. R., Numrich, S. K., and Frank, L. J. 1981. Calibration Technique for Acoustic Scattering Measurements. *Journal of the Acoustical Society of America*, 69: 1186–1189.
- Ehrenberg, J. E., and Torkelson, T. C. 2000. FM slide (chirp) signals: a technique for significantly improving the signal-to-noise performance in hydroacoustic assessment systems. *Fisheries Research*, 47: 193–199.
- Foote, K. G. 2006. Optimizing two targets for calibrating a broadband multibeam sonar. *Oceans 2006*, Vols 1–4: 1499–1502.
- Knudsen, V. O., Alford, R. S., and Emling, J. W. 1948. Underwater ambient noise. *Journal of Marine Research*, 7: 410–429.
- Korneliussen, R. J., Diner, N., Ona, E., Berger, L., and Fernandes, P. G. 2008. Proposals for the collection of multifrequency acoustic data. *ICES Journal of Marine Science*, 65: 982–994.
- Lavery, A., Bassett, C., Lawson, G. L., and Jech, J. M. 2017. Calibration and signal processing approaches for a wideband echosounder. *ICES Journal of Marine Science*. In press.
- MacLennan, D. N., and Dunn, J. R. 1984. Estimation of sound velocities from resonance measurements on tungsten carbide calibration spheres. *Journal of Sound and Vibration*, 97: 321–331.
- MacLennan, D. N., Fernandes, P. G., and Dalen, J. 2002. A consistent approach to definitions and symbols in fisheries acoustics. *ICES Journal of Marine Science*, 59: 365–369.
- Ona, E., and Mitson, R. B. 1996. Acoustic sampling and signal processing near the seabed: The deadzone revisited. *ICES Journal of Marine Science*, 53: 677–690.
- Oppenheim, A. V., Schafer, R. W., and Buck, J. R. 1999. *Discrete-Time Signal Processing*. Prentice Hall, Upper Saddle River, NJ, USA. ISBN: 0-13-754920-2. 896 pp.
- Orfanidis, S. J. 1996. *Introduction to Signal Processing*. Prentice-Hall, Englewood Cliffs, NJ, USA. 783 pp. <http://www.ece.rutgers.edu/~orfanidi/intro2sp/>.
- Pedersen, A. 2006. Effects of nonlinear sound propagation in fisheries research. PhD thesis, University of Bergen, Norway. 307 pp.
- Stanton, T. K., and Chu, D. 2008a. Calibration of broadband active acoustic systems using a single standard spherical target. *Journal of the Acoustical Society of America*, 124: 128–136. doi: 10.1121/1.2917387.
- Stanton, T. K., and Chu, D. Z. 2008b. Calibration of broadband active acoustic systems using a single standard spherical target. *Oceans 2008 – MTS/IEEE Kobe Techno-Ocean*, Vols. 1–3: 144–146. doi: 10.1109/OCEANSKOBE.2008.4530923.

- Turin, C. L. 1960. An introduction to matched filters. IRE Transactions on Information Theory, IT-6: 311–329.
- Warren, J. D., and Demer, D. A. 2010. Abundance and distribution of Antarctic krill (*Euphausia superba*) nearshore of Cape Shirreff, Livingston Island, Antarctica, during six austral summers between 2000 and 2007. Canadian Journal of Fisheries and Aquatic Sciences, 67: 1159–1170.

Annex 1: Simrad ES38-7 transducer

Historically, fisheries surveys have been conducted with 38 kHz echosounders and, in some cases, augmented with echosounders operating at other frequencies, e.g. 18, 70, 120, 200, and 333 kHz. Although the commonly used transducers for the higher frequencies (i.e. ES70-7C, ES120-7C, ES200-7C, and ES333-7C), may be operated over wide bandwidths, the 18 and 38 kHz transducers (ES18-11 and ES38B) have relatively small usable bandwidths. Therefore, a new 38 kHz split-beam transducer (Simrad ES38-7) has been developed to take better advantage of the wideband capability of the EK80.

The ES38-7 transducer has a nominal frequency = 38 kHz, a nominal beamwidth = 7°, a nominal side-lobe level = -21 dB, four sectors, each with a nominal 70 Ω impedance, and a sea temperature sensor. The maximum $SL = 230$ dB *re* μ Pa at 1 m. This transducer has a non-traditional arrangement of elements comprising three sectors circling a centre sector. Therefore, split-beam processing is different for this transducer compared to traditional four-quadrant configurations. Further specifications and data-processing details may be obtained at www.simrad.com and from the manufacturer.

Following the EK80 workshop, an ES38-7 transducer (SN 138) was evaluated in the SWFSC Technology Tank. Measurements were made of the transducer impedance, usable bandwidth, frequency-dependent beamwidth, frequency-dependent side-lobe levels, and transmit spectra.

A.1 Impedance

Impedance data were collected for the ES38-7 (SN 138) and ES70-7C (SN 234) transducers in the SWFSC Technology Tank on 11 October 2016. Both transducers were mounted on a rotary-pitch pole and positioned to project horizontally at a depth of ~5 m (Figure A1).

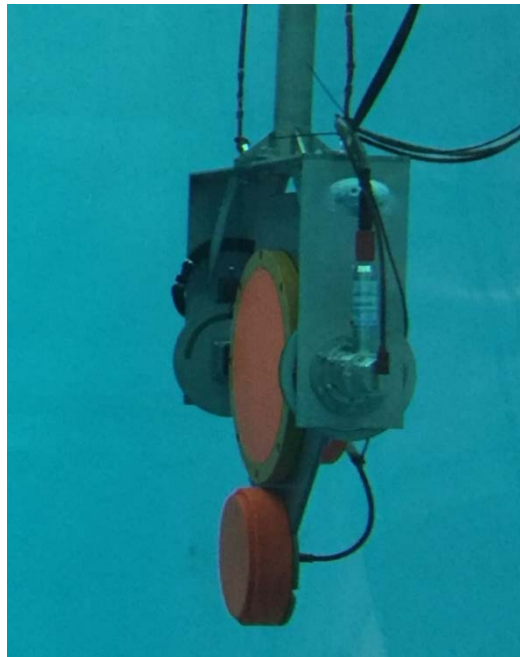


Figure A1. Simrad ES38-7 (upper) and ES70-7C (lower) transducers mounted on a pole with computer-controlled pitch and rotation motors located in the SWFSC Technology Tank.

Measurements were collected for each ES38-7 sector using a precision-impedance analyser (Agilent 4294A) from which 801 data points were collected over the measurement

bandwidth of 30–50 kHz. The impedance-analyser measurements were referred to the Amphenol connector on the transducer cable. Resistance R (Ω) and reactance X (Ω) were measured for the combined connector, cable, and transducer, and the following values were derived: impedance $Z = R + jX$ (Ω), magnitude of impedance $|Z| = \sqrt{R^2 + X^2}$ (Ω), phase of impedance $\theta = \arctan(X/R)$ (radians), admittance $Y = Z^{-1} = G + jB$ (Siemens), conductance $G = R/(R^2 + X^2)$ (Siemens), and susceptance $B = -X/(R^2 + X^2)$ (Siemens) (Figure A2). The measurements were repeated for each ES70-7C quadrant (Figure A3).

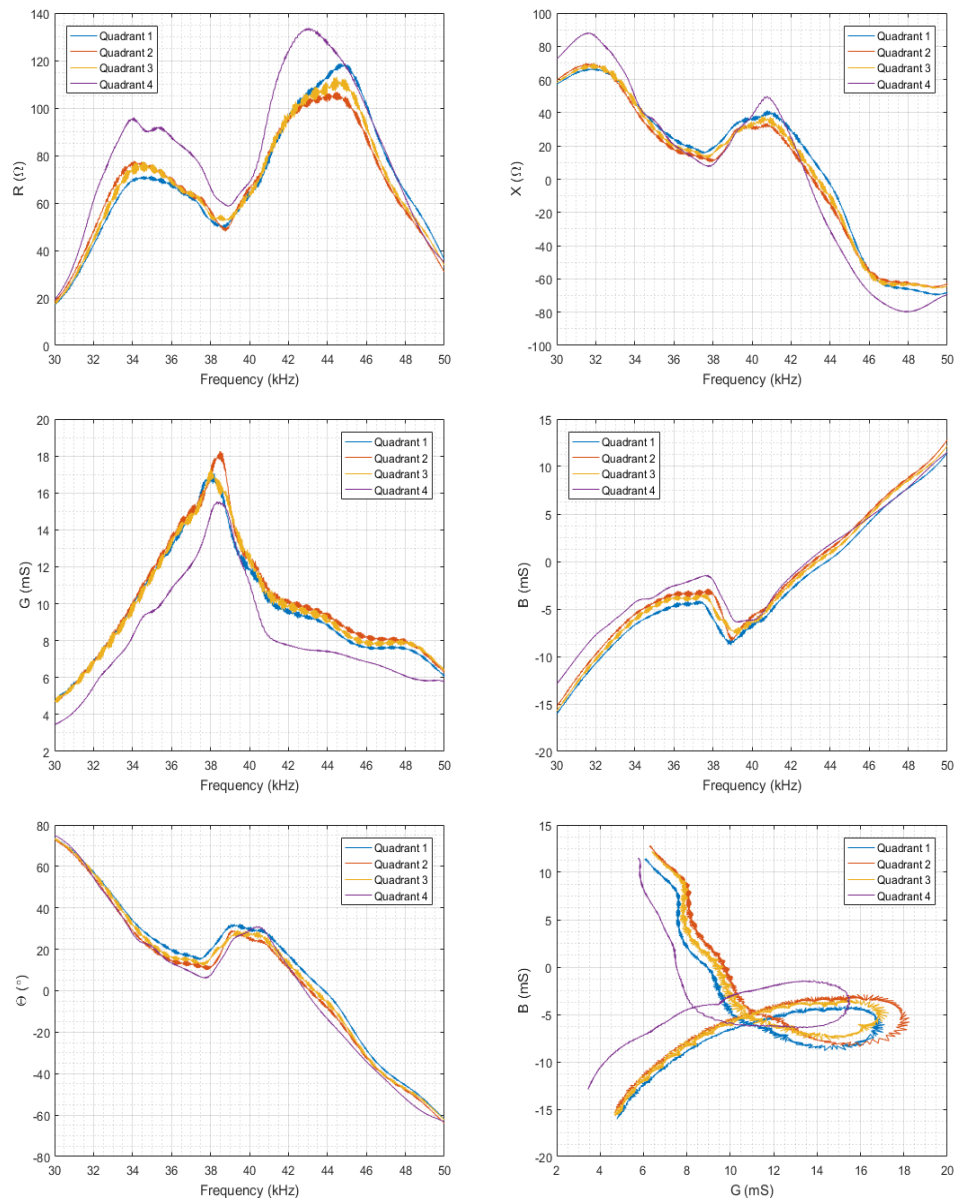


Figure A2. ES38-7 (SN 138) resistance (top left), reactance (top right), conductance (middle left), susceptance (middle right), phase vs. frequency (bottom left), and susceptance vs. conductance (bottom right).

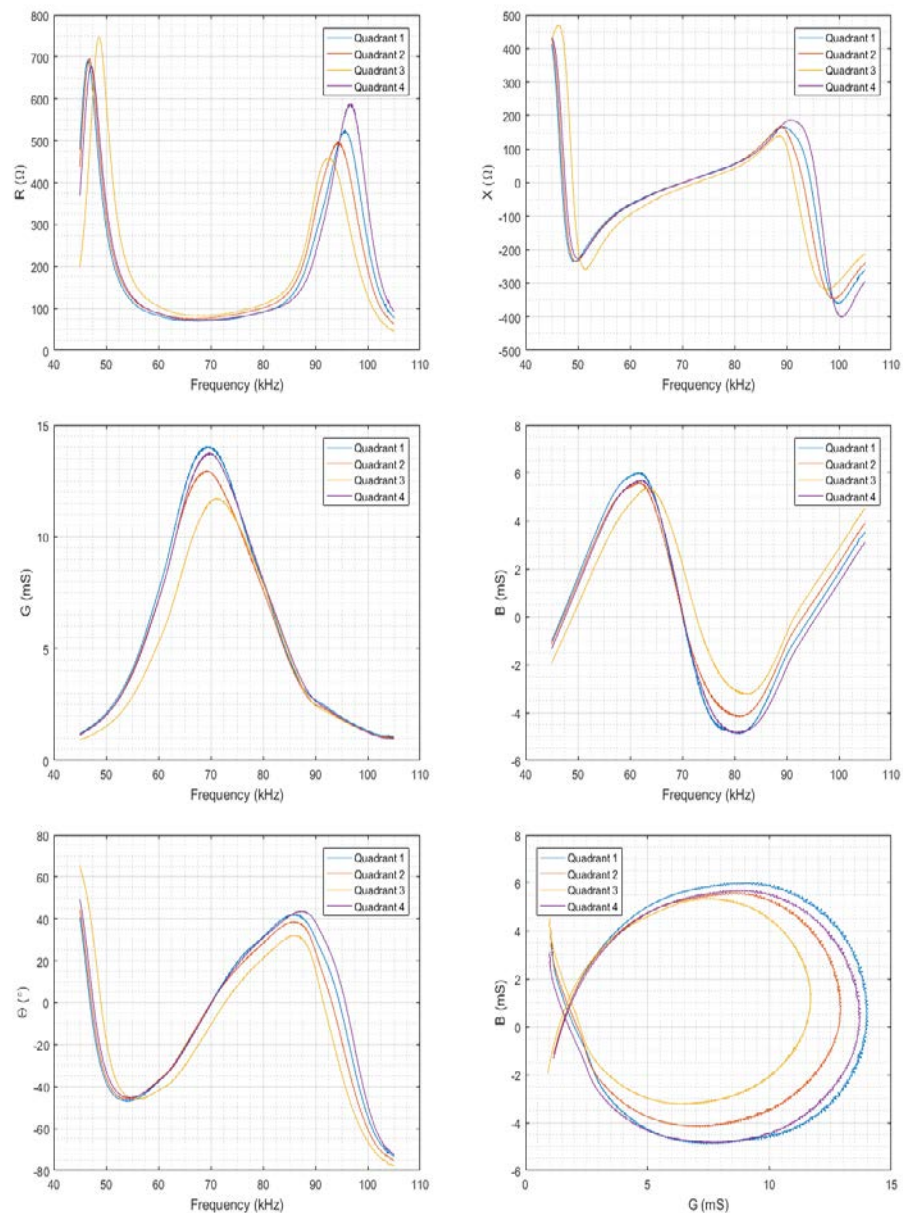


Figure A3. ES70-7C (SN 234) resistance (top left), reactance (top right), conductance (middle left), susceptance (middle right), phase vs. frequency (bottom left), and susceptance vs. conductance (bottom right).

A.2 Bandwidth

For FM transmissions, Simrad recommends using the frequency range where each sector or quadrant has $|Z| > 50 \Omega$ and $|\theta| < 45^{\circ}$. Strictly following these guidelines for the ES38-7, the usable bandwidth is ca. 33.1–47.2 kHz; for the ES70-7C, it is ca. 57.9–96.4 kHz (Figure A4). However, because the phase only slightly exceeds 45° before decreasing again, this ES70-7C should be usable from ~45 to 96.4 kHz.

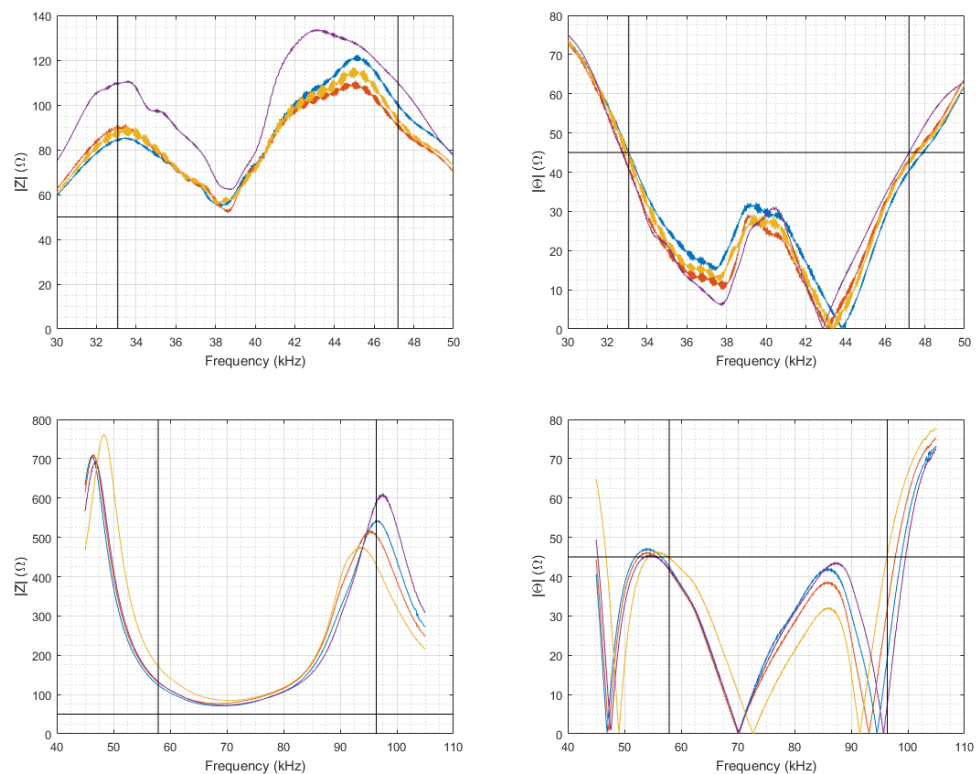


Figure A4. The usable bandwidth for the ES38-7 is ~33.1–47.2 kHz (top row), and for the ES70-7C ~57.9–96.4 kHz (bottom row), as defined by $|Z| > 50 \Omega$ (left column) and $|\theta| < 45^\circ$ (right column). However, the ES70-7C should be usable from ~45 to 96.4 kHz.

A.3 Beam pattern

The ES38-7 was placed on the rotator-pitch pole at ~ 5 m depth and oriented to project horizontally (Figure A1). Using the encoder from the rotary motor to modulate the athwartships plane and a compass attached to the transducer pitch tray to modulate the alongships plane, the transducer was positioned with a heading and pitch of 0° . A hydrophone (Reson TC4013), using EK80 single-target detection, was positioned on the beam axis at ~ 9.3 m range. The hydrophone was connected to a low-noise preamplifier (Stanford Research SR560) set for DC filtering and amplifying with a gain of 5. The output of the preamplifier was connected to channel 1 of an oscilloscope (Agilent 54624A). Channel 2 was connected to the EK80 output trigger and used to trigger the oscilloscope to display the transmit pulse. With the ES38-7 transmitting FM pulses of 33.1–47.2 kHz every second, a script (Matlab) was used to move the rotary motor between -15° and 15° in 0.1° increments. Transmit-pulse wave forms and their FFTs, with Hanning windows, were recorded for each position. The athwartships beam pattern was plotted (Figure A5).

To measure the two-dimensional beam pattern of the ES38-7, the rotary and pitch motors were used to orient the transducer between -5° and 5° in 0.5° increments. The plot of the beam pattern at 38 kHz is shown in Figure A6.

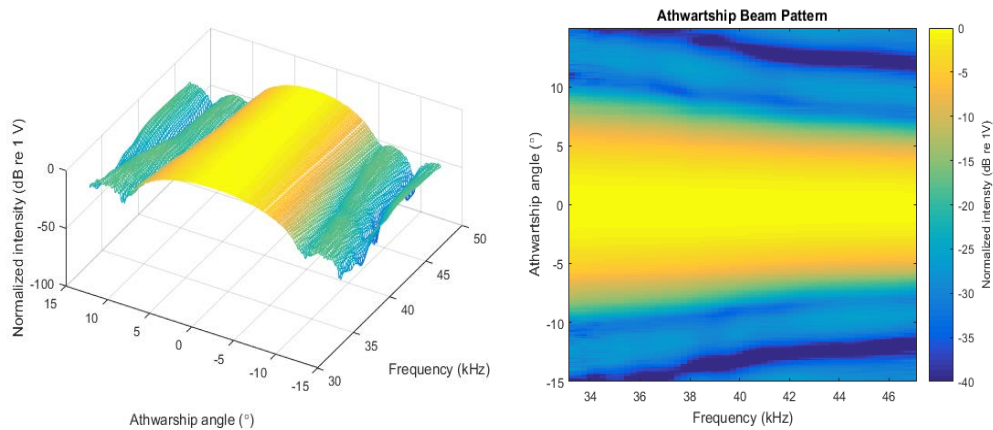


Figure A5. The frequency-dependent athwartships beam pattern of an ES38-7 transducer (3-D left; 2-D right).

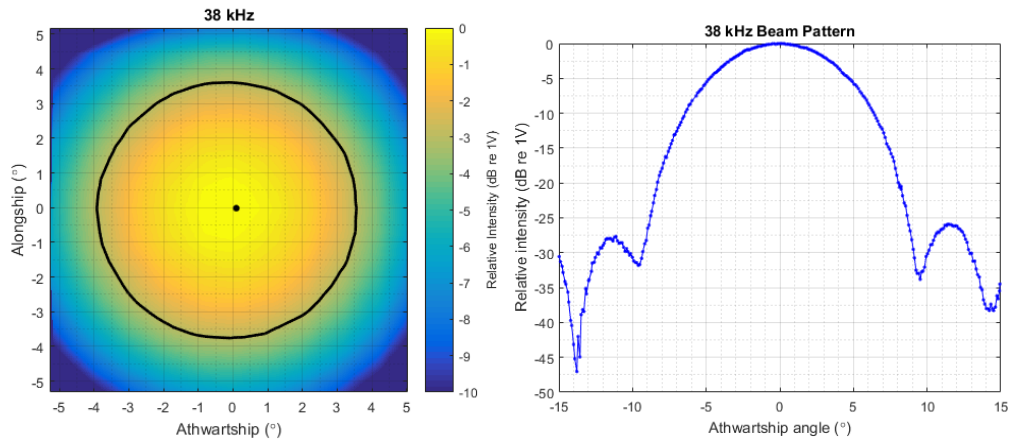


Figure A6. Beam pattern of an ES38-7 transducer at 38 kHz (left) showing the -3 dB beamwidth (black line) and the beam axis (dot), and the athwartships beam pattern at 38 kHz (right) showing side lobes less than -25 dB.

Relating the frequency-dependent beamwidth $b(f) = b_{ref}(f)f_{ref}/f$ to a reference beamwidth b_{ref} at a reference frequency f_{ref} , the measured beamwidths were compared to predicted values (Bodholt, 2002). Also calculated were the frequency-dependent beamwidths and the levels and positions of the side lobes (Figure A7).

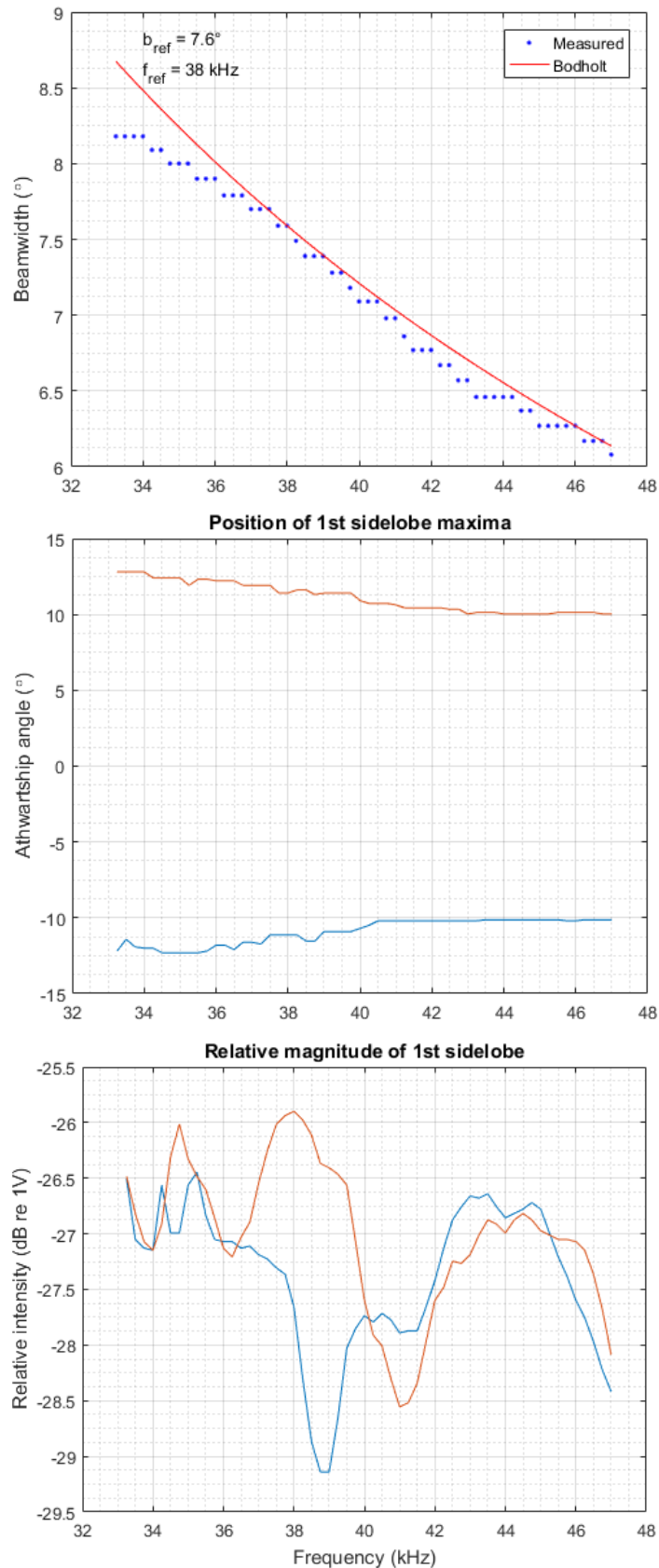


Figure A7. The beam pattern of an ES38-7 compared to theory (top); angular positions to port (red) and starboard (blue) of the side lobe peaks vs. frequency (middle); and the relative intensities to port (red) and starboard (blue) of the main and side lobes vs. frequency (bottom).

A.4 Transmit spectra

Sound-pressure level vs. frequency was measured for CW and fast-FM (33.1–47.2 kHz) pulses (2000 W power, 1.024 ms duration) generated by the EK80 and transmitted from an ES38-7 (SN 138). The $SPL = 20\log(u_{er}(f)) - M_u + 20\log(r)$ (dB re 1 μ Pa) spectra were calculated over the usable hydrophone frequency range (1 Hz to 170 kHz) using the power spectra = $20\log(u_{er}(f))$ dB re 1 V, the nominal receiving response $M_0 = -211\text{ dB} \pm 3\text{ dB re } 1\text{V}/\mu\text{Pa}$ for the hydrophone, and the range between the transducer and the hydrophone $r = 9.3\text{ m}$.

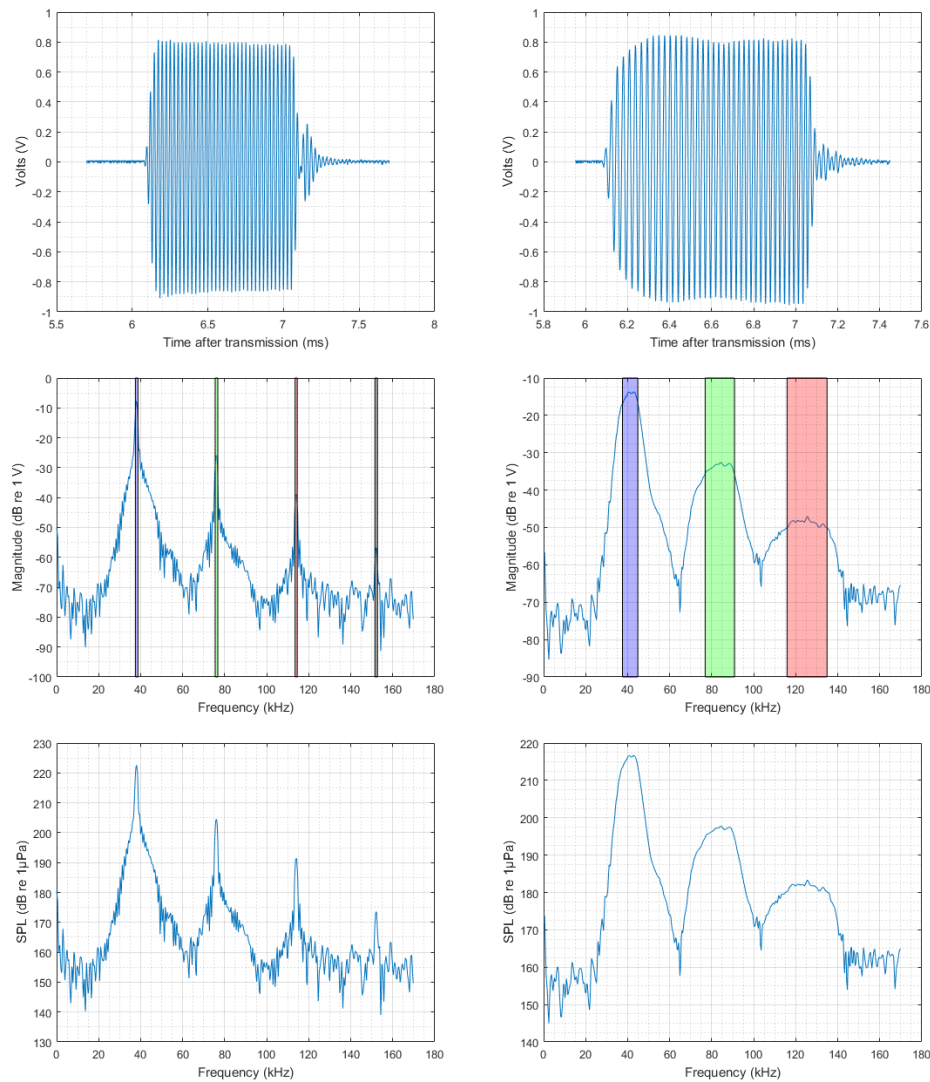


Figure A8. ES38-7 waveforms (top row), power spectra with -3 dB bandwidths (middle row), and SPL spectra (bottom row) for 38 kHz CW (left column) and 33.1–47.2 kHz fast-FM pulses (2000 W, 1.024 ms).

For CW, the pulse shape droops (Figure A8). The -3 dB bandwidth of the principal signal is 1.25 kHz (3.3%) from 37.50 to 38.75 kHz. The b_f of the first harmonic is 1.25 kHz (3.3%) from 75.50 to 76.75 kHz. The b_f of the second harmonic is 1.0 kHz (2.6%) from 113.50 to 114.50 kHz. The b_f of the third harmonic is 1.25 kHz (3.3%) from 151.50 to 152.75 kHz. The peaks of the first, second, and third harmonics are -18.12 , -31.29 , and -49.06 dB , respectively, relative to the principal peak.

For fast-FM, the -3 dB bandwidth of the principal signal is 7.34 kHz (19.3%) from 37.52 to 44.86 kHz. The b_f of the first harmonic is 14.01 kHz (36.9%) from 76.87 to 90.88 kHz. The b_f of the second harmonic is 19.01 kHz (50.0%) from 115.89 to 134.90 kHz. The b_f increases with higher harmonics. The peaks of the first and second harmonics are ca. -18.95 and -33.33 dB, relative to the principal peak.

A.5 Conclusion

For the test of ES38-7 at $f = 38$ kHz, the beamwidth $\theta_{-3\text{ dB}} = 7.6^\circ$ and the side lobes were -25 dB. The $\theta_{-3\text{ dB}}$ changed predictably vs. f . This transducer should be usable for a range of f values from 33.1 to 47.2 kHz, with consideration given to the appreciable harmonics. It could be expected that these measurements may differ for other transducers of the same model.

Annex 2: Terms, symbols, and units

The following terminology used in this document is based mostly on MacLennan *et al.* (2002) and follows the Système international d'unités (SI system). Symbols uniquely represent a term. All symbols for variables should be italicized. Any symbol for a variable (x) that is not logarithmically transformed should be lower case. Any symbol for a logarithmically transformed variable, e.g. $X = 10\log_{10}(x/x_{ref})$, with units of decibels referred to x_{ref} (dB *re* x_{ref}), should be capitalized. Deviations from these rules should be noted.

Term	Symbol	Unit	Description
Environmental			
Water temperature	t_w	Degree Celsius (°C)	Heat or average kinetic energy of particles in water
Water salinity	s_w	Practical salinity unit (psu)	The total amount of dissolved material in water
Water depth	d_w	Metre (m)	The vertical distance below the water surface
Water pressure	p_w	Pascal (Pa) (= 10^{-4} dbar)	The force per unit area in water
Water density	ρ_w	Kilogramme per cubic metre (kg m ⁻³)	The mass density of water
Electrical			
Voltage	u_e	Volt (V)	The square root of the mean of the squares (rms) of time-varying electric potential
Current	i_e	Ampere (A)	The rms electric current
Electrical impedance	z_e	Ohm (Ω)	The ability of a material to oppose the passage of an alternating electric current
Electrical power	p_e	Watt (W) or VA or V ² Ω^{-1} or A ² Ω	The rms electrical energy per unit time
Acoustic			
Water sound speed	c_w	Metre per second (m s ⁻¹)	The distance sound travels per unit time in water
Water acoustic impedance	z_{aw}	kg m ⁻² s ⁻¹	The product of ρ_w and c_w
Acoustic frequency	f	Hertz (Hz) = cycles s ⁻¹	The number of complete cycles of a periodic wave per unit time
Acoustic frequency bandwidth	b_f	Hz	The difference between the highest and lowest f in a signal or device
Acoustic wavelength	λ	m	The distance spanned by one cycle of a periodic pressure wave
Acoustic wave number	k	m ⁻¹	The number of periodic wavelengths per 2π -unit distance

Term	Symbol	Unit	Description
Pulse duration	τ	s	The duration of a signal pulse
Effective pulse duration	τ_{eff}	s	The duration of a square-shaped pulse that has the same energy as the echosounder-pulse shape after reception processing
Range	r	m	The direct-path distance between objects, e.g. the transducer and the target
Reference range	r_0	m	The r from an acoustic source or target to which measurements are referred, conventionally 1 m
Acoustic pressure	p	Pa (= N m^{-2} = $\text{kg m}^{-1} \text{s}^{-2}$)	The rms deviation of local pressure from the ambient
Reference acoustic pressure	p_{ref}	Pa	The reference p , conventionally 1 μPa for underwater sound
Acoustic power	p_a	W	The rms acoustic energy per unit time
Acoustic intensity	i	W m^{-2}	The rms p_a per unit area
Acoustic intensity at r_0	i_0	W m^{-2}	The rms i at r_0
Reference acoustic intensity	i_{ref}	W m^{-2}	The i of a plane wave with rms $p = p_{ref}$
Spherical spreading loss	No symbol	m^{-2}	The reduction in i with r resulting from spherical expansion of the wave front
Absorption loss	No symbol	m^{-1}	The reduction in i with r resulting from conversion to heat
Absorption coefficient	α_a	dB m^{-1}	A metric of absorption loss
Transduction			
Nominal frequency	f_{nom}	kHz	The transmit frequency used in CW mode
Centre frequency	f_c	kHz	The frequency in the middle of the range
Transmit voltage	u_{et}	V	The rms u_e input to a transducer
Transmit current	i_{et}	A	The rms i_e input to a transducer
Transducer electrical impedance	z_{et}	Ω	The ability of a transducer to oppose the passage of an alternating electric current
Receiver electrical impedance	z_{er}	Ω	The ability of an echosounder receiver to oppose the passage of an alternating electric current

Term	Symbol	Unit	Description
Transmit electric power	p_{et}	W	The electrical power input to a transducer
Transmit acoustic power	p_{at}	W	The acoustic energy per unit time output from a transducer
Transducer efficiency	η	Dimensionless	The proportion of p_{et} converted to p_{at}
Transmit pressure	p_t	Pa	The p output from a transducer
Directional angles	α, β	Degree ($^\circ$)	The angle coordinates in orthogonal planes, typically alongships and athwartships or aligned with the major and minor transducer axes, respectively
Gain	$g(\alpha, \beta)$ or $G(\alpha, \beta)$	Dimensionless or Decibel referred to 1 (dB <i>re</i> 1)	The ratio of i values, observed at a distant point, resulting from transmissions, with constant p_{et} , of a real transducer, and an idealized lossless omni-directional transducer. Gain accounts for losses referred to a point on the electrical side of the transducer
On-axis gain	g_0 or G_0	Dimensionless or dB <i>re</i> 1	The $g(\alpha, \beta)$ on the transducer beam axis ($\alpha = \beta = 0$)
Transducer directivity	$d(\alpha, \beta)$ or $D(\alpha, \beta)$	Dimensionless or dB <i>re</i> 1	The one-way directional gain of a real transducer, omitting losses
Transducer directivity pattern	$b(\alpha, \beta)$ or $B(\alpha, \beta)$	Dimensionless or dB <i>re</i> 1	The ratio of $d(\alpha, \beta)$ and its maximum value
Transducer beamwidth	$\theta_{-3 \text{ dB}}$ or $\alpha_{-3 \text{ dB}}$ or $\beta_{-3 \text{ dB}}$	$^\circ$	The angle from the transducer beam axis to the point of half-power, in the θ , α , or β planes
Transducer beamwidth offset	α_o or β_o	$^\circ$	The angular displacement of the transducer maximum-response axis beam from the axis of the zero split-beam phase in the α or β planes
Transducer angle sensitivity	Λ_α or Λ_β	Electrical $^\circ$ /geometric $^\circ$	A factor to convert split-beam electrical angles to target-bearing angles in the α or β planes
Source intensity or Source level	i_s or SL	W m $^{-2}$ or dB <i>re</i> 1 μ Pa at r_0	The i_0 in the direction (α, β) of the target

Term	Symbol	Unit	Description
Transmit intensity	i_t	W m ⁻²	The intensity of a plane wave transmitted from a real transducer
Omni-directional transmit acoustic intensity	$i_{t\ omni}$	W m ⁻²	The i_t for an idealized lossless omni-directional transducer.
Equivalent two-way beam angle	ψ or Ψ	steradian (sr) or dB <i>re</i> 1 sr	The solid angle subtended by an ideal conical beam that would produce the same volume integral as the square of the normalized transducer directivity
Effective receiving area	$a_r(\alpha, \beta)$	m ²	The area of a real transducer available to receive acoustic power and transfer it to a matched load (i.e. $z_{er} = z_{et}$), referred to the same point on the electrical side of the transducer as g_0
Received electric power	p_{er}	W or dB <i>re</i> 1 W	The p_e output from a transducer, referred to the same point as g_0 and a_r
On-axis received power	p_{er0} or P_{er0}	W or dB <i>re</i> 1 W	The p_{er} in the direction (α, β) of the maximum $b(\alpha, \beta)$
Transmit voltage sensitivity	s_u or S_u	$\mu\text{Pa V}^{-1}$ or dB <i>re</i> 1 $\mu\text{Pa V}^{-1}$	The SL resulting from a 1 V rms sinusoidal signal applied to the transducer terminals
Transmit current sensitivity	s_i or S_i	$\mu\text{Pa A}^{-1}$ or dB <i>re</i> 1 $\mu\text{Pa A}^{-1}$	The SL resulting from a 1 A rms sinusoidal signal applied to the transducer terminals
Receive voltage sensitivity	m_u or M_u	V μPa^{-1} or dB <i>re</i> 1 V μPa^{-1}	The unloaded u_e at a point on the electrical side of the transducer resulting from i_{ref} applied to the transducer surface
Reciprocity parameter	j	Dimensionless	The ratio of the response of a linear, passive, reversible electroacoustic transducer acting as a receiver, m_u , to its response as a transmitter, s_i
Original sampling frequency	f_s	Hz	The number of samples per second first digitized by an instrument
Sphere			
Sphere density	ρ_s	kg m ⁻³	Mass density of an elastic sphere

Term	Symbol	Unit	Description
Sphere compressional wave sound speed	c_c	m s^{-1}	The compressional (or longitudinal) wave sound speed of an elastic sphere
Sphere shear wave sound speed	c_s	m s^{-1}	The shear (or transverse) wave sound speed of an elastic sphere
Metrics			
Signal-to-noise ratio	r_{sn}	Dimensionless	The quotient of signal and noise power
Spherical scattering cross-section	σ_{sp}	m^2	The area of an acoustic target effectively scattering acoustic power
Backscattering cross-section	σ_{bs}	m^2	The area of an acoustic target effectively backscattering acoustic power $\sigma_{bs} = \sigma_{sp}/4\pi$, at r_0
or Target strength	or TS	or $\text{dB re } 1 \text{ m}^2$	
Point backscattering strength	S_p	$\text{dB re } 1 \text{ m}^2$	Calculated as TS , but for sample, not target, ranges
Sampled area	a	m^2	The area contributing to a received signal
Surface backscattering coefficient	s_s	$\text{m}^2 \text{ m}^{-2}$	The backscattering cross-section per unit of surface area, assuming the area is the intersection of ψ and a sphere with radius r centred on the transducer
or Surface backscattering strength	or S_s	or $\text{dB re } 1 \text{ m}^2 \text{ m}^{-2}$	
Sampled volume	v	m^3	The volume contributing to a received signal
Volume backscattering coefficient	s_v	$\text{m}^2 \text{ m}^{-3}$	The sum of σ_{bs} per unit of water volume
or Volume backscattering strength	or S_v	or $\text{dB re } 1 \text{ m}^2 \text{ m}^{-3}$	
Survey area	a_s	m^2	The area of the survey region
Area backscattering coefficient	s_a	$\text{m}^2 \text{ m}^{-2}$	The integral of s_v over a range of depths; or
or Nautical area backscattering coefficient	or s_A	or $\text{m}^2 \text{ nautical mile}^{-2}$	s_a multiplied by a scaling factor $(4\pi(1852)^2 \text{ nautical mile}^2 \text{ m}^{-2})$
Scatterer volume density	ρ_v	Number m^{-3}	The number of scatterers per unit of sampled volume
Scatterer areal density	ρ_a	Number m^{-2}	The number of scatterers per unit of sampled area
	or ρ_A	or Number nautical mile $^{-2}$	

Term	Symbol	Unit	Description
Scatterer abundance	n_b	Number	The number of scatterers within a sampled range and area
Scatterer biomass	m_b	kg	The mass of scatterers within a sampled range and area

Annex 3: Author contact information

Lars N. Andersen

Simrad AS
Strandpromenaden 50
NO-3183 Horten, Norway
lars.nonboe.andersen@simrad.com

Chris Bassett

NOAA Fisheries
Alaska Fisheries Science Center
7600 Sand Point Way N.E., Building 4
Seattle, WA 98115, USA
Chris.Bassett@noaa.gov

Laurent Berger

Centre IFREMER de Brest
BP 70
29280, Plouzané, France
Laurent.Berger@ifremer.fr

Naig Le Bouffant

Centre IFREMER de Brest
BP 70
29280 Plouzané, France
Naig.Le.Bouffant@ifremer.fr

Dezhang Chu

NOAA Fisheries
Northwest Fisheries Science Center
2725 Montlake Boulevard East
Seattle, WA 98112, USA
Dezhang.Chu@noaa.gov

Jeff Condiotty

Kongsberg Underwater Technologies,
Inc.
19210 33rd Ave. W.
Lynnwood, WA 98036, USA
Jeff.Condiotty@simrad.com

George R. Cutter Jr.

NOAA Fisheries
Southwest Fisheries Science Center
8901 La Jolla Shores Drive
La Jolla, CA 92037, USA
George.Cutter@noaa.gov

David Demer

NOAA Fisheries
Southwest Fisheries Science Center
8901 La Jolla Shores Drive
La Jolla, CA 92037, USA
David.Demer@noaa.gov

Briony Hutton

Echoview Software
1c/38 Montpellier Retreat
Battery Point, TAS 7004,
Australia
Briony.Hutton@echoview.com

Rolf Korneliussen

Institute of Marine Research
Nordnesgaten 50
5005 Bergen, Norway
Rolf.Korneliussen@imr.no

Gavin Macaulay

Institute of Marine Research
Nordnesgaten 50
5005 Bergen, Norway

Gavin.Macaulay@imr.no

William L. Michaels

NOAA Office of Science and Technology
1315 E-W Highway, SSMC3
Silver Spring, MD 20910, USA

William.Michaels@noaa.gov

David Murfin

NOAA Fisheries
Southwest Fisheries Science Center
8901 La Jolla Shores Drive
La Jolla, CA 92037, USA

David.Murfin@noaa.gov

Armin Pobitzer

Christian Michelsen Research
Fantoftvegen 38
5072 Bergen, Norway

Armin.Pobitzer@cmr.no

Josiah S. Renfree

NOAA Fisheries
Southwest Fisheries Science Center
8901 La Jolla Shores Drive
La Jolla, CA 92037, USA

Josiah.Renfree@noaa.gov

Thomas S. Sessions

NOAA Fisheries
Southwest Fisheries Science Center
8901 La Jolla Shores Drive
La Jolla, CA 92037, USA

Steve.Sessions@noaa.gov

Kevin L. Stierhoff

NOAA Fisheries
Southwest Fisheries Science Center
8901 La Jolla Shores Drive
La Jolla, CA 92037, USA

Kevin.Stierhoff@noaa.gov

Charles H. Thompson

NOAA Fisheries
Southeast Fisheries Science Center
Mississippi Laboratories
1021 Balch Blvd.
Stennis Space Center,
MS 39529, USA

Charles.H.Thompson@noaa.gov